Vertebrate Anatomy Morphology Palaeontology 10:65–110
ISSN 2292-1389

Problematic putative pachycephalosaurids: synchrotron µCT imaging shines new light on the anatomy and taxonomic validity of *Gravitholus albertae* from the Belly River Group (Campanian) of Alberta, Canada

Aaron D. Dyer[1,2,3,*], Mark J. Powers[3], and and Philip J. Currie[3]
[1]Department of Ecology and Evolutionary Biology, University of Toronto, Toronto, ON, Canada; aaron.dyer@mail.utoronto.ca
[2]Department of Natural History, Royal Ontario Museum, Toronto, ON, Canada
[3]Department of Biological Sciences, University of Alberta, Edmonton, AB, Canada; powers@ualberta.ca, pjcurrie@ualberta.ca

Abstract: The taxonomic validity of the holotype and sole specimen of the pachycephalosaurid *Gravitholus albertae* (TMP 1972.027.0001) from the Belly River Group (Alberta, Canada) remains unresolved forty years after its first description. The diagnosis for this species is tenuous at best and extensive cranial fusion has prevented a thorough description and taxonomic referral of TMP 1972.027.0001. We used synchrotron µCT imaging to identify fused sutures and segment the individual elements that comprise TMP 1972.027.0001. This allowed for a detailed description of the specimen in a more thorough comparative framework with other known pachycephalosaurian specimens. Using new observations of contacts between cranial elements, the morphological distinction of TMP 1972.027.0001 from other Belly River Group pachycephalosaurians was tested with bivariate and multivariate morphometric analyses. TMP 1972.027.0001 is morphologically and histologically consistent as an end-stage semaphorant of *Stegoceras validum*. Furthermore, we find no taxonomically significant morphometric distinctions between *Gravitholus albertae*, *Hanssuesia sternbergi*, and *Stegoceras validum*, and propose the former two are subjective junior synonyms of the latter. Large frontoparietals of *Stegoceras validum* are morphologically most disparate in frontonasal boss thickness. Pathologies consistent with intraspecific cranial combat appear restricted to frontoparietal domes with proportionally taller frontonasal bosses. This suggests that the high degree of intraspecific variation in frontonasal boss thickness represents intersexual variation, rather than interspecific variation. *Foraminacephale brevis* and *Stegoceras validum* are the only named pachycephalosaurids recognised in the Dinosaur Park Formation. The stratigraphic and temporal range of *Stegoceras validum* is extended into the underlying Oldman Formation. Pachycephalosaurid diversity in the Campanian is reduced as a result of these revised taxonomic hypotheses. A revised phylogenetic character matrix, recognising taxonomic synonymies and ontogenetically dependent character states results in a largely unresolved Pachycephalosauria.

INTRODUCTION

Pachycephalosauridae is the most recent common ancestor of *Pachycephalosaurus wyomingensis* and *Stegoceras validum* and all of its descendants (so long as *Heterodontosaurus tucki* is not the common ancestor or a descendant; Madiza et al. 2021). They were a Late Cretaceous clade of thick-, often dome-headed, small to medium sized ornithischian dinosaurs. Like most small bodied dinosaurs, taphonomic processes have disproportionately limited the preservation potential of their skeletal remains (Brown et al. 2013a; Evans et al. 2013). However, their characteristic thickened skull roof elements are overrepresented compared to the rest of the skeleton (Brown et al. 2013b). These elements are often diagnostic at the species level (Sullivan 2003; Evans et al. 2013). Several pachycephalosaurid species are solely known

Published February 18, 2023
*corresponding author. submitted August 23, 2022; revisions received January 24, 2023; accepted January 25, 2023. Handling editor: Robert Holmes. DOI 10.18435/vamp29388

from a single cranial element of a single individual (e.g., *Alaskacephale gangloffi*, Sullivan 2006; *Sinocephale bexelli*, Evans et al. 2021), or are solely known from the fused and domed frontals and parietals (frontoparietal dome) of multiple individuals (e.g., *Acrotholus audeti*, Evans et al. 2013).

Of the hundreds of pachycephalosaurid specimens recovered from the Upper Cretaceous Belly River Group (Alberta, Canada), none have been more contentious than the partial skull roof TMP 1972.027.0001, the holotype and only specimen of *Gravitholus albertae* (Table 1). Extensive cranial fusion has prevented a thorough identification and description of incorporated elements, which have ranged from designating the specimen as a fused frontoparietal representing a distinct genus and species (Wall and Galton 1979) to an incomplete skull roof of an indeterminate pachycephalosaurid (Sullivan 2003).

Wall and Galton (1979) described TMP 1972.027.0001 as a frontoparietal dome (fused frontals and parietals; Maryańska et al. 2004). They erected it as the holotype of a new taxon *Gravitholus albertae*, diagnosed as possessing extreme dome width and thickness, a large depression and associated pits on the parietal, a relatively small braincase, and absence of node-like ornamentation. Wall and Galton (1979) incompletely described the type locality and horizon of *Gravitholus albertae*. They reported TMP 1972.027.0001 was donated to the then Provincial Museum of Alberta by Ted Malach, that it was collected from the Oldman Formation (prior to the recognition of the Dinosaur Park Formation; Eberth and Hamblin 1993) near the Jenner Ferry in Alberta, Canada (latitude and longitude coordinates were reported). However, the reported coordinates are 9 km south of the modern Jenner Bridge, and ~6 km from the nearest bedrock outcrop. Sullivan (2003) reported a personal communication from Dr. David Eberth (TMP) confirmed that TMP 1972.027.0001 came from the Oldman Formation, not the Dinosaur Park Formation.

Validity of *Gravitholus albertae* was supported in subsequent publications (e.g., Sues and Galton 1987). Chapman et al. (1981) performed a Principal Component Analysis on various linear measurements of North American pachycephalosaurid domes. They recovered *Gravitholas albertae* separated from a cluster of *Stegoceras* (which then included specimens currently referred to *Colepiocephale lambei*, *Foraminacephale brevis*, *Hanssuesia sternbergi*, *Sphaerotholus buchholtzae*, *Sphaerotholus edmontonensis* and *Stegoceras validum*; Schott and Evans 2017; Woodruff et al. 2021). However, the measurements used in that analysis were not based on homologous landmarks (Goodwin, 1990). Giffin (1989a) reported braincase (endocranial) measurements for TMP 1972.027.0001 and supported Wall and Galton's (1979) claim that it had a relatively small endocast compared to other pachycephalosaurid specimens (namely CMN 138 and UALVP 8501; currently regarded as *Stegoceras validum* and *Foraminacephale brevis*, respectively; Schott and Evans 2017).

Table 1. Taxonomic history of TMP 1972.027.0001.

Study	Taxonomic referral
Wall and Galton (1979) Chapman et al. (1981) Sues and Galton (1987) Giffin (1989a) Maryańska (1990)	*Gravitholus albertae*
Williamson and Carr (2002)	*Stegoceras* sp.
Sullivan (2003)	Pachycephalosauridae indet.; similar to *Hanssuesia sternbergi*
Maryańska et al. (2004)	*Gravitholus albertae*
Sullivan (2006)	Pachycephalosauridae indet. similar to *Hanssuesia sternbergi*
Lehman (2010) Longrich et al. (2010)	*Gravitholus albertae*
Jasinski and Sullivan (2011)	Pachycephalosauridae indet.
Peterson et al. (2013)	*Gravitholus albertae*

Maryańska (1990) suggested the dorsal depression on the parietal of TMP 1972.027.0001 is pathologic, now regarded as an instance of post-traumatic infection (Peterson et al., 2013). Sullivan (2000) recognised that TMP 1972.027.0001 was not solely a frontoparietal (as described by Wall and Galton 1979) and suggested it included both fused postorbital + postfrontals and parts of both supraorbital IIs. He suggested that these peripheral elements were not fully incorporated into the dome, resulting in an apparently posteriorly wide frontoparietal. He stated (without reporting measurements) that TMP 1972.027.0001 is similar in size to the holotypes of *Colepiocephale lambei* and *Hanssuesia sternbergi* (CMN 8818 and CMN 8817 respectively, at that time considered specimens of *Stegoceras*). Despite recognising that the description and diagnosis presented by Wall and Galton (1979) for *Gravitholus albertae* were incomplete, Sullivan (2000) did not reject the taxon, but suggested it was similar to *Stegoceras sternbergi* (currently *Hanssuesia sternbergi*).

Williamson and Carr (2002) hypothesised TMP 1972.027.0001 was referable to *Stegoceras* sp. (at the time, *Stegoceras* included what would become *Colepiocephale*

lambei, *Foraminacephale brevis*, *Hanssuesia sternbergi*, and *Stegoceras validum*) and tested this by including TMP 1972.027.0001 in a specimen level pachycephalosaurian cladistic analysis. TMP 1972.027.0001 was recovered in a polytomy that included (what would later be named) *Colepiocephale lambei, Hanssuesia sternbergi*, and *Stegoceras validum*. TMP 1972.027.0001 and *Stegoceras* "unambiguously" shared grooved frontals, a pear-shaped dome, a tall and convex frontonasal boss, and a posterior dome margin perpendicular to a parietosquamosal shelf rather than forming a down-turned parietal. They concluded that *Gravitholus albertae* is nomen dubium and that TMP 1972.027.0001 represented an adult *Stegoceras* sp.

Sullivan (2003) elaborated on the incomplete description and diagnosis provided by Wall and Galton (1979). Sullivan identified both postorbitals and a right posterior supraorbital, then speculated on the preservation of the right anterior supraorbital (palpebral) and prefrontal. Sullivan (2003) argued that dome size was a poor defining character, and that the parietal depression was an artifact of pathology or weathering (in part citing Maryańska 1990). Sullivan (2003) regarded the endocranial cavity of TMP 1972.027.0001 as similar in size to specimens of *Hanssuesia sternbergi* (without providing measurements or specimen numbers). Sullivan observed TMP 1972.027.0001 shared a lack of dome incorporated peripheral elements (postorbital, posterior supraorbital, and palpebral (anterior supraorbital)) with *Colepiocephale lambei*, and a broad frontonasal boss with *Hanssuesia sternbergi*. He interpreted that there was a posteriorly directed extension of the parietals, uninflated anterolateral regions of the frontal, and that it lacked a parietosquamosal shelf. He noted minor ornamentation on the posteromedial extension of the parietal. Sullivan (2003) agreed with Williamson and Carr (2002) in regarding *Gravitholus albertae* as a nomen dubium, but considered TMP 1972.027.0001 as Pachycephalosauridae indet., although noted its similarity to *Hanssuesia sternbergi*.

Sullivan (2006) and Jasinski and Sullivan (2011) followed Sullivan's (2003) referral of TMP 1972.027.0001 without adding additional comments. However, some studies continue to consider *Gravitholus albertae* valid (Lehman 2010; Longrich et al. 2010; Peterson et al. 2013). Schott and Evans (2017) excluded TMP 1972.027.0001 when discussing pachycephalosaurid diversity in the Belly River Group due to the fusion of cranial elements. This precluded identifying the homologous landmarks necessary for morphometric analysis (pers. comm. David Evans ROM 2020).

The goal of this study is to resolve the anatomical and taxonomic problems posed by TMP 1972.027.0001. We applied synchrotron radiation micro computed tomography (SμCT) imaging to identify the fused cranial sutures within TMP 1972.027.0001 (which appear to be heavily fused, Sullivan 2003). This allowed us to provide a detailed description of this specimen. Identification of homologous frontoparietal landmarks from these images enables us to test its distinction from other Belly River Group pachycephalosaurians through bivariate and multivariate morphometric analyses of frontoparietal measurements (e.g., Schott and Evans 2017). Specifically, we focused on its possible synonyms with *Hanssuesia sternbergi* or *Stegoceras validum*. Resolving the taxonomic identity of TMP 1972.027.0001 will refine pachycephalosaurian faunal change through the Belly River Group, and refine patterns of pachycephalosaurian diversity and evolution.

MATERIALS AND METHODS

Institutional Abbreviations

AMNH, American Museum of Natural History, New York City, New York, United States of America; BMNH, Natural History Museum, London, United Kingdom; CMN, Canadian Museum of Nature, Ottawa, Ontario, Canada; MPC, Paleontological and Geological Center of the Mongolian Academy of Sciences, Ulaan Baatar, Mongolia; NMMNH, New Mexico Museum of Natural History and Science, Albuquerque, New Mexico, United States of America; ROM, Royal Ontario Museum, Toronto, Ontario, Canada; TMP, Royal Tyrrell Museum of Palaeontology, Drumheller, Alberta, Canada; UALVP, University of Alberta Laboratory of Vertebrate Palaeontology, Edmonton, Alberta, Canada; UCMP, University of California Museum of Paleontology, Berkeley, California, United States of America; UCMZ(VP), University of Calgary Museum of Zoology (Vertebrate Palaeontology), Calgary, Alberta, Canada; UWBM, University of Washington Burke Museum, Seattle, Washington, United States of America.

SμCT Imaging and Segmentation

TMP 1972.027.0001 was photographed with a Canon T4i rebel camera (Fig. 1). Photographs were touched up using Adobe Lightroom Classic (such as brightness and white balance corrections). TMP 1972.027.0001 was additionally scanned using a LMI Technologies 3D scanner. Models were created in FlexScan 3D (Fig. 2), then imported into Geomagic Design X for imaging.

TMP 1972.027.0001 was subjected to SμCT imaging at Canada Light Source at the University of Saskatchewan in Saskatoon, Canada. Scanning was performed on the BMIT 05ID-2 beamline at 80 KeV with a Wiggler field of 3.8T and 3.0 mm filters of aluminum and copper respectively (mounted at an angle to the beam; actual transverse distance of 3.31 mm). Images were captured

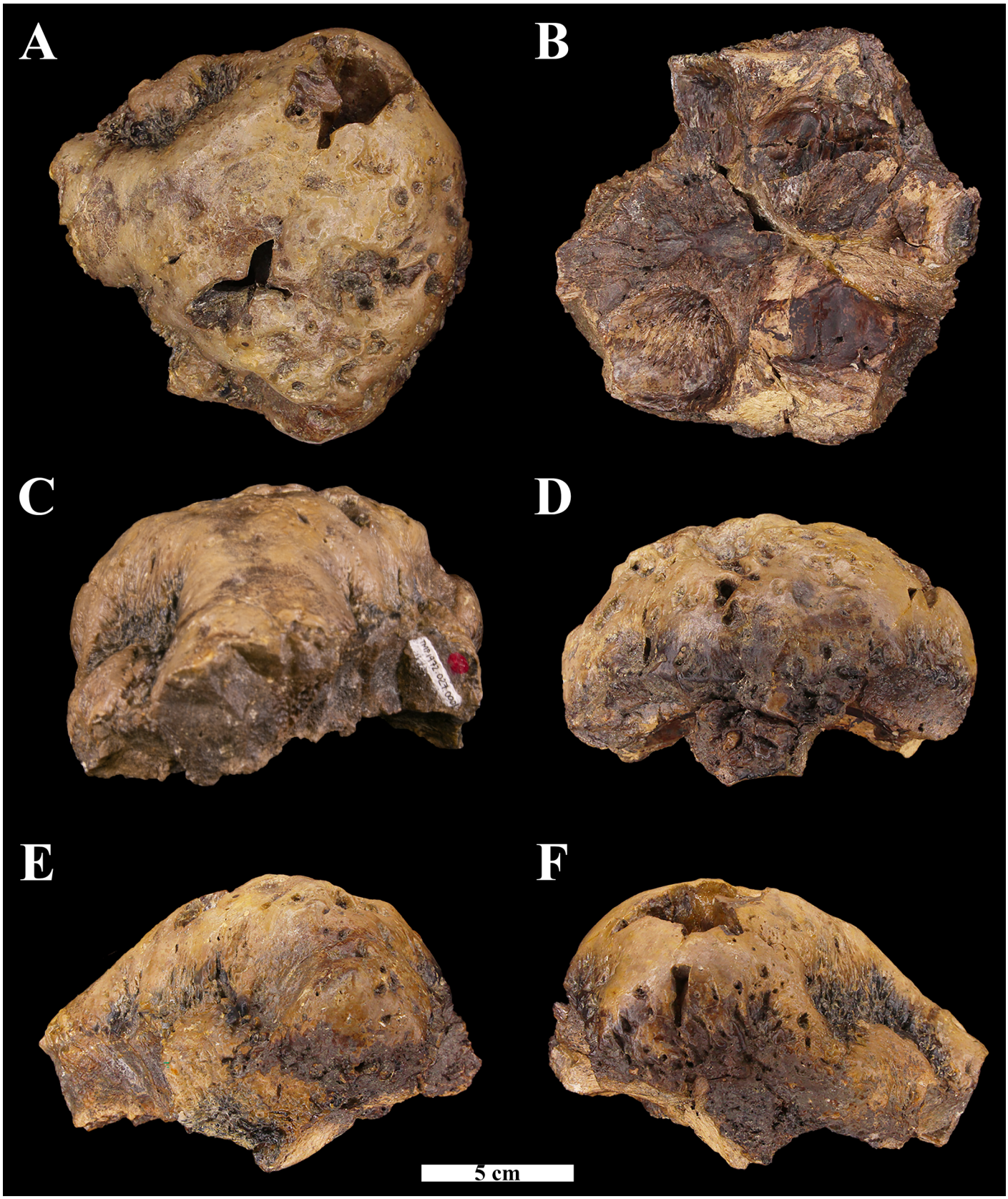

Figure 1. TMP 1972.027.0001, the holotype of "*Gravitholus albertae*" Wall and Galton 1979. Photographs of the skull roof in dorsal (A), ventral (B), anterior (C), posterior (D), left lateral (E), and right lateral (F) views.

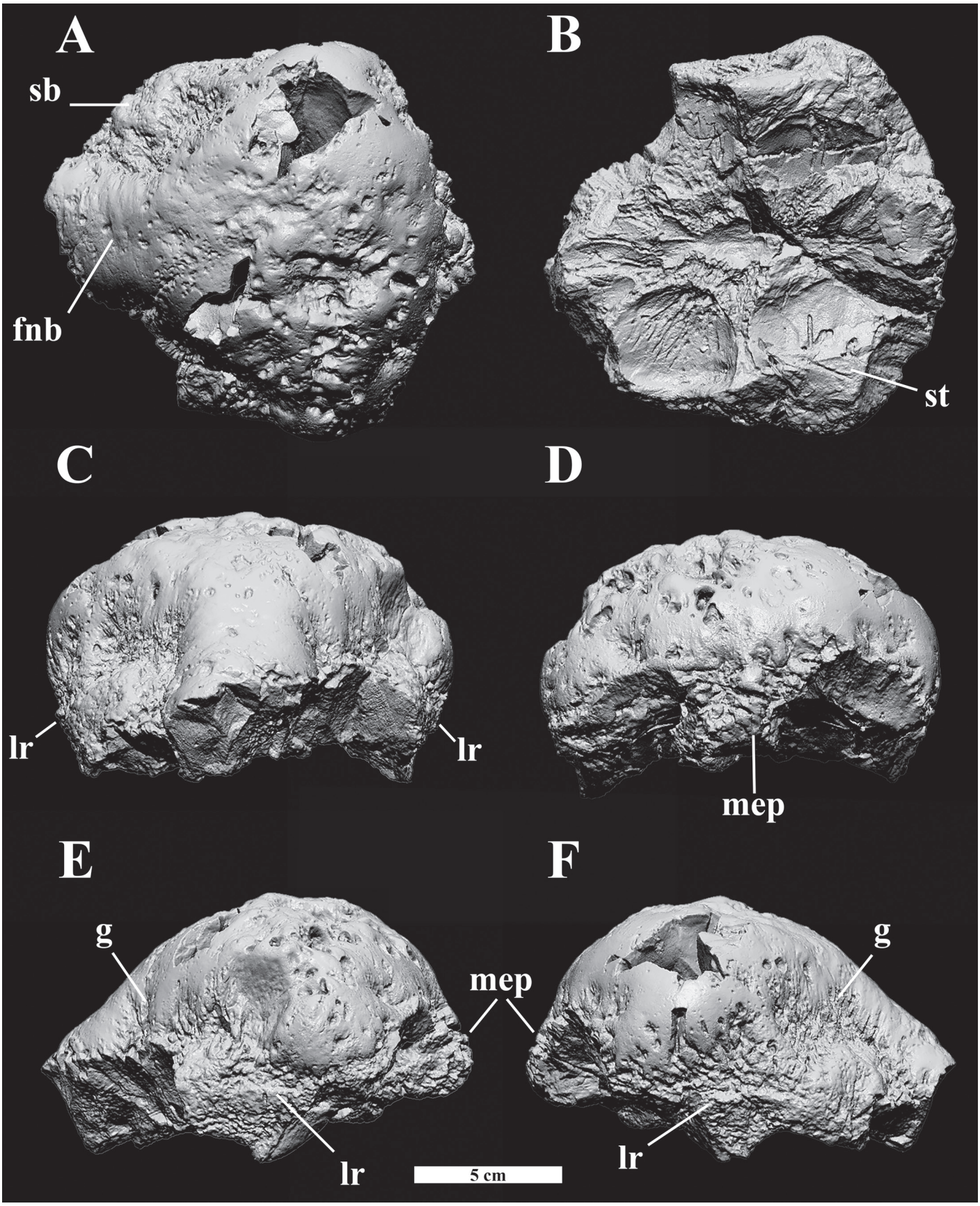

Figure 2. Orthographic projections of TMP 1972.027.0001. Laser 3-D scan images in dorsal (A), ventral (B), anterior (C), posterior (D), left lateral (E), and right lateral (F) views. Abbreviations: fnb, frontonasal boss; g, groove; lr, lateral ridge; mep, medial extension of the parietal; sb, supraorbital boss; st, groove for the squamosal tongue.

with a DALSA Shad-o-box detector (115 mm by 65 mm field of view; pixel size = 50 μm) with 100 ms exposure. Three thousand projection images were captured over a 180º rotation per vertical step. Seventeen vertical steps were performed with 1 mm overlap between adjacent steps. Both high energy photons and the highest possible photon flux were required to obtain adequate transmission because TMP 1972.027.0001 is highly x-ray absorbent. A combination of glass microspheres (packed around TMP 1972.027.0001 within a 150 mm diameter PVC tube) and an aluminum U-shaped profiler (the "U" shape matched the dimensions of the PVC tube) were used to normalize absorption and prevent detector oversaturation. This also required the use of a D-shaped absorber when collecting flat images. The combined absorption of the D-shaped absorber and the U-shaped profiler was exactly the combined absorption of the U-shaped profiler and the PVC tube filled with glass microspheres. The amount of available glass microspheres was insufficient to completely immerse TMP 1972.027.0001. Several aluminum bars were used to fill additional space. However, this was still insufficient to immerse the entire specimen. The most posterior portion of TMP 1972.027.0001 was left exposed and was not scanned. The horizontal field of view of the detector was too small to capture the entire width of TMP 1972.027.0001. Therefore, it was positioned such that the more complete (right) side fit in the field of view. Cranial elements of TMP 1972.027.0001 were then manually segmented in Dragonfly v.4.0 (Object Research Systems (ORS) INC, Montreal, Canada, 2020; software available at http://www.theobjects.com/dragonfly). The ROI Painter 3D mode was used in combination with a range threshold to segment each individual element. The slab average and slab minimum intensity projection functions were occasionally used to better visualise sutural contacts (Fig. 3B', D', E'). Some contacts were open ventrally and internally, but fused dorsally. In these cases, segmentation continued along the most dorsal orientation of the sutures until the dorsal surface. The frontoparietal of ROM 53555 was also segmented from CT images (see Schott et al. 2011 for imaging methods) to increase the sample of large *Stegoceras validum* in morphometric analyses performed in this study. Regions of interest (ROIs) created in Dragonfly v4.0 were converted into mesh objects, then imported into Geomagic Design X and underwent the fix normal and smooth functions. These and a segmented frontoparietal model of UALVP 2 (http://n2t.net/ark:/87602/m4/M43121) were measured and imaged in Geomagic Design X.

Void Density

TMP 1972.027.0001 has previously been proposed to be a mature individual of *Stegoceras* sp. (Williamson and Carr, 2002). Goodwin and Horner (2004) suggested a test of maturity by histologically examining a multitaxic ontogenetic series of pachycephalosaurid crania. They proposed the relative amount of vasculature in the frontoparietal decreased through ontogeny. Several studies have replicated these results among pachycephalosaurid species using non-destructive high resolution computed tomography (HRCT) images of frontoparietals (*Foraminacephale brevis*, Schott and Evans 2017; *Sphaerotholus buchholtzae* Woodruff et al. 2021; and *Stegoceras validum*, Schott et al. 2011), although Nirody et al. (2022) demonstrated that vascular space initially increases from flatheaded to partially domed *Stegoceras validum*. HRCT images have also been used to assess the ontogenetic stages of individual pachycephalosaurid specimens (TMP 2008.045.0001, *Acrotholus audeti*, Evans et al. 2013; ROM 53672, *Pachycephalosaurus wyomingensis*, Goodwin and Evans 2016; and NMMNH P-33898, "*Stegoceras novomexicanum*", Williamson and Brusatte 2016).

To test histologically the maturity of TMP 1972.027.0001, pixels from SμCT slices were binarized based on a brightness threshold to quantify the proportion of void space in its frontoparietal dome, following the methods outlined by Schott et al. (2011). Pixels with brightness values below the threshold were made black, whereas pixels with brightness values above the threshold were made white. Void space (black pixels in binarized images) was used as a proxy for vascular space, although some void space would have contained nervous tissues and lymphatic tissues (Starck and Chinsamy 2002). A standard coronal plane at the contact between the posterior supraorbital and postorbital was binarized. Unfortunately, TMP 1972.027.0001 was scanned at a slight off angle, so the SμCT slices are ~7º off from a true coronal plane (see Evans et al. 2013 for issues with resampling). Slices were imported into imageJ 1.53e, and binarized using the Huang threshold method. A rectangular region of interest was specified for calculating relative void space. Landmarks for the corners of this region were positioned medioventrally by the interfrontal contact along the endocavity, lateroventrally at the frontal-posterior supraorbital-postorbital contact, and dorsolaterally along the dorsal margin of the frontal.

Previous studies using single slice binarization thresholding have not addressed slice thickness and slice resolution when interpreting relative void space from HRCT slices of pachycephalosaurid frontoparietals, which can influence the ability to adequate binarize pixels (Nirody et al. 2022). Scanning resolutions of previously binarized pachycephalosaurid frontoparietals vary from 250 μm (ROM 53555; Schott et al. 2011) to 36.22 μm (TMP 1985.043.0068; Schott and Evans 2017). The slice thickness and resolution of the SμCT slices of TMP 1972.027.0001, are thinner and higher (respectively) than Schott et al. (2011)

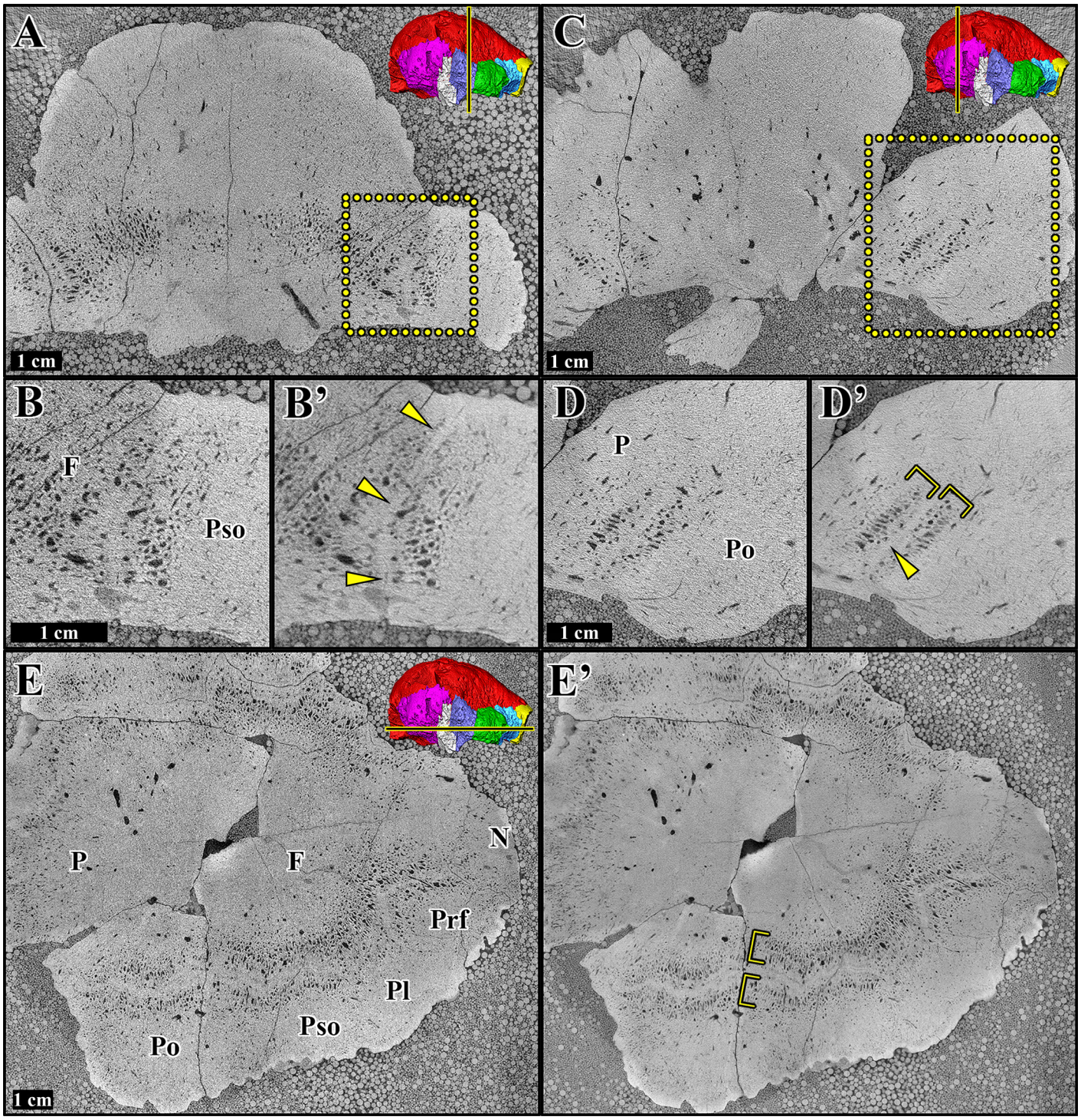

Figure 3. SμCT images of TMP 1972.027.0001; A) Coronal plane across the frontal-posterior supraorbital sutures in posterior view. B) Enlarged area around the right frontal-posterior supraorbital suture. B') Same area, averaged from five 50 μm thick slices. Arrows identify the frontal-posterior supraorbital suture. C) Coronal plane across the parietal-postorbital sutures in posterior view. D) Enlarged area around the right parietal-postorbital suture. D') Same area, averaged from five 50 μm thick slices. Arrow identifies the parietal-postorbital suture. Brackets identify the vascularized area adjacent to the suture. E) Horizontal plane across the lower half of the peripheral element contacts in dorsal view. E') Same area, averaged from five 50 μm thick slices. Brackets identify the vascularized area adjacent to the sutures.

HRCT slices of the ontogenetic series of *Stegoceras validum*, particularly when compared to the similarly sized skull of ROM 53555 (250 μm). Thus, the binarized SμCT slices are not directly comparable to the results of Schott et al. (2011). The slice parameters of this study are nearly identical to those used to assess the two smaller *Stegoceras validum* specimens presented in Nirody et al. (2022), and are appropriate for direct comparison with their results.

To make the SμCT images TMP 1972.027.0001 more comparable to the HRCT images of ROM 53555, a combination of averaging slices and size (resolution) reduction were performed. First, the proceeding and following two images (five images total) were averaged together using the default settings of the z-project function in ImageJ 1.53e. As each image (slice) was 50 μm thick, averaging five together approximated the slice thickness of ROM 53555 (250 μm; Schott et al. 2011). Second, the original SμCT image of TMP 1972.027.0001 was reduced from a size of 2304 by 2304 pixels to 461 by 461 pixels, to approximate the pixel size of the HRCT slices of ROM 53555. Finally, the same size reduction was performed on the averaged slice image of TMP 1972.027.0001. Separately performing slice averaging and size reduction allowed respective examination of their effects on calculating void density.

Morphometrics

Specimens and measurements: Linear measurements from 136 pachycephalosaurian frontoparietals were used in morphometric analyses (Supplemental Data 1). Most of these measurements were obtained from Schott and Evans (2017). A total of 57 newly measured specimens were examined, including TMP 1972.027.0001, seven *Colepiocephale lambei*, 23 *Foraminacephale brevis*, three *Hanssuesia sternbergi*, and 23 *Stegoceras validum*, from the AMNH, ROM, TMP, and UALVP collections. Linear measurements reported from some specimens, including CMN 8817 (the holotype of *Hanssuesia sternbergi*; Brown and Schlaikjer 1943), appeared erroneous and were re-measured (Supplemental Data 2). Linear measurements were taken using a traditional digital caliper, or a proportional caliper when the traditional caliper could not be fit to the landmarks (frontoparietal thickness, heights from articulated specimens). Some measurements were estimated based on published photographs (e.g., AMNH 5388; Brown and Schlaikjer 1943). These measurements are based on homologous landmarks at the contacts between cranial elements (Fig. 4), initially proposed by Goodwin (1990). Additionally, endocranial lengths and widths were measured from the anterior extent of the olfactory bulbs to the pit for the supraoccipital cartilage (L:olf/soc) and along the frontoparietal suture (cerebrum width; W:cer) respectively (Giffin 1989a).

Schott et al. (2011) and Schott and Evans (2017) doubled the preserved widths of isolated frontals to obtain the width across both frontals. However, width measurements in those studies were not taken from numerous available fused frontoparietals that only preserved one of the bilateral width landmarks. These are as complete as isolated frontals, for which width measurements were reported.

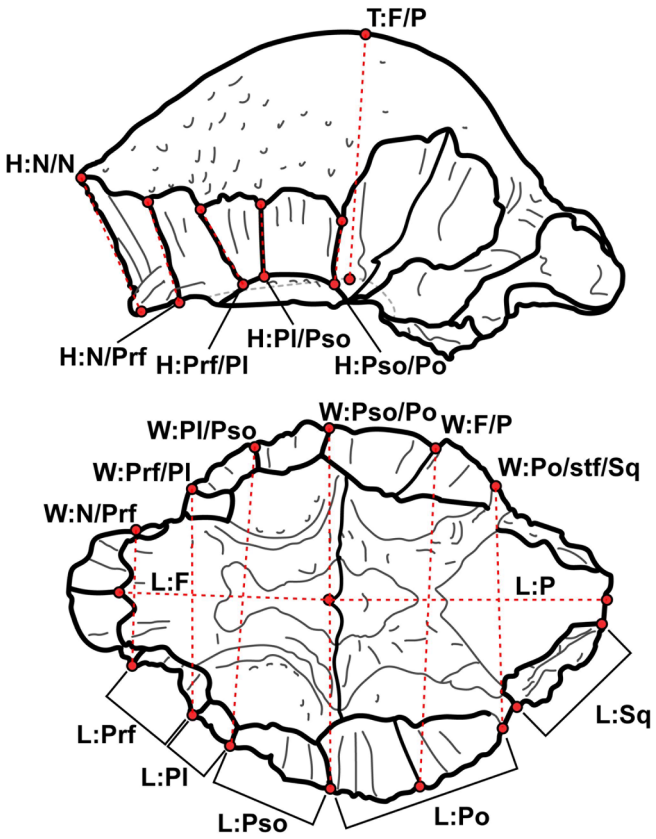

Figure 4. Linear measurements used in morphometric analyses. Line drawings based on UALVP 2. Abbreviations: H:N/N, height at the nasal/nasal contact; H:N/Prf, height at the nasal/prefrontal contact; H:Prf/Pl, height at the prefrontal/palpebral contact; H:Pl/Pso, height at the palpebral/posterior supraorbital contact; H:Pso/Po, height at the posterior supraorbital/postorbital contact; T:F/P, frontoparietal thickness; W:N/Prf, dorsal width at the nasal/prefrontal contact; W:Prf/Pl, dorsal width at the prefrontal/palpebral contact; W:Pl/Pso, dorsal width at the palpebral/posterior supraorbital contact; W:Pso/Po, dorsal width at the posterior supraorbital/ postorbital contact; W:F/P, dorsal width at the frontal/parietal contact. W:Po/stf/Sq, dorsal width at the postorbital/squamosal contact (or at posterior extent of postorbital if the supratemporal fenestra is present; L:F, ventral length of the frontal; L:P, ventral length of the parietal; L:Prf, dorsal length of the prefrontal contact; L:Pl, dorsal length of the palpebral contact; L:Pso, dorsal length of the posterior supraorbital contact; L:Po, dorsal length of the postorbital; L:Sq, dorsal length of the squamosal contact.

Frontoparietal width measurements were estimated from several previously reported specimens, including fused ones that preserved either the left or the right landmark.

Previous analyses of frontoparietal linear measurements have not addressed bilateral measurements – the heights and lengths of the peripheral element contacts with the frontoparietal – but instead reported single measurements when two could have been measured (left and right; Schott et al. 2011; Evans et al. 2013; Williamson and Brusatte 2016; Schott and Evans 2017; Woodruff et al. 2021). In this study, left and right measurements (when preserved) were measured from new specimens, and some previously studied specimens were re-measured. Left and right measurements, when both are preserved, were then averaged. These averages were used in morphometric analyses.

Identities of TMP 2000.026.0001 and TMP 2017.012.0019: TMP 2000.026.0001 has been inconsistently referred to as *Hanssuesia sternbergi* and *Stegoceras validum*. Sullivan (2003) figured and discussed the specimen as *Stegoceras validum*, but included TMP 2000.026.0001 in the lists for both *Stegoceras validum* and *Hanssuesia sternbergi*. Schott et al. (2011) regarded TMP 2000.026.0001 as *Stegoceras validum*. Evans et al. (2013) reported TMP 2000.026.0001 as *Hanssuesia sternbergi*. Finally, Schott and Evans (2017) referred TMP 2000.026.0001 to *Stegoceras validum*.

The domes of both TMP 2000.026.0001 and TMP 2017.012.0019 appear to preserve depressed (or shallow) parietal portions of the dome compared to the frontals (Figs. S1, S2), and the latter preserves an apparent broad frontonasal boss. Both features were considered diagnostic of *Hanssuesia sternbergi* (Sullivan 2003). Although TMP 2017.012.0019 has not been referred to this taxon in the literature, it is consistent with the diagnosis provided by Sullivan (2003). Therefore, prior to any analysis, TMP 2000.026.0001 and TMP 2017.012.0019 were included in a cohort of specimens historically referred to as *Hanssuesia sternbergi*.

Bivariate analyses: All bivariate regressions in this study were Reduced Major Axis (RMA) regressions performed on $\log_{10}$-transformed linear measurements in PAST 4.10 (Hammer et al. 2001). RMA regressions account for error in both the y and x variables (appropriate given the inclusion of estimated linear measurements in this dataset) and is an appropriate method to interpret patterns of allometry (Smith 2009). Additionally, regressions examining independent variables (multiple elements) with no apparent association preclude these variables from examination in Ordinary Least Squares regression, which infers a correlation between an independent and dependent variable (Kilmer and Rodrigues 2017). Scaling was considered positively allometric when the lower bound of the 95% confidence interval around the slope was above a value of 1, and negatively allometric when the upper bound was below 1. RMA regressions were performed for each individual Belly River Group pachycephalosaurian taxon, and on the total sample.

Diagnostic small endocranium - *Gravitholus albertae*: RMA regressions were performed to test if TMP 1972.027.0001 has a uniquely small endocranium amongst Belly River Group pachycephalosaurians. In this study, we attempt to correlate both endocranial length (L:olf/soc) and endocranial width (W:cer) with two standard frontoparietal size measurements, the dorsal width across the frontoparietal contact (W:F/P) and the length of the frontal (L:F). L:F was chosen instead of frontoparietal length (L:FP) due to the low number of complete parietals, particularly amongst *Colepiocephale lambei*. When TMP 1972.027.0001 was recovered with the greatest negative residual amongst Belly River Group pachycephalosaurians, a Grubbs test was performed in PAST 4.10 to determine if TMP 1972.027.0001's residual was an outlier amongst the total sample.

Diagnostic wide frontoparietals and inflated supraorbital lobes - *Hanssuesia sternbergi*: Most of the diagnosis for *Hanssuesia sternbergi* (Sullivan 2003) is constructed on proportional relationships of the frontoparietal dome and can therefore be tested using bivariate analyses. This can also be used to test referral of TMP 1972.027.0001 to *Hanssuesia sternbergi*, and the morphological distinction of *Hanssuesia sternbergi* from the other Belly River Group pachycephalosaurian taxa (*Colepiocephale lambei*, *Foraminacephale brevis*, and *Stegoceras validum*). The purported diagnostic width was tested using RMA regressions comparing frontoparietal widths to frontal length (L:F). Frontoparietal length (L:FP) may be a more appropriate baseline for comparing frontoparietal widths, rather than a portion of that length (L:F). However, only two specimens of *Hanssuesia sternbergi* preserve complete parietals, compared to six that preserve complete frontal lengths. Additionally, five of the six frontoparietal width measurements occur on the frontals; therefore, frontal length is an appropriate measurement to assess relative frontoparietal width. RMA regressions were also used to assess the diagnostic inflated supraorbital lobes of *Hanssusia sternbergi* by comparing the peripheral supraorbital heights (H:Prf/Pl, H:Pl/Pso, H:Pso/Po) to frontoparietal thickness (T:F/P).

Principal Component Analysis: Principal Component Analysis (PCA) was used to visualize the morphometric distinctness of the frontoparietal of TMP 1972.027.0001 from the other Belly River Group pachycephalosaurian taxa. These were performed on 43 frontoparietal specimens (TMP 1972.027.0001, seven *Colepiocephale lambei*, 11 *Foraminacephale brevis*, five *Hanssuesia sternbergi*, 19 *Stegoceras validum*; Supplemental Data 1) from 16 preserved linear measurements (excluding L:cer, L:FP, L:olf/

soc, L:P, L:Prf, L:Sq due to low sample sizes; Fig. 4) in PAST 4.10 using a variance-covariance matrix. Four PCA iterations were performed using different data standardisation methods on these 43 frontoparietal specimens. The first iteration $\log_{10}$-transformed each linear measurement, similar to previous PCA of pachycephalosaurian frontoparietals (Evans et al. 2013; Williamson and Brusatte 2016; Schott and Evans 2017). The second PCA iteration was performed on the original, non-transformed linear measurements. In both of these analyses, a standard size variable (dorsal width across the frontal-parietal contact; W:F/P) was excluded, and used to test if the PC scores of the entire dataset and of individual taxa correlated with frontoparietal size (as in Schott and Evans 2017). PC scores from the $\log_{10}$-transformed PCA iteration were regressed (using RMA regressions) to $\log_{10}$-transformed W:F/P, whereas PC scores from the non-transformed PCA iteration were regressed on non-transformed W:F/P (mm). The final two PCA iterations were performed with size standardized measurements, with each variable divided by either frontal length (L:F) or W:F/P (Supplemental Data 1). Given that six of the 16 linear measurements are width measurements, size standardising based on the length of the frontal may inflate the effects of width measurements, such as the purported diagnostic frontoparietal width of *Hanssuesia sternbergi* (Sullivan 2003).

The initial PCA iterations did not recover any size-independent distinction between TMP 1972.027.0001, *Hanssuesia sternbergi*, and *Stegoceras validum*. A second round of the four PCA iterations were performed on this reduced sample (n = 25), to explore any potential subtle distinction between these specimens.

Analyses of frontoparietal dimorphism: PC 2 of the $\log_{10}$-transformed, non-transformed, and frontal length (L:F) proportionate PCA iterations of *Hanssuesia sternbergi*, *Stegoceras validum*, and TMP 1972.027.0001 appeared to separate large frontoparietal specimens (W:F/P > 80 mm) into two clusters, but were not separated based on previous taxonomic referrals. Following taxonomic revisions, these clusters were hypothesised to represent mature dimorphs of *Stegoceras validum*. Dimorphism was tested following the methods outlined by Mallon (2017). Normalities of the distribution of PC 2 scores of large presumed mature individuals (W:F/P > 80 mm; see Fig S3 for associated gap in the distribution of W:F/P around 80mm; Schott et al. 2011) were tested with the Shapiro-Wilk and Anderson-Darling tests (performed in PAST 4.10). A Hartigan's Dip test, with 10,000 iterations, was used to test for unimodality (performed in R v1.4.1103, using the diptest package). Mixture analyses were performed in PAST 4.10 to determine if the data (PC 2 scores) were better fit to a single (unimodal) or two normal distributions (bimodal). Akaike information criterion (AIC) values were used to determine the best-fitting distribution. Lower AIC values indicate a better fitting model, with differences of at least 2 indicating a significantly better-fitting model. A Jenks Natural Breaks Optimization function was additionally performed to assess the presence of a natural break in the distributions of PC 2 scores. These were performed in R v1.4.1103 using the GmAMISC package, and tested for a single natural break (two groups; n = 2). A goodness of variance fit (GVF) of 0.7 or greater was considered acceptable to identify the presence of a natural break (Powers et al. 2020).

Galton (1971) predicted that if the dome was used in intraspecific combat, there should be a high degree of intraspecific variation in dome thickness. As the purported dimorphism we observed was largely explained by frontonasal boss thickness, we hypothesised that this intraspecific variation was concurrent with intersexual variation, whereby the "thicker-bossed" sex engaged in intraspecific combat. We predicted that instances of post-traumatic pathologies consistent with intraspecific cranial combat would be restricted to "thicker-bossed" individuals. Peterson et al. (2013) observed that the frequencies of these pathologies are consistent between pachycephalosaurian species. Therefore, the occurrence of pathologies on both "thicker-bossed" and "thinner-bossed" specimens would suggest that the purported dimorphism represented distinct taxa.

To test if post-traumatic pathologies consistent with intraspecific combat (Peterson et al. 2013; Dyer et al. 2021) were restricted to "thicker-bossed" individuals (consistent with sexual dimorphism), we assessed the distribution of pathological specimens, amongst the samples used in PCA. Unequal variance between pathological and non-pathological specimens' PC 2 scores were assessed using a F test. Student's t tests assuming equal/unequal variance (depending on the results of the F test) were used to test if the average PC 2 scores of pathological specimens (CMN 9148, TMP 1972.027.0001, TMP 1979.014.0853, TMP 1992.002.0003; UALVP 8502; Peterson et al. 2013, although see Supplemental Data 2 for reinterpretation of CMN 9148) significantly differed from non-pathological specimens. Post-traumatic pathologies are not restricted to large specimens in this sample and occur in some of the smallest specimens (TMP 1992.002.0003, W:F/P = 46.07 mm). Therefore, all specimens used in these reduced taxon PCA (*Hanssuesia sternbergi*, *Stegoceras validum*, and TMP 1972.027.0001) were used to test for a difference in average PC 2 scores between pathological and non-pathological specimens.

Analyses of frontoparietal allometry: Following taxonomic revisions, frontoparietal allometry in *Stegoceras validum* was re-examined. Frontoparietal width is the

strongest statistical predictor of other frontoparietal measurements (Schott et al. 2011; Schott and Evans 2017) and was used as the standard variable (x) to assess allometry. RMA regressions were performed on $\log_{10}$-transformed linear measurements. Allometry was identified in regressions where the 95% confidence interval around the slope excluded 1 (positive if above 1, negative if below), and indistinguishable from isometry if it encompassed 1.

PHYLOGENETIC ANALYSES

Character revisions: The initial character matrix was obtained from Woodruff et al. (2021) and supplemented with the scoring of *Sinocephale bexelli* and re-assessments proposed by Evans et al. (2021). Characters were revised based on our observations and interpretations. Focus was placed on recognition of ontogenetically correlated characters and reinterpretation of taxonomic identification. We changed absence scoring in the outgroup taxa to inapplicable when dealing with characters defining derived structures such as the frontoparietal dome as well as unique ornamentation and variable peripheral elements. Additionally problematic characters were identified following Simões et al. (2017) and corrected when possible (Supplemental Data 2). Published L:Pl measurements were used to justify reassessments for Woodruff et al. (2021) character 31 (extent of the "anterior supraorbital" - frontal contact). We interpret the anterior supraorbital as homologous with the palpebral due to topological relationships with other cranial elements, and adjust our character coding/scoring accordingly. Probable ontogimorphs are also synonymized with species described for the adult stage semaphoront (e.g., *Dracorex hogwartsia* and *Stygimoloch spinifer* as ontogenetic semaphoronts of *Pachycephalosaurus*; Horner and Goodwin 2009; Goodwin and Evans 2016). We agree with Williamson and Brusatte (2016) that "*Stegoceras novomexicanum*" is not sufficiently morphologically distinct from other domed pachycephalosaurians (although see Jasinski and Sullivan 2016 responses to Williamson and Brusatte 2016 conclusions) and did not include the species in our phylogenetic analyses. Character revisions and taxonomic synonymy led to a character-taxon matrix of 52 characters and 18 terminal taxa.

Parsimony analysis: Maximum parsimony analyses were performed in TNT 1.5 (Goloboff and Catalano 2016) using an implicit enumeration (exhaustive) search. A strict consensus tree and 50% majority consensus tree were constructed from the resulting most parsimonious trees (MPTs). Additionally, an agreement subtree was created, which prunes all taxa with inconsistent positions amongst the MPTs, resulting in a reduced taxon tree that depicts identical interrelationships recovered in all MPTs.

Bayesian analysis: Bayesian analyses were performed using Mr. Bayes v 3.2.7 on CIPRES Science Gateway v 3.3. Methods follow Powers et al. (2021) with slight modifications. Instead of 50000000 generations, our dataset was set to 10000000 generations but retained a burn in phase of 0.25, discarding the first 2500000 trees. Temp = 0.01 was added and all other parameters were left the same as initially produced by Mesquite v 3.6. Two datasets were created for the Bayesian analysis, one which was left as described, and a second that included the "contype=allcompat" function. This function was included to produce a fully resolved tree to examine hypothetical sister relationships with the understanding that they would have less support than more robust clades. This approach was favoured due to the incredible phylogenetic uncertainty of many pachycephalosaurian taxa known from sparse and incomplete material. Pachycephalosaurian phylogenetics are a great example of when Bayesian analyses can be beneficial because they handle missing data and homoplastic characters more effectively than parsimony analyses (Wright and Hillis, 2014).

Both datasets were run through Mr. Bayes v 3.2.7 for 6x8 CPU hours. The analysis only took about 45 minutes, because the dataset is small. Parameters were set to use those outlined in the nexus files produced by Mesquite v 3.6. A majority rules consensus tree and a fully resolved tree were produced and posterior probabilities reported in percentages and added to their respective nodes in each tree for figures. The fully resolved tree was used to create a time calibrated tree following the methods of Powers et al. (2021). The "strap" package was used in RStudio to develop the time calibrated tree. Node age estimation was performed using the "equal" method in the "scaletree" function. The resulting tree was modified in Adobe Illustrator CS 6 to include posterior probabilities and colour code the terminal unit time intervals with their geographic location of discovery.

SYSTEMATIC PALAEONTOLOGY

DINOSAURIA Owen, 1842
ORNITHISCHIA Seeley, 1887
PACHYCEPHALOSAURIA Maryańska and Osmólska, 1974
PACHYCEPHALOSAURIDAE Sternberg, 1945
Stegoceras Lambe, 1902
Stegoceras validum Lambe, 1902

Lectotype: CMN 515, frontoparietal

Type locality: East side of the Red Deer River below the mouth of Berry Creek, Alberta, Canada.

Synonymy: *Troodon validus* Gilmore, 1924; *Troodon sternbergi* Brown and Schlaikjer 1943; *Stegoceras stern-*

bergi Sternberg 1945; *Gravitholus albertae* Wall and Galton 1979; *Stegoceras browni* Wall and Galton 1979; *Ornatotholus browni* Galton and Sues 1983; *Hanssuesia sternbergi* Sullivan 2003.

Referred Material: TMP 1972.027.0001, incomplete skull roof. See Supplemental Data 1 for additional referred material.

Emended diagnosis: Modified from Schott et al. (2011). A medium-sized pachycephalosaurid differing from all other pachycephalosaurians, where known, by possessing six or more nodes in the primary parietosquamosal node row, a row of small, keel-shaped nodes on lateral margins of postorbitals and squamosal, numerous minute tubercles on lateral and posterior sides of the postorbitals and squamosals, no ventrolateral corner node on the posterior surface of the squamosals, no nasal ornamentation, a greatly reduced maxillary-premaxillary diastema, and a pubic peduncle of the ilium that is mediolaterally compressed and platelike. Differs from all other domed pachycephalosaurians (except possibly *Colepiocephale lambei*), where known, in possessing a parietosquamosal shelf (may be fully incorporated into the dome in mature individuals), as opposed to the dome extending to the posterior margin of the skull. The palpebral and prefrontal are not incorporated into the dome, as in *Acrotholus audeti, Pachycephalosaurus wyomingensis, Prenocephale prenes,* and *Sphaerotholus* spp.

Comments: This study continues to demonstrate that *Stegoceras validum* had great morphological variability. The parietosquamosal shelf, which has been a crucial diagnostic feature, is known to decrease in relative size through ontogeny (Schott et al. 2011). Here the ontogenetic end stage of that reduction is identified in TMP 1972.027.0001, with posterior progression of the dome (reducing the parietosquamosal shelf) reaching the posterior extent of the parietal, which forms a "downturned" medial extension of the parietal. The depressed parietal of "*Hanssuesia sternbergi*" may represent either delayed inflation of the parietal, or possibly healed pathologies. Frontonasal boss thickness is highly variable amongst adult individuals, which may represent intersexual morphological variation.

RESULTS

Description

General overview: TMP 1972.027.0001 is an incomplete pachycephalosaurid skull roof with a preserved length of 130.73 mm and a maximum skull width of 133.50 mm (Figs. 1, 2). It includes a damaged frontoparietal, partial right nasal, right prefrontal, right palpebral, complete left and right posterior supraorbitals, nearly complete left and right postorbitals, and fragments of the left prefrontal and squamosal (Fig. 5). Nearly all the bones appear indistinguishably fused to each other; however, their sutures are observable in SμCT images (Fig. 3) except for the interfrontal, frontoparietal, and right posterior supraorbital-postorbital ones. Most of the dorsal surface of the specimen forms a massive "pear-shaped" cranial dome in dorsal view (narrowing anteriorly), typical of *Stegoceras validum* and *Colepiocephale lambei* (Schott et al. 2009). The cranial dome excludes the prefrontal and palpebral from the dome, which are incorporated in "derived" pachycephalosaurid domes (e.g., *Pachycephalosaurus* and *Sphaerotholus*, Evans et al. 2013).

The frontoparietal and interfrontal sutures are externally fused, although a faint trace of the frontoparietal contact is observable within the cerebellar fossa (Fig. 2B). The frontoparietal suture is unobservable in SμCT images (Fig. 3E). An internal fracture occurs where the interfrontal suture is expected (Fig. 3A, E), thus the state of internal interfrontal fusion is unknown (cracks may form along fused interfrontal sutures; Dyer et al. 2021). The peripheral elements are typically more fused with each other than any is to the frontoparietal. The nasal-prefrontal suture is an exception; it remains mostly open. This unfused contact extends through to the prefrontal–frontal suture. The prefrontal–palpebral suture is heavily fused. The entire right posterior supraorbital–postorbital suture is indistinguishably fused. The frontal–nasal and right frontoparietal–postorbital sutures are indistinguishably dorsally fused. The left squamosal appears to have been more fused to the postorbital and parietal than the right, as indicated by attached fragments of the left squamosal (particularly on the postorbital) and the clean sutural surface for the right squamosal (Figs. 1D, 2D). Otherwise, the left peripheral elements appear less fused to each other and to the frontoparietal than the right elements. The sutural surface for the left palpebral on the frontal is clean, without any remnant of the left palpebral or damage to the frontal. The same is true for most of the left sutural surface for the prefrontal. Part of the left prefrontal remains attached, although its suture with the frontal remains unfused. The left posterior supraorbital and postorbital appear to have broken and been reattached along their sutures with the frontoparietal. The most medial portion of the left posterior supraorbital–postorbital suture remains internally open, although its lateral extent was not imaged during SμCT scanning.

Nasal: TMP 1972.027.0001 preserves a fragmentary posterior portion (~ 20 mm anteroposterior) of the right nasal. The medial portion that formed the internasal suture is missing. The nasal contacts the frontal posteromedially and the prefrontal posterolaterally. The contact with the frontal is slightly anteriorly concave when viewed dorsally (Fig. 5A), so that the nasal partially surrounds the anterior boss of the frontal. The contact with the prefrontal is most-

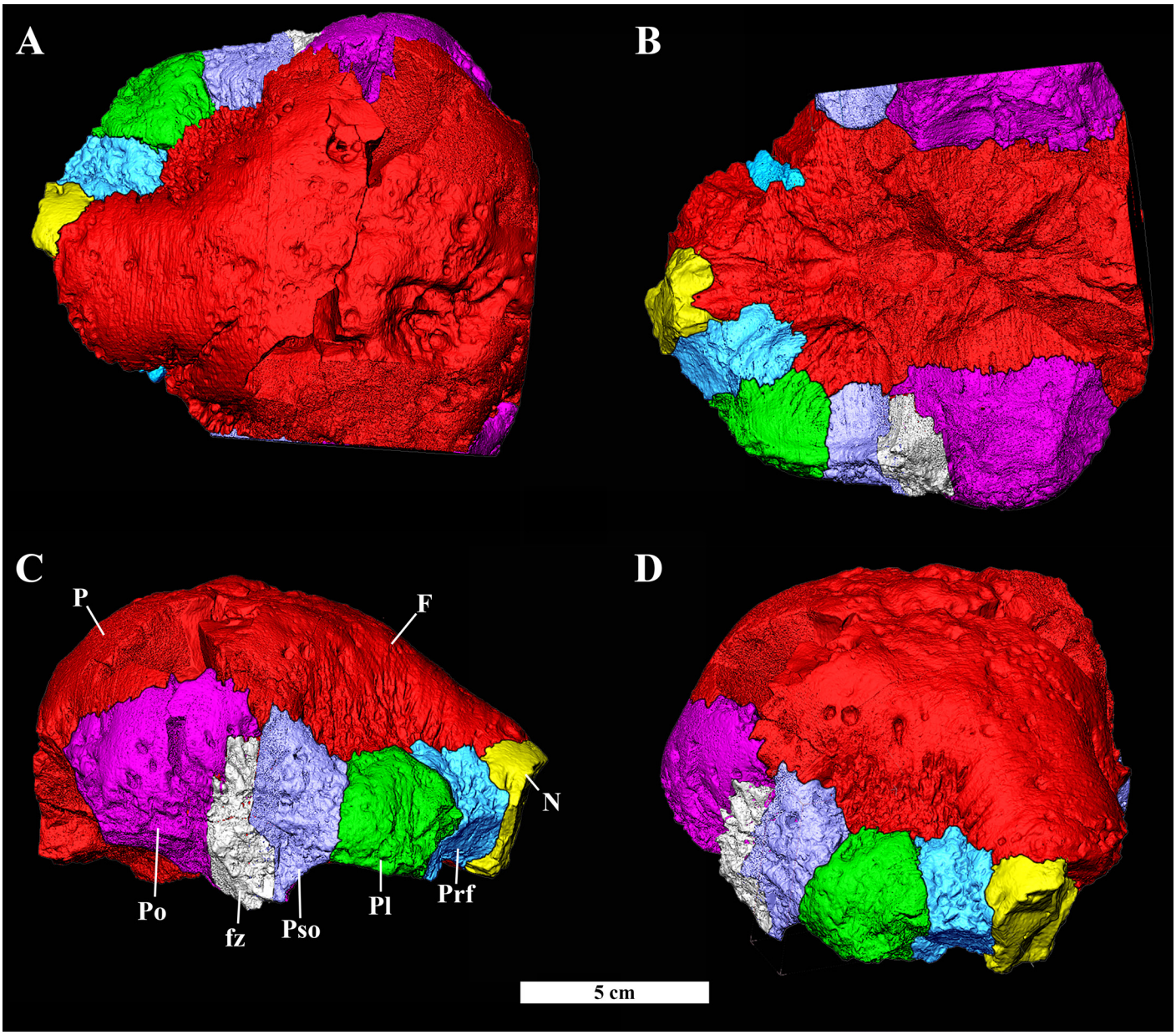

Figure 5. Segmented model of TMP 1972.027.0001. Skull roof in dorsal (A), ventral (B), right lateral (C), and right anterodorsal (oblique) views (D). Abbreviations: F, frontal; fz, fused zone containing postorbital-posterior supraorbital contact, N, nasal; P, parietal; Pl, palpebral; Prf, prefrontal; Po, postorbital; Pso, posterior supraorbital.

ly directed anterolaterally. The nasal-prefrontal contact is slightly concave on the lateral surface of the nasal, such that the dorsal portion of the nasal overhangs laterally.

The nasal is dorsoventrally thick, both sagittally (H:N/N = 35.13 mm) and laterally (H:N/Prf = 26.79 mm). It contributes to a distinct frontonasal boss. The dorsal surface is smooth, lacking the tesserate (Williamson and Carr 2002; Woodruff et al. 2021; "tuberculate", Schott et al. 2011) texture seen in *Stegoceras validum* (UALVP 2, Gilmore 1924), aside from a groove (positioned at the lateral margin of the boss) that extends anterodorsally to the prefrontal. Similar grooves occur on the dorsal surface of the frontals near the contact with the palpebral and prefrontal.

The contact area for the frontal on the nasal's ventral surface is broadly V-shaped, which corresponds to the anteroventral flange of the frontal (Fig. 6). The ventral surface of the nasal is slightly depressed, forming part of the roof of the nasal cavity. Within this surface, the nasal preserves a facet for the anteroventral projection of the frontal (Fig. 6D, E). Two posteriorly directed ridges on this facet (Fig. 6D, E) correspond to the anteroventrally directed grooves on the dorsal surface of the anteroventral projection of the frontal (Fig. 6B, C). Lateral to the facet is a short (~ 3 mm) posteriorly directed process, positioned at the ventral base of the nasal between the contacts with the frontal and prefrontal. A ventrolateral ridge extends anteriorly from this posterior projection. The

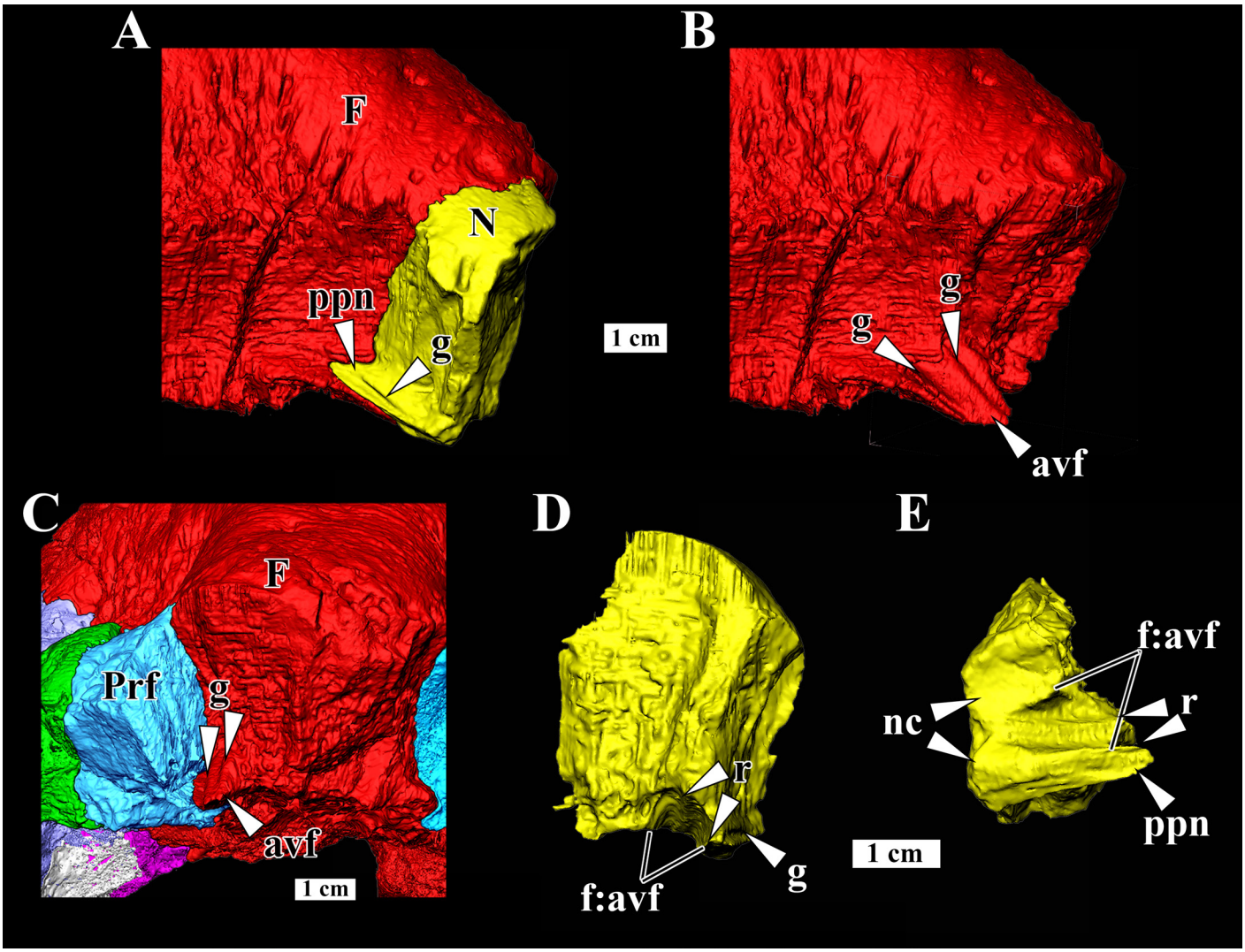

Figure 6. Anterior anatomy of TMP 1972.027.0001. A) Right lateral view of the segmented models of the frontals and nasal with the right prefrontal and palpebral removed. B) Right lateral view of the segmented model of the frontal with the nasal removed. C) Anterior view of the segmented model with the nasal removed. D) Posterior view of the nasal segmented model. E) Ventral view of the nasal segmented model (anterior left). Abbreviations: avf, anteroventral flange of the frontal; F, frontals; f:avf, facet for the anteroventral projection of the frontal; g, groove; N, nasal; nc, nasal cavity; ppn, posterior projection of the nasal; r, ridge.

ridge contacts the prefrontal dorsally and anteroventrally, and the frontal posteroventrally. A shallow anteroposteriorly directed groove rests on the dorsal surface of this ridge.

Prefrontal: Most of the right prefrontal is preserved, with only the most anterior portion missing (Fig. 5B). The prefrontal contacts the nasal anteromedially, the frontal medially and posteriorly (which forms a "L" shaped notch on the frontal in dorsal view), and the palpebral laterally. The prefrontal is incipiently incorporated into the frontonasal boss (Fig. 5C), a unique feature amongst known pachycephalosaurids. This portion is smooth; the remainder of the dorsal surface is rugose. Anteriorly and medially (aside from the frontonasal boss), the rugosity resembles the tuberculate ornamentation seen in uninflated cranial roof elements of *Stegoceras validum* (Schott et al. 2011). Laterally and posteriorly, the tubercles appear coalesced, and are less distinct than the surrounding tubercles. Along with the palpebral, the prefrontal contributes to a larger supraorbital boss that is distinct from the cranial dome (Figs. 1A, 5D). The prefrontal is not incorporated into the frontoparietal dome.

The ventral surface of the prefrontal contributes to the roofs of both the orbit and the nasal cavity. These surfaces are separated by an anterolaterally directed ridge that extends from the frontal (Fig. 5B). Several vessels enter the orbital roof on the prefrontal. Medioventrally, the prefrontal receives the ventrolateral ridge of the nasal and most of the anteroventral projection of the frontal (Fig. 6C). The

contact with the palpebral is nearly straight, except for a shallow horizontal ridge that extends along the ventral margin of the contact.

Palpebral (anterior supraorbital): The palpebral (see Supplemental Data 2 for revised nomenclature) contacts the prefrontal medially, frontal posteromedially, and posterior supraorbital posteriorly (Fig. 5). The contacts with the frontal and posterior supraorbital are straight. The contact with the frontal appears extensive, unlike the restricted contact described in derived pachycephalosaurids (*Acrotholus audeti*, *Prenocephale prenes*, and *Sphaerotholus* spp.; Evans et al. 2013).

The dorsal surface of the palpebral is convex and rugose, and forms most of a supraorbital boss (Figs. 1A, 5D) like in *Prenocephale prenes* (Maryańska and Osmólska 1974, although they mention each peripheral element is separated from each other, there is no discernible groove along the contacts of the prefrontal and palpebral in *Prenocephale prenes*). This rugosity is shallow and more irregular than the typical tesserate rugosity of uninflated cranial roof bones (such as the palpebral of UALVP 2). This rugosity extends onto the lateral surface, such that the lateral (supraorbital) ridge does not extend onto the palpebral (Fig. 2F; Schott et al. 2011; Schott and Evans 2012), whereas a lateral ridge is retained in the holotype of *Prenocephale prenes*. *Pachycephalosaurus wyomingensis* (AMNH 1696, Brown and Schlaikjer 1943) and *Sphaerotholus buchholtzae* (DMNH EPV.97077, Woodruff et al. 2021) do not appear to have a supraorbital boss, and the dorsal surfaces for the supraorbital elements are smooth and continuous with each other and the frontal.

The preserved ventral surface of the palpebral contributes to the orbital roof, which is slightly depressed from the rounded orbital rim (Fig. 5B). The ventral surface is pierced by numerous canals (Fig. 7B). These enter the palpebral at shallow angles and are oriented perpendicular to the frontal – palpebral contact. Some canals rest in furrows that extend onto (and then enter) the frontal.

Posterior supraorbital: The posterior supraorbital contacts the palpebral anteriorly, the frontal medially, and the postorbital posteriorly (Fig. 5). Although the right posterior supraorbital – postorbital suture appears obliterated, the respective contacts of these two bones with the frontal are identifiable and are dorsally separated by a diastema (both have a dorsally arched contact with the frontoparietal). The left posterior supraorbital appears to have been reattached to the frontoparietal, with the break running along the frontal-posterior supraorbital suture (Figs. 1B, 2B).

The dorsal margin of the posterior supraorbital that contacts the frontal is strongly arched, with the maximum height of the contact skewed posteriorly (Fig. 5C; unique to TMP 1972.027.0001). The dorsal surface extending perpendicular from the middle of the frontal contact is smooth. The dorsal surface becomes rugose towards the contact with the palpebral and postorbital, and towards the lateral margin. The dorsal inflation extends to the lateral margin, but a slight anteroposterior ridge may represent the remnants of a dorsolateral ridge. The left posterior supraorbital is not incorporated into the dome, although this may be due to a pathological depression that also affects the postorbital and frontoparietal (Fig. 7C). The lateral surfaces of the posterior supraorbitals are rugose, and are characterized by bumps rather than depressions.

The ventral surface of the posterior supraorbital contributes to most of the posterodorsal region of the orbital roof. Vascular canals along the orbital roof are oriented perpendicular to the frontal – posterior supraorbital contact, some resting in furrows like on the prefrontal and palpebral (Fig. 7B). A possible muscle scar is marked by a small peg-like rugosity resting in a shallow depression in the posterolateral corner of the orbit roof (Fig. 7A, B). The orbital rim on the posterior supraorbital is sharper than that on the palpebral.

Postorbital: Both postorbitals are nearly complete, although the ventrolateral margins of both are weathered. The roofs of the temporal chamber remain intact, but not the ventral surface of either postorbital bar. The postorbital contacts the posterior supraorbital anteriorly, the frontoparietal medially, and the squamosal posteriorly. The sutural surfaces for the squamosals are continuous from the postorbitals onto the parietal (Figs. 2, 5), eliminating the supratemporal fenestrae.

The postorbital is completely incorporated into the frontoparietal dome (Fig. 5), contrary to Sullivan (2003). The dome continuously extends from the frontoparietal to the lateral edge of the postorbital, such that there is no lateral shelf. The postorbital's contribution of the dome slightly overhangs the lateral surface of the postorbital-squamosal bar, and forms the maximum width of the skull (Figs. 1C, 2C). The dorsal surface is extremely smooth, but becomes rugose towards the anterior, lateral, and posterior margins. Fragments of the left squamosal appear fused onto the postorbital. A deep pathological depression exposes an open frontoparietal-postorbital suture on the left side (Fig. 7C).

The preserved ventral surface of the postorbital forms part of the temporal roof. The temporal roof contains two shallow mediolaterally oriented depressions, which extend onto the parietals. Vascular canals rest in furrows that cross the parietal-postorbital contact and enter each element. The surface for the squamosal tongue is preserved on the right postorbital (Fig. 2B).

Frontoparietal: The frontoparietal (fused frontals and parietals) is nearly complete but is dorsally and ventrally damaged. Two large holes along the dorsal surface extend through most of the frontoparietal (Figs. 1A, B, 2A, B, 3). Ventrally, the frontoparietal is damaged along the

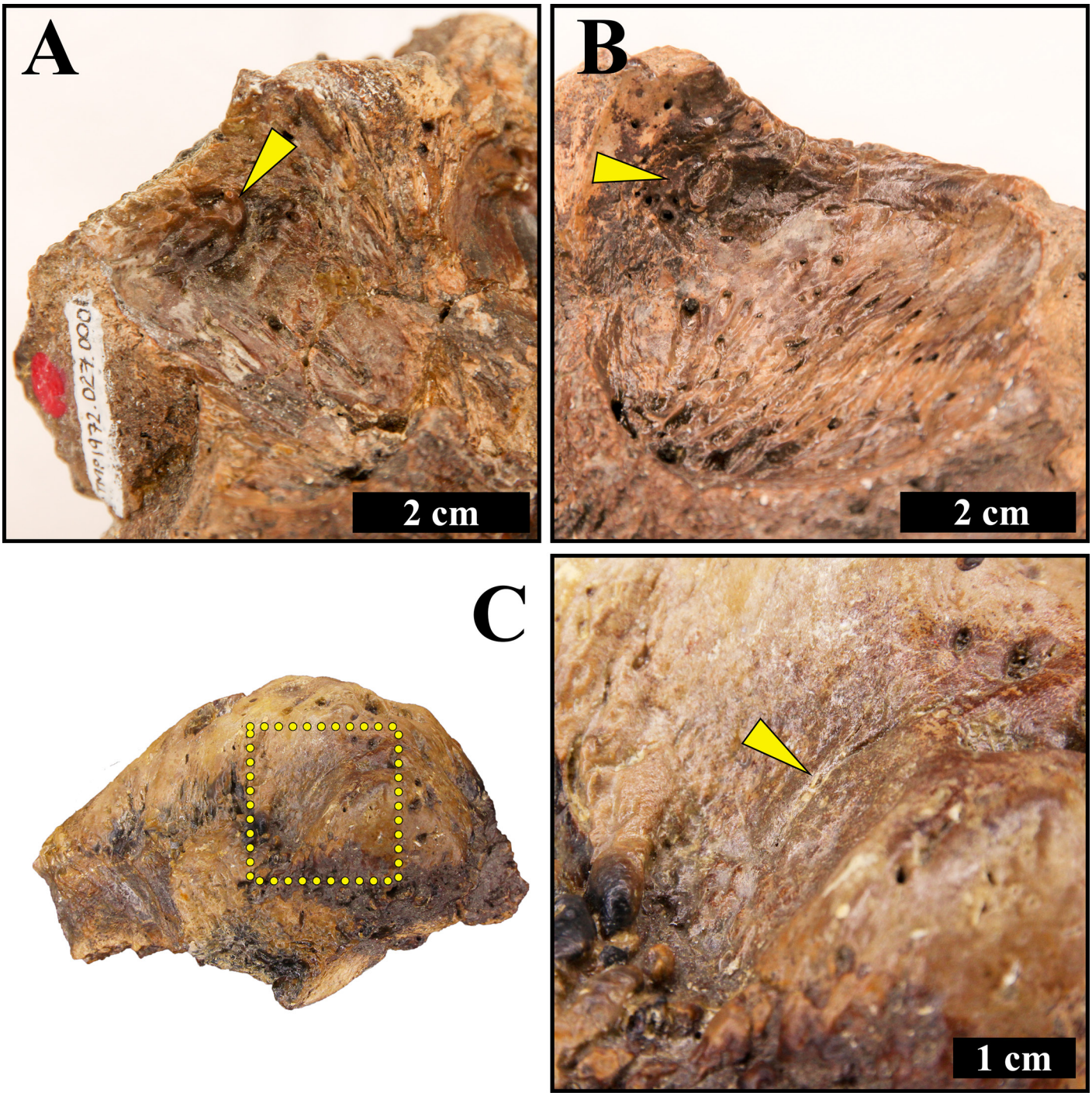

Figure 7. Additional photographs of TMP 1972.027.0001. Posterodorsal muscle scars (arrows) on the left (A) and right (B) orbital roof. C) An open frontoparietal/postorbital suture (arrow) situated within a depressed lesion. The dashed box in the large image indicates the position of image C.

left anterolateral corner of the frontonasal boss (missing the anteroventral flange, Fig. 5B). Many of the posterior neurocranial contacts are damaged, including the left posterior portion of the cerebral fossa, the contacts for the supraoccipital and left laterosphenoid, and the right sutural surface for the prootic and opisthotic (Figs. 1B, 2B). Missing portions are inferred from the neurocranial arrangement described by Giffin (1989a). The ventral and posterior portion of the occipital surface of the parietal, including the ventral and posterior sutural surfaces for the right squamosal, are damaged.

TMP 1972.027.0001 is the absolutely and proportionally widest frontoparietal of any unquestionable known Belly River Group pachycephalosaurian (108.99 mm (W:F/P)/51.62 mm (L:F) = 2.11; see Sullivan 2003 for discussion on the provenance of BMNH R 8648, an incom-

plete skull roof of *Pachycephalosaurus wyomingensis* originally reported from the Oldman Formation). Despite its great width, the frontoparietal is only 6.24 mm longer than in UALVP 2 (121.24 mm, 115.18 mm respectively; W:F/P = 80.98 mm), and is 15.7 mm shorter than the longest unquestionable Belly River Group pachycephalosaurian frontoparietal (TMP 2017.012.0019; L:FP = 137.12 mm).

The dorsal surface forms a massive dome, which is continuous with the frontonasal boss, the posterior supraorbital and the postorbital, and which extends to the posterior margin of the parietal (Figs. 1, 2, 5). The dome apex is relatively flat and broad where it is unaltered by pathologies (Figs. 1C, D, 2C, D). The largest lesion is situated on the left side of the parietal and is 24 mm by 30 mm, and 16 mm at its deepest. It has a terraced appearance, with narrower but deeper depressions lying inside wider, shallower ones.

The broad frontonasal boss is posterolaterally separated from the supraorbital lobes by a distinct groove on either side (the left groove is dorsally bifurcated; Fig. 2 E, F). The frontonasal boss of TMP 1972.027.0001 is anteroposteriorly distinct, similar to UALVP 2, whereas "*Hanssuesia sternbergi*" typically possesses anteroposteriorly short frontonasal bosses (Figs. S2, S9, S10). The anteroposterior extent of the frontonasal boss varies in *Colepiocephale lambei* (e.g., TMP 1992.088.0001, short; CMN 8818, long; Schott et al. 2009), *Foraminacephale brevis* (e.g., TMP 1985.036.0292, short; TMP 1987.050.0029, long; Schott and Evans 2017) and *Sphaerotholus buchholtzae* (ROM 53584, short; UWBM 89701 long; Woodruff et al. 2021).

The peripheral margins of the supraorbital lobes are quite rugose, but smooth posteromedially into the dome. The dome is steep towards the supraorbital lobes (134º along the palpebral contact) but does reach the dorsal margins of the supraorbital elements (prefrontal, palpebral, and posterior supraorbital; Fig. 5). The sutural surface for the right posterior supraorbital is concave in dorsal view. The posterior extent of the supraorbital lobe is greater in *Colepiocephale lambei*, and is marked by an indentation in the lateral surface of the frontoparietal at the contact between the posterior supraorbital and postorbital (Sternberg 1945; Sullivan 2003), an apomorphy of the taxon (Schott et al. 2009). In dorsal view, the frontoparietal of TMP 1972.027.0001 is not indented between the sutural surfaces for the posterior supraorbital and postorbital.

The posterior medial extension of the parietal of TMP 1972.027.0001 is not visible in lateral view photographs of previous publications (Wall and Galton 1979; Sullivan 2003), although it is visible in a figured lateral line drawing in Wall and Galton (1979, fig. 1). It is more distinct in orthographic views of the laser model (Fig. 2E, F) compared to photographs (Fig. 1E, F). The posterior medial extension of the parietal is confluent with the dome, eliminating a posterior shelf (the parietosquamosal shelf; contra to Williamson and Carr 2002) and instead forms a "down-turned" parietal (Sternberg 1945), a unique feature amongst specimens of *Stegoceras validum*. Otherwise, a dome extending to the posterior margin of the parietal is restricted to other domed pachycephalosaurians, except for *Colepiocephale lambei* (which presumably has a narrow posterior projection portion of the parietal in-between the supratemporal fenestrae; Schott et al. 2009). The medial extension of the parietal preserves a shallow sagittal node (also present in UALVP 2, although Evans et al. 2021 described this as a ridge) that is laterally and ventrally bordered by a tuberculate rugosity. There is no indication that a primary node row extended on the parietal, although the right side of the medial extension of the parietals that contacts the squamosal is damaged, and possibly could have otherwise preserved a coalescing medial node. *Stegoceras validum* variably preserves a coalescing node, or the medial node is completely positioned on the squamosal (Schott and Evans 2012). This state was historically unknown for "*Hanssuesia sternbergi*". However, TMP 2017.012.0019 preserves a coalescing node on the right side, but not on the left side of the medial extension of the parietal (Fig. S2A, D). The ventral surface of the medial extension of the parietal in TMP 1972.027.0001 has a shallow groove that follows the posterior border of the parietal (Figs. 1B, 2B).

The ventral surface of the frontoparietal is divided into five fossae: the median endocranial fossa (which includes the olfactory bulbs and the cerebellar fossa), the paired orbital fossae, and the paired temporal roofs. The relative length of the endocranial fossa (from the anterior extent of the olfactory bulbs to the pit for the supraoccipital cartilage – L:olf/soc; see Giffin 1989a) is similar to "*Hanssuesia sternbergi*" and large *Stegoceras validum* (e.g., TMP 2000.026.0001 and UALVP 2). TMP 1972.027.0001 does have the shortest L:olf/soc (32.41 mm) amongst these large specimens, although it is ~ 1.6 mm shorter than UALVP 2. TMP 2017.012.0019 preserves the longest L:olf/soc (46.03 mm) amongst the examined specimens (Fig. S2). Compared to frontoparietal length (as in Giffin 1989a), the L:olf/soc of UALVP 2 (29.7%) is indistinct from TMP 1972.027.001 (26.7%) and TMP 2017.012.0019 (33.6%).

The orbital fossae are separated from the endocranial fossa by thick sutures for the accessory orbital ossifications, orbitosphenoid, and laterosphenoid (see Giffin 1989b for neurocranial anatomy), as in "*Hanssuesia sternbergi*" (Brown and Schlaikjer 1943) and large *Stegoceras validum* (e.g., UALVP 2). The medial border of the orbital fossa is pierced by numerous vascular canals, some of which are situated within furrows that extend onto the supraorbital elements.

The parietal portion of the temporal chamber is extremely narrow, and the roof is horizontal as in "*Hanssuesia*

sternbergi", *Foraminacephale brevis*, and *Stegoceras validum* (Williamson and Carr 2002; Schott and Evans 2017). The roofs of the temporal chambers preserve a pair of deep furrows on each side. These cross the parietal-postorbital suture and lead to vascular foramina. Similar vascular furrows were described from the parietals of *Colepiocephale lambei* (Schott et al. 2009).

Relative Void Space

The binarized original SμCT slice at the contact of between the frontal-posterior supraorbital-postorbital of TMP 1972.027.0001 produced a relative frontoparietal void space of 36.09% (Fig. 8A), 15% higher than in the flatheaded juvenile *Stegoceras validum* AMNH 5450 (20.1%, Schott et al. 2011; ~20% Nirody et al. 2022). Averaging the pixel intensities of the proceeding and following two slices (five slices total) resulted in a lower relative void space after binarization (22.25%; Fig 8B). Similarly, reducing the resolution of the single SμCT slice to 22% original resolution (2403 by 2403 pixels reduced to 461 by 461 pixels) greatly reduced the binary relative void space (8.53%, Fig. 8C). Reducing the number of pixels in the image averaged from five sequential slices resulted in the lowest relative void space (7.23% Fig. 8D), similar to the relative void space calculated for ROM 53555 (7.27%; Schott et al. 2011).

Diagnostic Endocranial Size of "*Gravitholus albertae*"

Amongst the total Belly River Group pachycephalosaurian sample, endocranial length (L:olf/soc) and endocranial width (W:cer) poorly correlate with frontoparietal width (W:F/P) and frontal length (L:F) ($r^2 < 0.5$), and W:cer did not correlate with L:F (Fig. 9; Table S6). Covariance values (r^2) were higher in RMA regressions including L:olf/soc compared to W:cer. L:olf/soc scales with negative allometry relative to W:F/P, and isometrically scales relative to L:F. W:cer scales with negative allometry relative to W:F/P. No significant correlations were identified within individual taxa. L:olf/soc appears proportionally similar between Belly

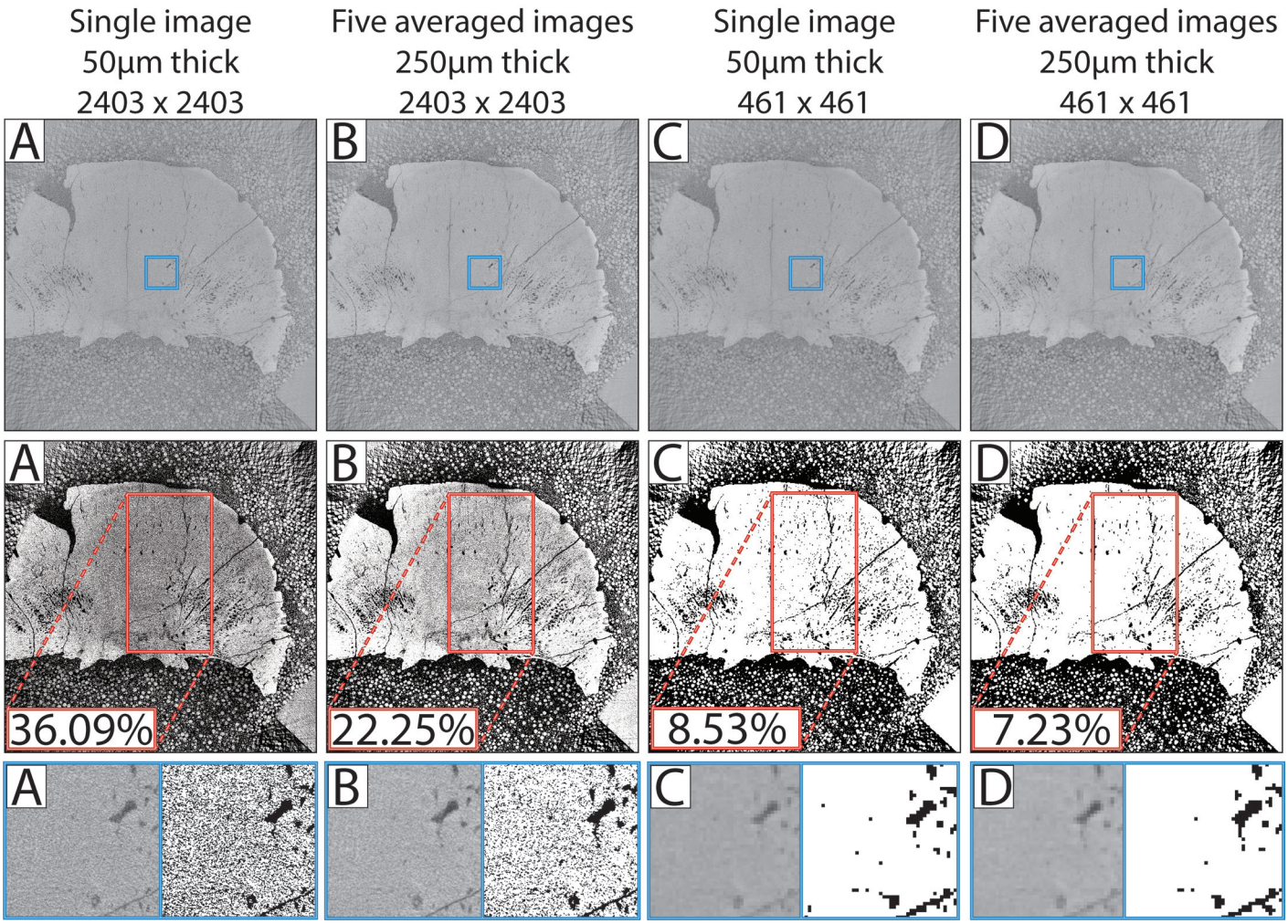

Figure 8. Void binarization of TMP 1972.027.0001. Top row of images – SμCT images. Middle row of images – Huang threshold images. Red box captures area assessed for void density. Void density reported below images. Bottom row – enlarged area of SμCT and Huang threshold images (blue box in top row). Note that calculated void density is less in thicker SμCT slices (B and D) as well as in lower resolution SμCT images (C and D)

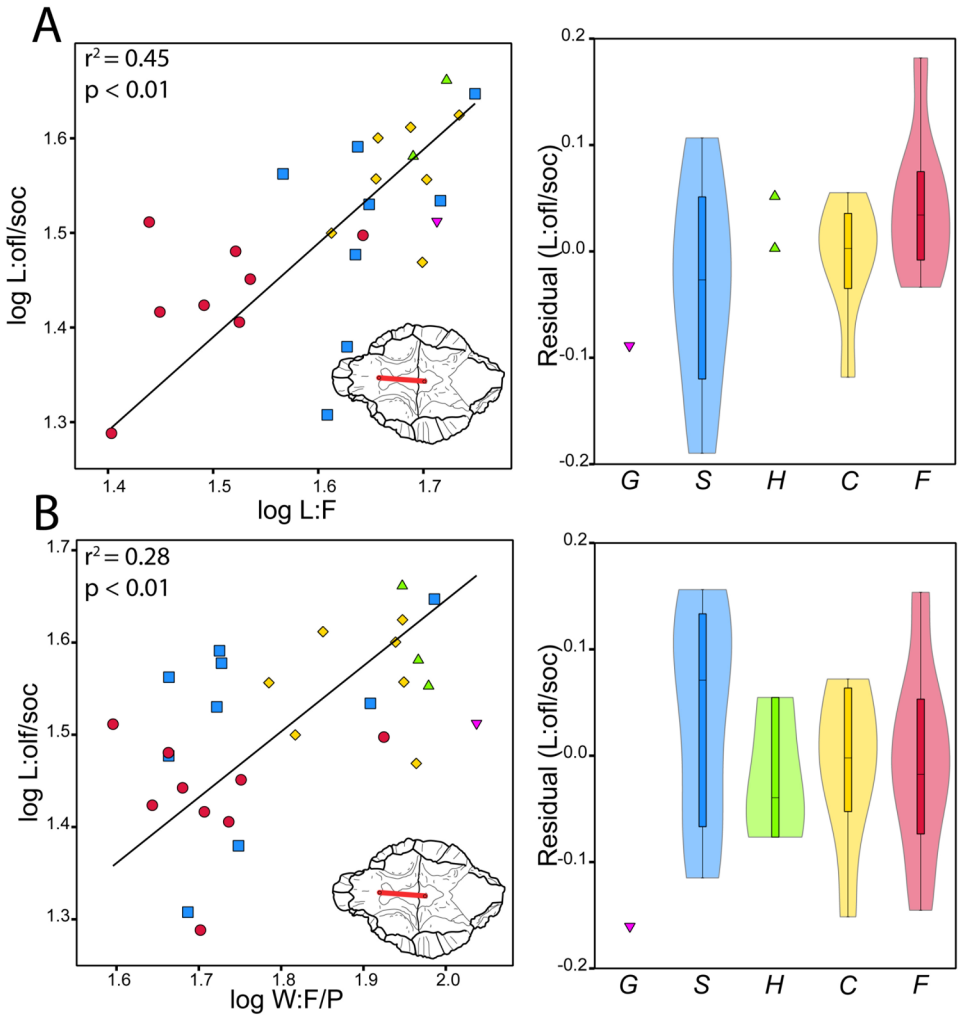

Figure 9. Relative endocranial length amongst Belly River Group pachycephalosaurians. RMA regressions of endocranial length (L:olf/soc) against; A) frontal length (L:F), and B) frontoparietal width (W:F/P). Symbols: purple inverted triangle, TMP 1972.027.0001; blue squares, *Stegoceras validum*; green triangles, "*Hanssuesia sternbergi*"; yellow diamonds, *Colepiocephale lambei*; red circles, *Foraminacephale brevis*. RMA regression results are for the total sample. The distribution of residuals (violin boxplots) from the best fit line for the total sample are shown to the right. Boxes capture the 25-75% quartiles. Horizontal line within box = median. While TMP 1972.027.0001 has the smallest L:olf/soc residual relative to its frontoparietal width, it is not a statistical outlier from the total Belly River Group sample (G = 1.78, p = 1.00).

River Group pachycephalosaurian taxa. The L:olf/soc residual of TMP 1972.027.0001 relative to the L:F is within the range of both *Colepiocephale lambei* and *Stegoceras validum*. The L:olf/soc residual of TMP 1972.027.0001 relative to the W:F/P is the smallest amongst Belly River Group pachycephalosaurians, but is similar to some specimens of *Colepiocephale lambei* and *Foraminacephale brevis*, and ~ 0.05 less than the smallest residual amongst *Stegoceras validum*. There were no significant outliers in the distribution of these residuals (G = 1.78, p = 1.00).

Belly River Group pachycephalosaurian taxa are somewhat distinguished by endocranial width (W:cer), particularly relative to frontal length (L:F) (Fig. 10). *Colepiocephale lambei* and *Foraminacephale brevis* tend to have wider cerebral impressions on the frontoparietal, compared to "*Hanssuesia sternbergi*", *Stegoceras validum*, and TMP 1972.027.0001. TMP 1972.027.0001 has a cerebral width impression that falls within the range of *Stegoceras validum*, and is similar to specimens of "*Hanssuesia sternbergi*". The W:cer of residual of TMP 1972.027.0001 compared to L:F is the smallest amongst Belly River Group pachycephalosaurians. However, it is only 0.02 smaller than the residual for CMN 515, the lectotype of *Stegoceras validum*. There were no significant outliers in the distribution of these residuals (G = 2.21, p = 0.81).

Diagnostic Morphometrics of "*Hanssuesia sternbergi*"

Frontoparietal width: Frontal length (L:F) did not significantly correlate with the width of the frontonasal boss (W:N/Prf), anterior dome width (W:Pl/Pso), or posterior dome width (W:Po/stf/Sq) in "*Hanssuesia sternbergi*" (Fig. 11; Table S7). However, L:F did significantly positively correlate with these widths in *Colepiocephale lambei*, *Foraminacephale brevis*, and *Stegoceras validum*. W:N/Prf, W:F/P, and W:Po/stf/Sq show significant positive correlation with L:F amongst all Belly River Group pachycephalosaurians, and all scale with positive allometry relative to frontal length. There is no taxonomic separation in the distribution of residuals for W:N/Prf and W:Pl/Pso. The W:N/Prf residual of TMP 1972.027.0001 is not within the range of "*Hanssuesia sternbergi*", but is within the range of both *Foraminacephale brevis* and *Stegoceras validum* (Fig. 11A). The distribution of W:N/Prf residuals for *Stegoceras validum* completely encompassed the distribution of all other Belly

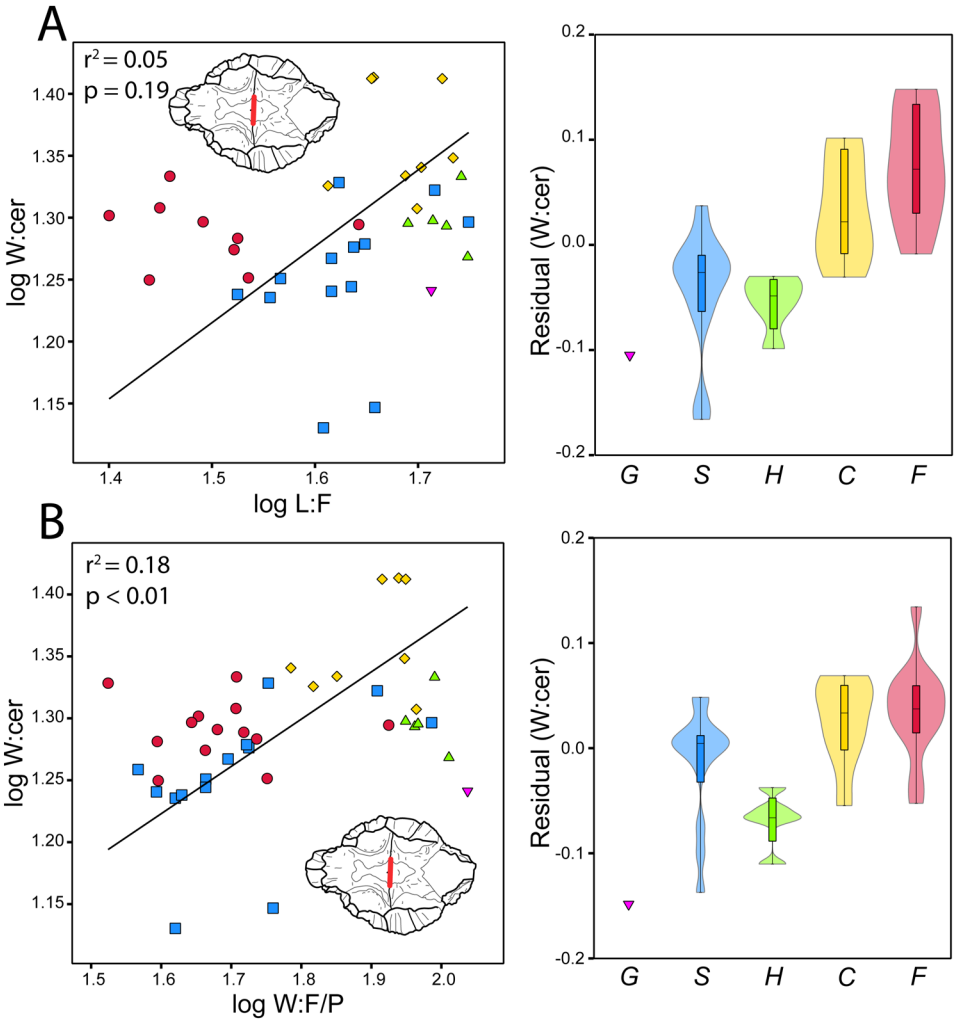

Figure 10. Relative endocranial width amongst Belly River Group pachycephalosaurians. RMA regressions of endocranial width (W:cer) against: A) frontal length (L:F), and B) frontoparietal width (W:F/P). Symbols: purple inverted triangle, TMP 1972.027.0001; blue squares, *Stegoceras validum*; green triangles, "*Hanssuesia sternbergi*"; yellow diamonds, *Colepiocephale lambei*; red circles, *Foraminacephale brevis*. RMA regression results are for the total sample. The distribution of residuals (violin boxplots) from the best fit line for the total sample are shown on the right. Boxes capture the 25-75% quartiles. Horizontal line within box = median. While TMP 1972.027.0001 has the smallest W:cer residual relative to its frontoparietal width, it is not a statistical outlier from the total Belly River Group sample (G = 2.21, p = 0.81).

River Group pachycephalosaurians. The averages of W:N/Prf residuals between Belly River Group pachycephalosaurian taxa (excluding TMP 1972.027.0001) did not significantly differ (F = 1.86, p = 0.15). The W:Pl/Pso residuals amongst *Stegoceras validum* nearly encompassed all other Belly River Group pachycephalosaurians, except for a single specimen of *Foraminacephale brevis* (Fig. 11B). The average of W:Pl/Pso residuals between Belly River Group pachycephalosaurian taxa (excluding TMP 1972.027.0001) did significantly differ (F = 10.89, p < 0.01); a subsequent Tukey's pairwise (Table S8) identified that the average for *Stegoceras validum* is significantly smaller than "*Hanssuesia sternbergi*" and *Foraminacephale brevis* respectively (p < 0.01). No other significant differences in residual averages were identified. TMP 1972.027.0001's W:Pl/Pso residual falls within the range of all Belly River Group pachycephalosaurian taxa.

The residuals for posterior dome width (W:Po/stf/Sq) are more taxonomically separated (Fig. 11C). The residual for TMP 1972.027.0001 falls within the range of *Colepiocephale lambei* and "*Hanssuesia sternbergi*". "*Hanssuesia sternbergi*" is almost entirely positively separated from *Stegoceras validum*; however, both overlap with *Colepiocephale lambei* extensively. The variation in relative frontoparietal width amongst specimens of *Colepiocephale lambei* is similar to the combined variation of "*Hanssuesia sternbergi*", *Stegoceras validum*, and TMP 1972.027.0001. The range of *Foraminacephale brevis* slightly overlaps with both *Colepiocephale lambei* and "*Hanssuesia sternbergi*", and shows greater positive separation (wider) than other Belly River Group pachycephalosaurians. The average of W:Po/stf/Sq residuals amongst Belly River Group pachycephalosaurian taxa (excluding TMP 1972.027.0001) did significantly differ (F = 49.92, p < 0.01). All pairwise comparisons were significantly different (p < 0.01), except for the averages of *Colepiocephale lambei* and "*Hanssuesia sternbergi*" (p = 0.27; Table S9).

Supraorbital lobe inflation: The height of the posterior supraorbital-postorbital contact (H:Pso/Po) was the only supraorbital height that may correlate with frontoparietal thickness (T:F/P) amongst "*Hanssuesia sternbergi*" specimens (Fig. 12; Table S10). Neither heights for the prefrontal-palpebral contact (H:Prf/Pl) nor palpebral-posterior supraorbit-

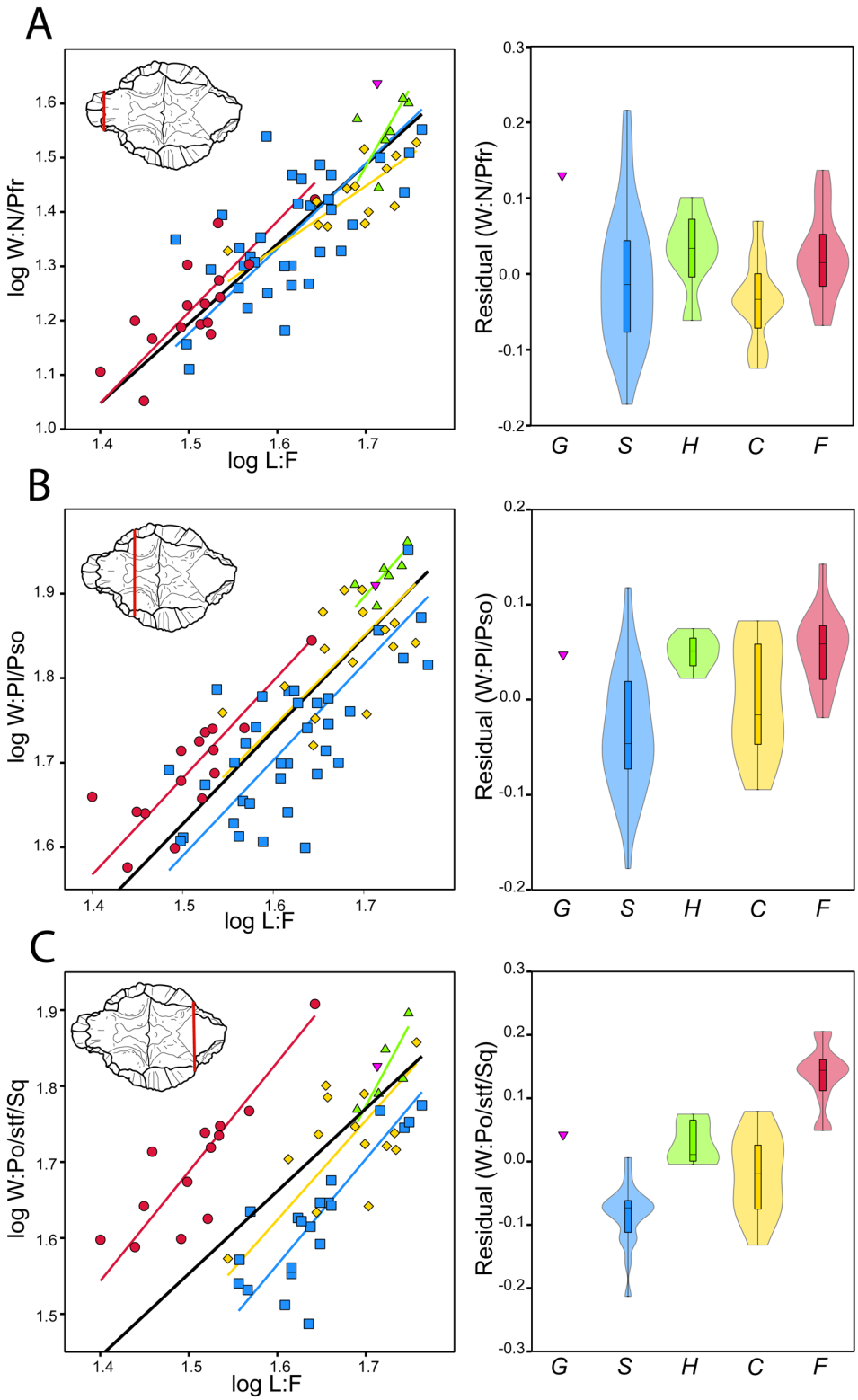

Figure 11. Relative frontoparietal widths amongst Belly River Group pachycephalosaurids. A) width of the frontonasal boss (W:N/Prf), B) anterior (frontal) dome width (W:Pl/Pso). C) Posterior (parietal/temporal) dome width. Symbols: purple inverted triangle, TMP 1972.027.0001; blue squares, *Stegoceras validum*; green triangles, "*Hanssuesia sternbergi*"; yellow diamonds, *Colepiocephale lambei*; red circles, *Foraminacephale brevis*. Black line = best fit line for the total sample. The distribution of residuals (violin boxplots) from the best fit line for the total sample are shown to the right. Boxes capture the 25-75% quartiles. Horizontal line within box = median. Note that frontoparietals of "*Hanssuesia sternbergi*" are not uniquely wider from other Belly River Group pachycephalosaurians.

al contact (H:Pl/Pso) correlated with frontoparietal thickness (T:F/P) amongst "*Hanssuesia sternbergi*". Otherwise, all supraorbital heights significantly correlated positively with frontoparietal thickness in *Colepiocephale lambei*, *Foraminacephale brevis*, and *Stegoceras validum*. The H:Prf/Pl residual representing TMP 1972.027.0001 falls within the range of all other Belly River Group pachycephalosaurian taxa. The other two supraorbital residuals for TMP 1972.027.0001 fall within the range of "*Hanssuesia sternbergi*", *Foraminacephale brevis*, and *Stegoceras validum*, but not *Colepiocephale lambei*. Supraorbital height residuals for all Belly River Group pachycephalosaurians taxa overlap. The distribution of H:Pl/Pso residuals amongst "*Hanssuesia sternbergi*" specimens slightly overlap with *Colepiocephale lambei*.

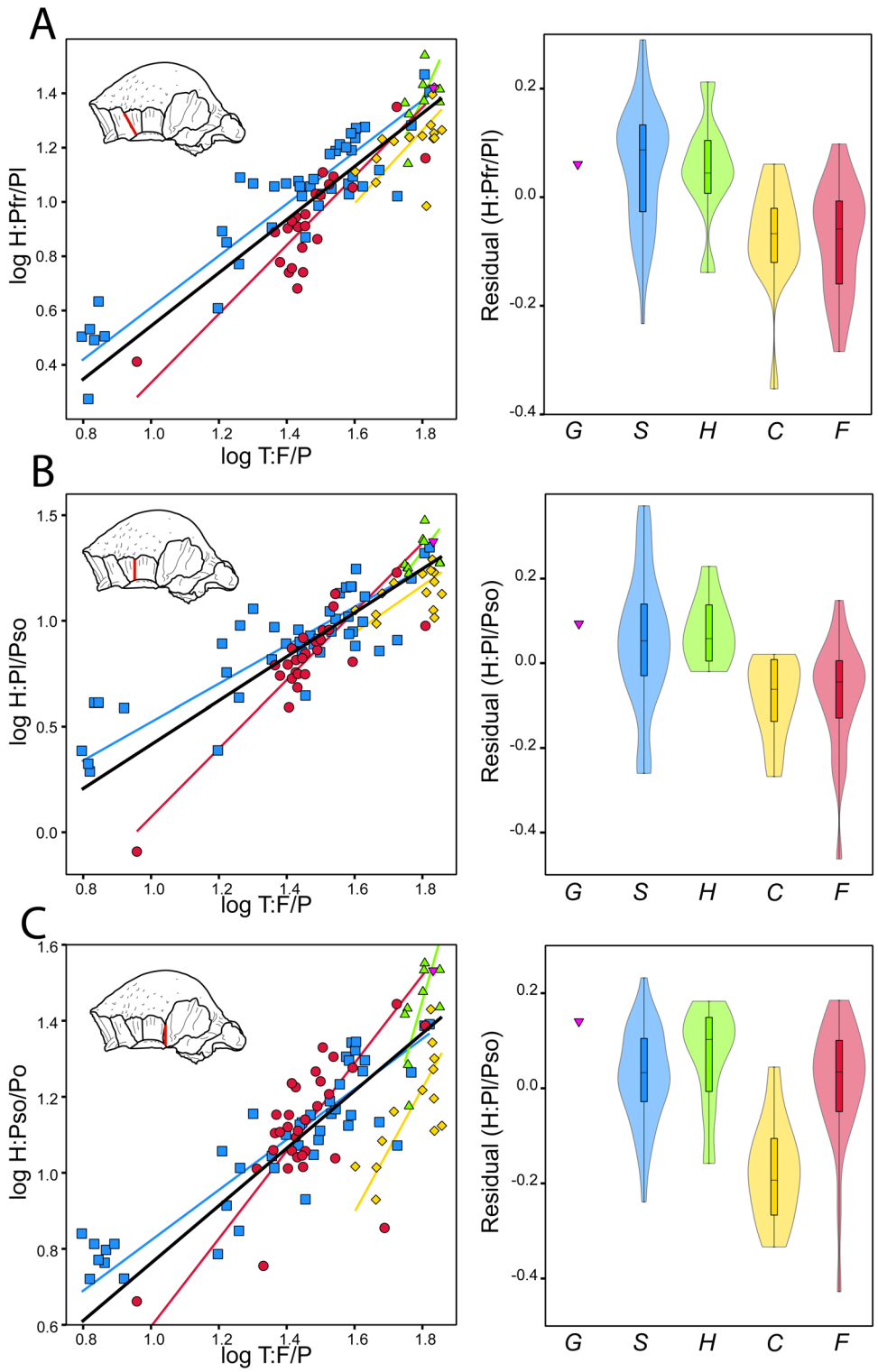

Figure 12. Relative supraorbital inflation amongst Belly River Group pachycephalosaurians. A) Height at the contacts of the prefrontal and palpebral (H:Prf/Pl) vs. frontoparietal thickness (T:F/P). B) Height at the contacts of the palpebral and posterior supraorbital (H:Pl/Pso) vs. T:F/P. C) Height at the contacts of the posterior supraorbital and postorbital (H:Pso/Po) vs. T:F/P. Symbols: purple inverted triangle, TMP 1972.027.0001; blue squares, *Stegoceras validum*; green triangles, "*Hanssuesia sternbergi*"; yellow diamonds, *Colepiocephale lambei*; red circles, *Foraminacephale brevis*. Black line = best fit line for the total sample. The distribution of residuals (violin boxplots) from the best fit line for the total sample are shown to the right. Boxes capture the 25-75% quartiles. Horizontal line within box = median. Note that the peripheral supraorbital thicknesses of "*Hanssuesia sternbergi*" frontoparietals are not unique amongst Belly River Group pachycephalosaurians.

The averages of all three supraorbital height residuals significantly differed between Belly River Group pachycephalosaurian taxa (H:Prf/Pl, $F = 11.23$, $p < 0.01$; H:Pl/Pso, $F = 7.13$, $p < 0.01$; H:Pso/Po, $F = 12.72$, $p < 0.01$). The average H:Prf/Pl and H:Pl/Pso residuals of "*Hanssuesia sternbergi*" and *Stegoceras valium* were significantly larger than *Colepiocephale lambei* and *Foraminacephale brevis* (Tables S11, S12). The average H:Pso/Po of *Colepiocephale lambei* was significantly smaller than all other Belly River Group pachycephalosaurian taxa (Table S13).

Belly River Group Principal Component Analyses

Iteration loadings: Tables S14-S17 (Supplemental Data 2) summarise the PC variances and loadings for

the total Belly River Group PCA iterations. Results for the $\log_{10}$-transformed and non-transformed PCA will be discussed subsequently. The results for both size standardized PCAs are discussed in the Supplemental Data 2. All variable loadings in PC 1 of the $\log_{10}$-transformed and non-transformed iterations were positive. PC 1 in the $\log_{10}$-transformed and non-transformed iterations explained 72.6% and 84.2% of the total variance, respectively. Variables with the largest range had the highest loadings on PC 1 of all iterations (Fig. S9). PC 1 in the $\log_{10}$-transformed iteration was strongly positively loaded by frontoparietal heights (excluding H:Pso/Po and T:F/P). PC 1 in the non-transformed iteration was strongly loaded by the two posterior frontal widths and frontoparietal thickness.

PC 2 in the $\log_{10}$-transformed iteration explained 6.5% of the variance, and represents variation in the sagittal height of the frontonasal boss, contact lengths for the peripheral supraorbital elements (palpebral and posterior supraorbital), and temporal width across the parietal. It was strongly positively loaded by L:Pl, W:Po/stf/Sq, L:Pso, and H:Pso/Po, and strongly negatively loaded by H:N/N. PC 2 in the non-transformed iteration explained 5.6% of the total variance, and represents variation in the temporal width across the parietal. It was strongly positively loaded by W:Po/stf/Sq, and strongly negatively loaded by L:Po.

PC 3 in the $\log_{10}$-transformed iteration explained 5.0% of the total variance, and largely explains the lateral thickness of the frontonasal boss. It was strongly positively loaded by T:F/P, and strongly negatively loaded by H:N/Prf and H:Pso/Po. PC 3 in the non-transformed iteration explained 2.9% of the total variance, and explains the variation in the height of the posterior supraorbital postorbital contact relative to frontoparietal thickness. It was strongly positively loaded by H:Pso/Po, and strongly negatively loaded by T:F/P.

PC 4 in the $\log_{10}$-transformed iteration explained 2.6% of the total variance, and explains the height of the palpebral-posterior supraorbital contact on the frontal. It was strongly negatively loaded by H:Pl/Pso, and H:N/Prf had the highest positive loading. PC 4 in the non-transformed iteration explained 2.4% of the total variance, and explains the thickness of the frontonasal boss and frontoparietal. It was strongly positively loaded by H:N/Prf, H:N/N, and T:F/P, and strongly negatively loaded by W:Prf/Pl.

Iteration Scoring: TMP 1972.027.0001 had the highest and second highest PC 1 score in the $\log_{10}$-transformed (Fig. 13) and non-transformed PCA (Fig. 14), respectively. PC 1 scores for all specimens and amongst individual taxa significantly correlated with the dorsal width across the frontal-parietal contact (W:F/P) in both the $\log_{10}$-transformed (Fig. 15; Table S18) and non-transformed PCA iterations (Fig. 16: Table S19), except for PC 1 scores of "*Hanssuesia sternbergi*" from the $\log_{10}$-transformed PCA. *Colepiocephale lambei* and *Foraminacephale brevis* tended to have lower PC 1 scores relative to W:F/P, compared to "*Hanssuesia sternbergi*" and *Stegoceras validum*. This is more apparent in the non-transformed PC 1 scores. PC scores of the entire Belly River Group from subsequent axes did not correlate with W:F/P (Table S18, S19).

Pachycephalosaurian taxa were most distinct in the frontal length (L:F) proportionate PCA (Fig. 17; Fig. S4), followed by the non-transformed iteration (Fig. 14D), W:F/P proportionate (Fig. S5), and finally $\log_{10}$-transformed iteration (Fig. 13D). *Foraminacephale brevis* is broadly distinct in PC 2 of the $\log_{10}$-transformed and non-transformed. Some specimens of "*Hanssuesia sternbergi*" and large *Stegoceras validum* overlapped with *Foraminacephale brevis* in PC 2 of the $\log_{10}$-transformed iterations (Fig. 13). Some large specimens of *Colepiocephale lambei* and "*Hanssuesia sternbergi*" overlap with smaller *Foraminacephale brevis* in PC 2 of the non-transformed PCA (Fig. 14). *Colepiocephale lambei* completely overlapped with "*Hanssuesia sternbergi*", *Stegoceras validum*, and TMP 1972.027.0001 in PC 2 of both PCA iterations (Figs. 13, 14). "*Hanssuesia sternbergi*" is positively separated from larger *Stegoceras validum* and TMP 1972.027.001, although it does overlap with a smaller specimen of *Stegoceras validum*. PC 2 scores of *Stegoceras validum* do significantly correlate with W:F/P in both iterations (Figs. 15, 16, Tables S18, S19), and PC 2 scores of *Foraminacephale brevis* correlated with W:F/P in the non-transformed PCA (Fig. 16; Table S19).

Smaller specimens of *Colepiocephale lambei* were separated along the positive axis from other pachycephalosaurians in PC 3 of the $\log_{10}$-transformed PCA (Fig. 13). Three specimens of *Hanssuesia sternbergi* (CMN 8817, TMP 1987.036.853, TMP 2017.012.0019) are distinct from *Stegoceras validum*, and TMP 1972.027.0001, but overlap with *Colepiocephale lambei*. PC 3 scores of *Colepiocephale lambei* in the $\log_{10}$-transformed PCA were negatively correlated with W:F/P (Fig. 15; Table S18).

Colepiocephale lambei is separated along the negative axis from other Belly River Group pachycephalosaurians in PC 3 of the non-transformed PCA (except for one *Colepiocephale lambei* that overlaps with a small number of other specimens) (Fig. 14). TMP 1972.027.0001 has the highest PC 3 score in the Belly River Group non-transformed PCA, followed closely by specimens of "*Hanssuesia sternbergi*" and *Stegoceras validum*.

There was no taxonomic separation in PC 4 of the $\log_{10}$-transformed and non-transformed PCAs (Figs. 13, 14). PC 4 scores of *Colepiocephale lambei* in the $\log_{10}$-transformed PCA positively correlated with W:F/P (Fig 15; Table S18). CMN 8817, TMP 1987.036.853, and TMP 2017.012.0019 ("*Hanssuesia sternbergi*") are negative-

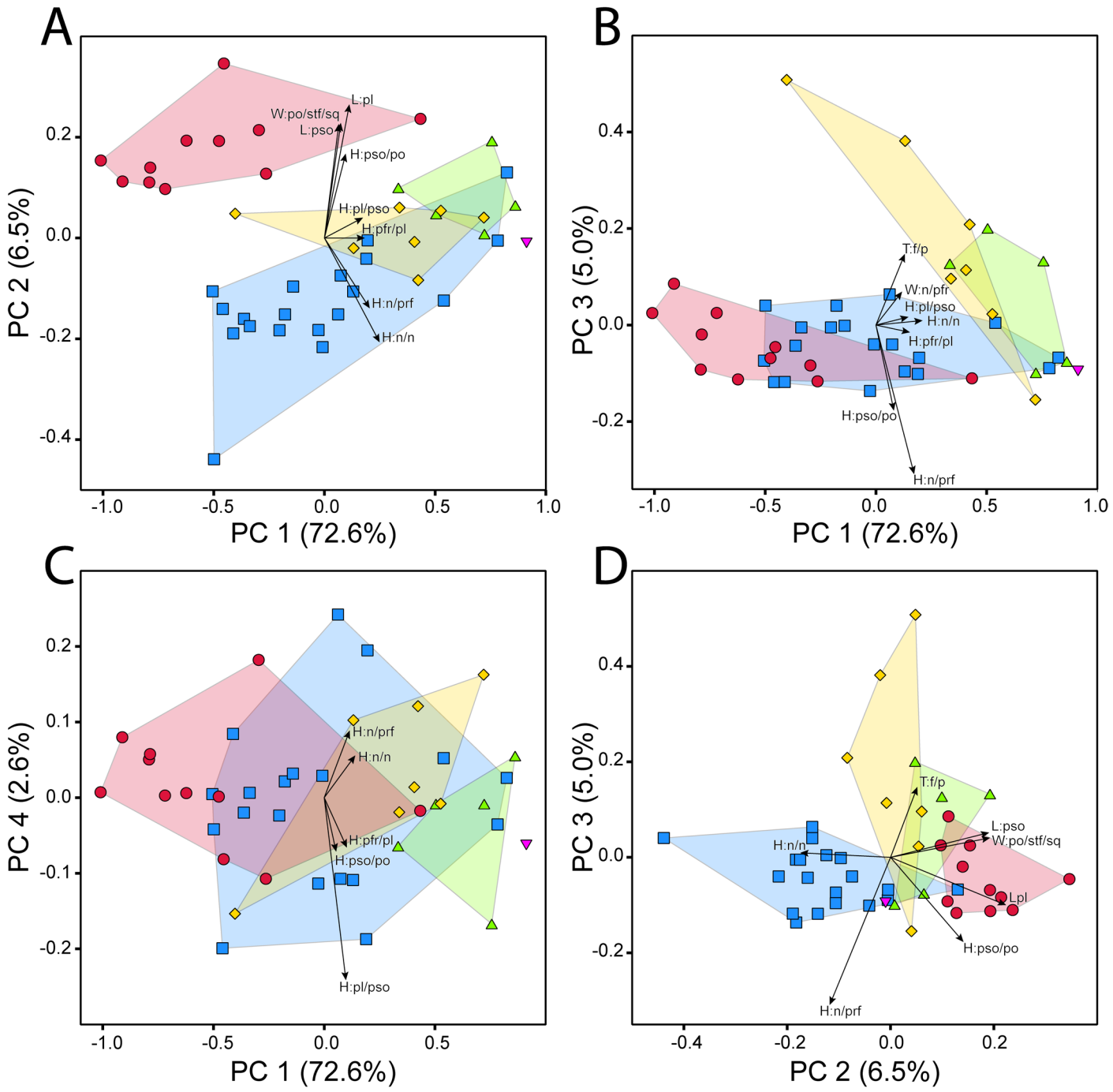

Figure 13. PCA of $\log_{10}$-transformed linear measurements from Belly River Group pachycephalosaurian frontoparietals. Symbols: purple inverted triangle, TMP 1972.027.0001; blue squares, *Stegoceras validum*; green triangles, "*Hanssuesia sternbergi*"; yellow diamonds, *Colepiocephale lambei*; red circles, *Foraminacephale brevis*. Arrows indicate the eigenvectors of variable loadings; only variables that loaded at least |0.3| in either axis are displayed. Pachycephalosaurian taxa are most disparate in PC 2 and PC 3.

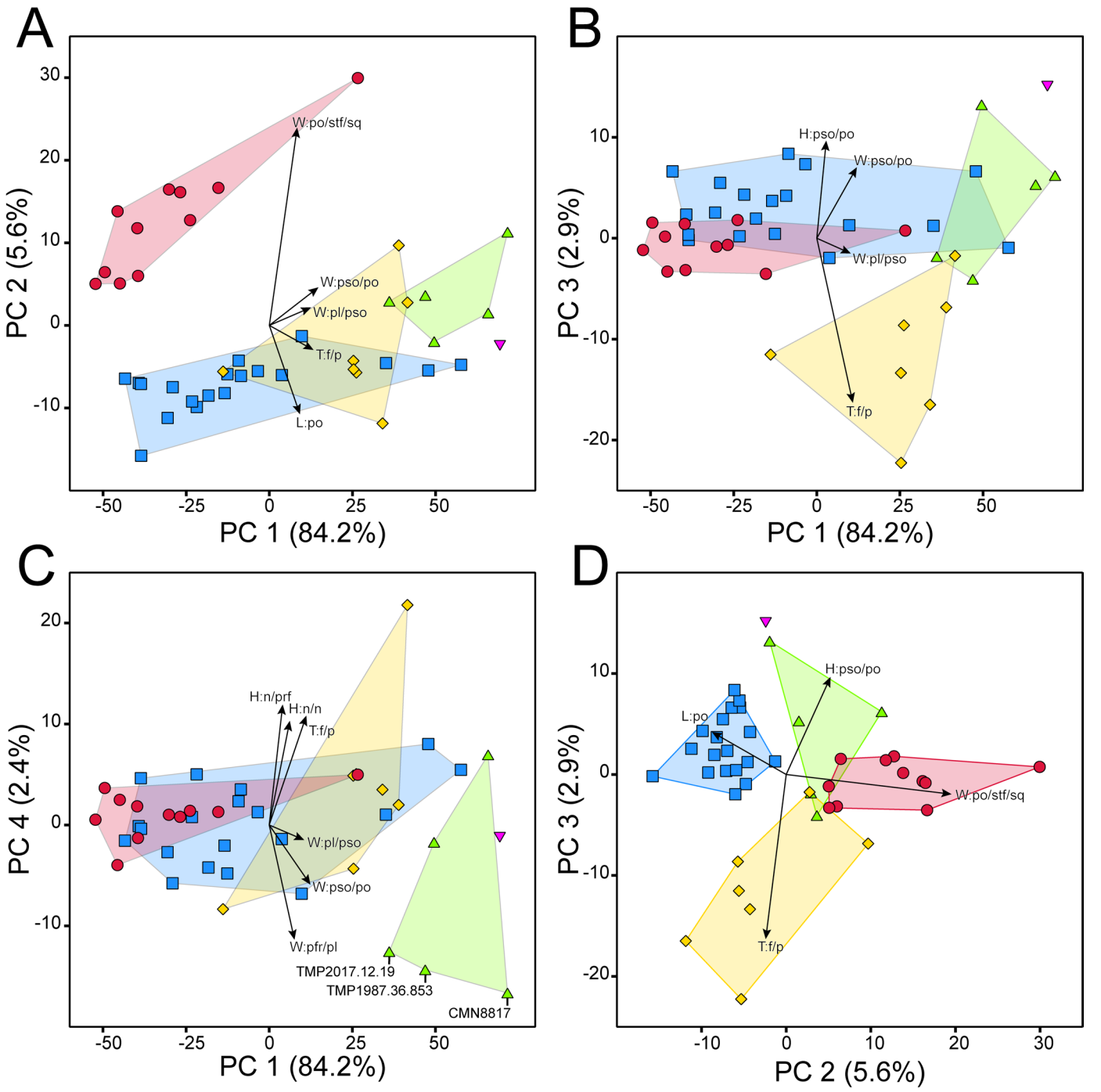

Figure 14. PCA of non-transformed linear measurements from Belly River Group pachycephalosaurian frontoparietals. Symbols: purple inverted triangle, TMP 1972.027.0001; blue squares, *Stegoceras validum*; green triangles, "*Hanssuesia sternbergi*"; yellow diamonds, *Colepiocephale lambei*; red circles, *Foraminacephale brevis*. Arrows indicate eigenvectors of variables; only variables that loaded at least |0.3| in either axis are displayed. Pachycephalosaurian taxa are most disparate in PC 2 and PC 3.

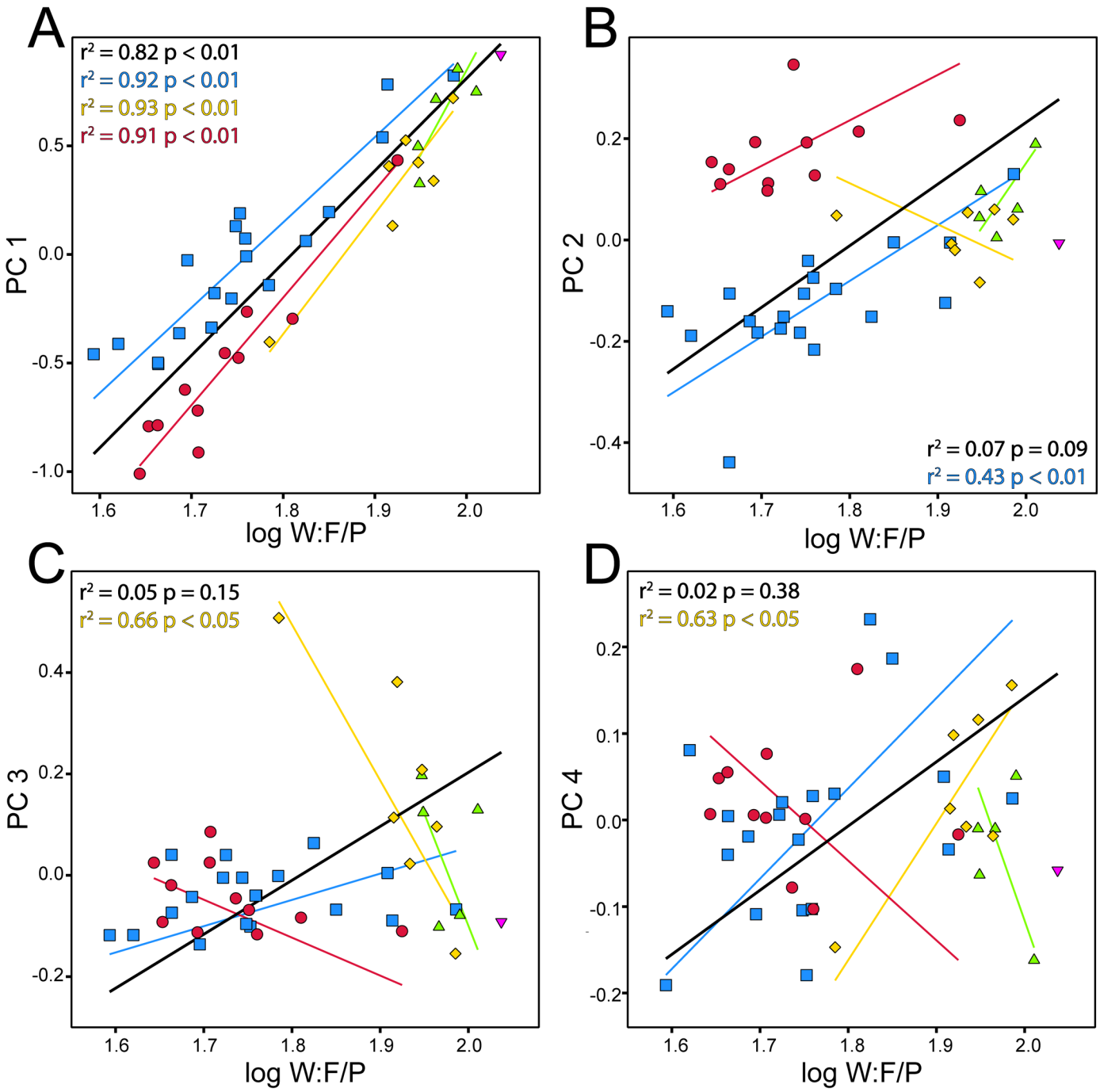

Figure 15. Relationship between PC scores from the PCA of log_{10}-transformed linear measurements and frontoparietal size. Symbols: purple inverted triangle, TMP 1972.027.0001; blue squares, *Stegoceras validum*; green triangles, "*Hanssuesia sternbergi*"; yellow diamonds, *Colepiocephale lambei*; red circles, *Foraminacephale brevis*. RMA regression results reported for the total sample (black line), followed by individual taxa if a significant relationship was identified. Regression results in descending order, after the total sample: A) PC 1, *Stegoceras validum*, *Colepiocephale lambei*, and *Foraminacephale brevis*. B) PC 2, *Stegoceras validum*. C) PC 3, *Colepiocephale lambei*. D) PC 4, *Colepiocephale lambei*. Note that while the total sample PC 2-4 scores do not correlate with frontoparietal width, scores for individual taxa may significantly correlate with frontoparietal width.

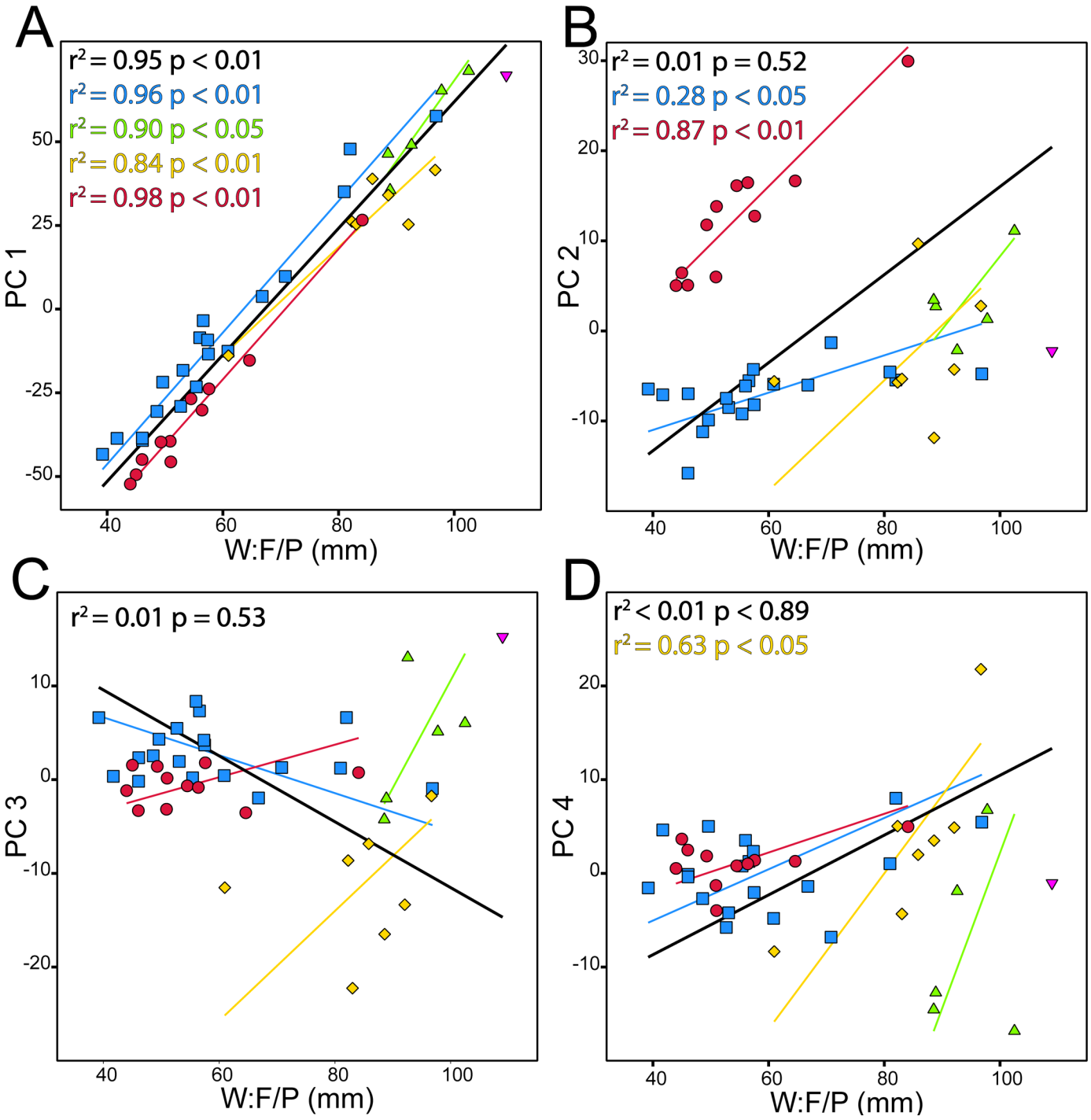

Figure 16. Relationship between PC scores from the PCA of non-transformed linear measurements and frontoparietal size. Symbols: purple inverted triangle, TMP 1972.027.0001; blue squares, *Stegoceras validum*; green triangles, "*Hanssuesia sternbergi*"; yellow diamonds, *Colepiocephale lambei*; red circles, *Foraminacephale brevis*. RMA regression results reported for the total sample (black line) and for individual taxa if a significant relationship was identified. Regression results in descending order, after the total sample: A) PC 1, *Stegoceras validum*, "*Hanssuesia sternbergi*", *Colepiocephale lambei*, and *Foraminacephale brevis*. B) PC 2, *Stegoceras validum* and *Foraminacephale brevis*. Note that while the total sample PC 2 scores do not correlate with frontoparietal width, scores for individual taxa may significantly correlate with frontoparietal width.

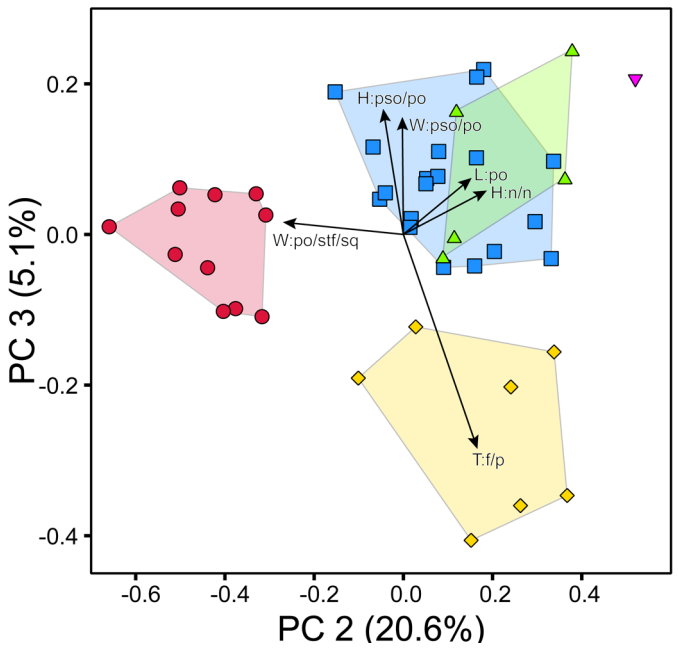

Figure 17. PC 2 and PC 3 of the L:F proportionate PCA of Belly River Group pachycephalosaurian frontoparietals. Symbols: purple inverted triangle, TMP 1972.027.0001; blue squares, *Stegoceras validum*; green triangles, "*Hanssuesia sternbergi*"; yellow diamonds, *Colepiocephale lambei*; red circles, *Foraminacephale brevis*. Arrows indicate eigenvectors of variables; only variables that loaded at least |0.3| in either axis are displayed. Belly River Group pachycephalosaurians are most disparate in this PCA iteration.

ly displaced from other "*Hanssuesia sternbergi*", large *Stegoceras validum*, and TMP 1972.027.001 in PC 4 of the non-transformed PCA (Fig. 14).

PCA of "*Hanssuesia sternbergi*", *Stegoceras validum*, and TMP 1972.027.0001: PC 1 variable loadings in the reduced taxonomic PCA's were similar to the Belly River Group PCA's (Tables S20-S23). PC 1 of the $\log_{10}$-transformed PCA explained 81.2% of the total variation. PC 1 of the $\log_{10}$-transformed PCA was not strongly loaded by H:N/Prf, but was by L:Pl. PC 2 of the $\log_{10}$-transformed PCA explained 4.2% of the total variation. It was strongly loaded positively by H:N/Prf and H:N/N, and strongly loaded negatively by L:Pl and H:Pl/Pso. PC 3 of the $\log_{10}$-transformed PCA explained 4.2% of the total variation. It was strongly loaded negatively by H:Pl/Pso, and W:Po/stf/Sq had the highest positive loading.

PC 1 of the non-transformed PCA explained 89.9% of the total variation. Variable loading along PC 1 were all similar to the Belly River Group non-transformed PCA, although it was additionally strongly loaded positively by W:Po/stf/Sq. PC 2 explained 2.9% of the total variation. PC 2 of the non-transformed PCA was strongly loaded positively by H:N/Prf and H:N/N, and strongly loaded negatively by W:Po/stf/Sq. PC 3 explained 1.8% of the total variation. It was strongly loaded positively by L:Pso,W:Prf/Pl, W:Pl/Pso, and L:Pl, and strongly loaded negatively by W:Pso/Po and L:Po.

"*Hanssuesia sternbergi*", *Stegoceras validum*, and TMP 1972.027.0001 do not show any separation in PC 2 or PC 3 of the $\log_{10}$-transformed, frontal length (L:F) proportionate, and dorsal width across the frontal-parietal contact (W:F/P) proportionate PCA (Figs. 18A, S6-8). Three specimens of "*Hanssuesia sternbergi*" (CMN 8817, TMP 1987.036.853, and TMP 2017.012.0019) are negatively separated from *Stegoceras validum*, TMP 1972.027.0001, and other "*Hanssuesia sternbergi*" (CMN 9148, TMP 1979.014.0853) along the PC 2 axis of the non-transformed PCA (Fig. 18B), but there is no taxonomic separation evident in PC 3 (Fig. S6). Both PCA iterations appeared to recover two distinct clusters of large frontoparietals (W:F/P > 80 mm), one cluster comprised of three "*Hanssuesia sternbergi*" (CMN 8817, TMP 1987.036.853, TMP 2017.012.0019), and the other with *Stegoceras validum*, TMP 1972.027.0001, and the remaining "*Hanssuesia sternbergi*". In PC 2 of the $\log_{10}$-transformed PCA, these three specimens of "*Hanssuesia sternbergi*" score similar to smaller specimens of *Stegoceras validum* which preserve diagnostic squamosal ornamentation (Fig. 18A; ROM 64183 and TMP 1984.005.0001; Schott and Evans 2012).

Dimorphism

The distribution of large frontoparietals (W:F/P > 80 mm) across PC 2 scores from the $\log_{10}$-transformed PCA iterations (of the reduced taxonomic sample, only including "*Hanssuesia sternbergi*", *Stegoceras validum*, and TMP 1972.027.0001) were indistinct from normal distributions (Fig. 18A; W = 0.89, p = 0.21; A = 0.45, p = 0.21). The Hartigan's Dip test did not indicate that this distribution was significantly multimodal (D = 0.13, p = 0.17). The distribution of PC 2 scores amongst large frontoparietals was significantly best fit by a unimodal distribution (AIC = -25.33). However, the Jenks Natural Break Optimization identified a natural break in the distribution (GVF = 0.87). This natural gap separates three "*Hanssuesia sternbergi*" (CMN 8817, TMP 1983.036.0363, TMP 2017.012.0019) from other "*Hanssuesia sternbergi*", *Stegoceras validum*, and TMP 1972.027.0001 (Table 2).

The distribution of large frontoparietals in PC 2 of the non-transformed PCA was significantly different from a uniform distribution (Fig. 18B; W = 0.83, p = 0.04; A = 0.72, p = 0.04). However, the Hartigan's Dip test did not identify a significantly multimodal distribution in the non-transformed PC 2 scores (D = 0.13, p = 0.17). This distribution was significantly best fit by a unimodal distribution (AIC = 57.16). The Jenks Natural Break Optimization identified a natural

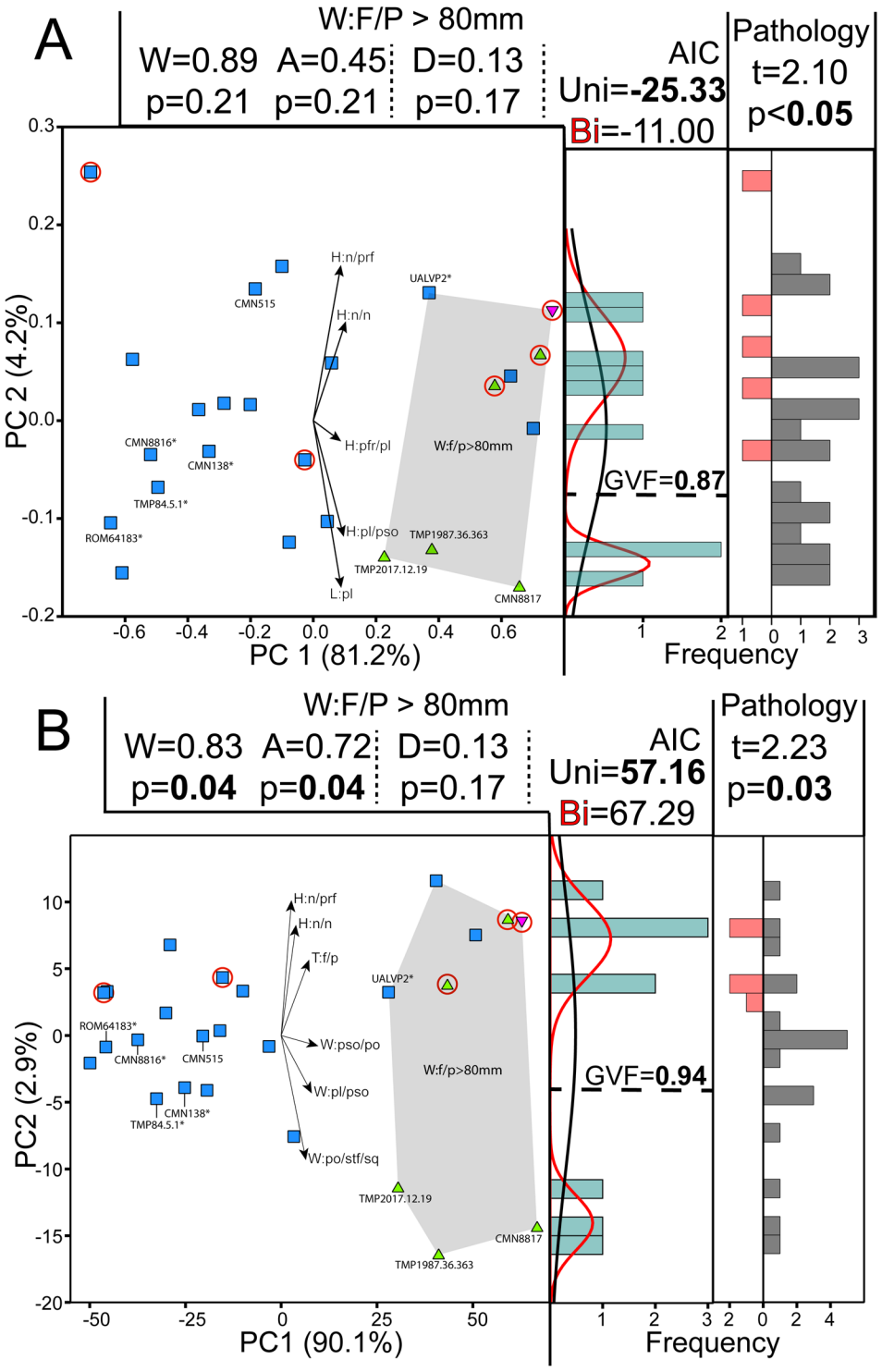

Figure 18. PCA's of frontoparietals from TMP 1972.027.0001, "*Hanssuesia sternbergi*", and *Stegoceras validum*. A) $\log_{10}$-transformed linear measurement results. B) non-transformed linear measurement results. Symbols: purple inverted triangle, TMP 1972.027.0001; green triangles, "*Hanssuesia sternbergi*"; blue squares, *Stegoceras validum*; red circles, pathological specimens. Grey convex hull: frontoparietal specimens with W:F/P > 80 mm. Specimens associated with squamosal ornamentation diagnostic of *Stegoceras validum* are labeled and identified with an asterisk. The lectotype of *Stegoceras validum* (CMN 515), and select specimens of "*Hanssuesia sternbergi*" are also labeled. Arrows indicate eigenvectors of variables; only variables that loaded at least |0.3| in either axis are displayed. Left histogram: distribution of large *Stegoceras validum* across PC 2. Black line: best fitting unimodal distribution; red lines: best fitting bimodal distribution (based on mixture analysis). Dashed line indicates the position of a natural gap based on a Jenks Natural Break Optimization function. AIC values from mixture analysis; AIC values of significantly "better fitting" distributions are bolded if applicable. Right (bi) histogram: distribution of pathological (red, left) and non-pathological (grey, right) *Stegoceras validum* across PC 2. Abbreviations: A, Anderson-Darling statistic; Bi, AIC for bimodal distribution; D, Hartigan's Dip statistic; GVF, goodness of variance fit; t, Student's t statistic (assuming equal variance); Uni, AIC for unimodal distribution; W, Shapiro-Wilk statistic. While large frontoparietals are not significantly bimodal, pathological specimens have a significantly higher average PC 2 score compared to non-pathological specimens.

break in this distribution (GVF = 0.94). The natural break separated large frontoparietals into the same groups as in the log_{10}-transformed PCA.

All pathological specimens were restricted to the positive side of PC 2 in both iterations (except for UALVP 8502 in the log_{10}-transformed PCA, PC 2 = -0.04, Fig. 18). The variance of pathological and non-pathological specimen PC 2 scores did not significantly differ in either iteration (log_{10}-transformed F = 1.16, p = 0.72; non-transformed F = 6.95, p = 0.08). The average PC 2 scores of pathological specimens are significantly larger than non-pathological specimens in both PCA iterations (log_{10}-transformed t = 2.10, p = 4.7 E-2, non-transformed t = 2.23, p = 0.03; Fig. 18).

Frontoparietal Allometry in *Stegoceras validum* (= "*Gravitholus albertae*" and "*Hanssuesia sternbergi*")

Table 3 summarises the RMA regression results for bivariate regressions of *Stegoceras validum* (including "*Hanssuesia sternbergi*" and "*Gravitholus albertae*"). All log_{10}-transformed linear measurements significantly positively correlated with the width across the frontoparietal contact (W:F/P; Fig. 19). The r^2 values ranged from 0.59

Table 2. Statistical group assignments of large (W:F/P > 80 mm) *Stegoceras validum*. Groupings based visual inspection and Jenks Natural Break Optimizations of PC 2 scores from the reduced taxon PCAs (Fig. 18). All specimens are derived from within or near Dinosaur Provincial Park, AB, Canada. Holotypes are designated with an asterisk. Abbreviations: OF, Oldman Formation; DPF, Dinosaur Park Formation.

Specimen	Stratigraphic horizon	Previous taxonomic assignment	Frontonasal boss morph
AMNH 5388	OF or DPF (uncertain); Evans et al. (2013)	*Stegoceras validum*; Brown and Schlaikjer (1943)	Tall
CMN 8817*	OF or DPF (uncertain); Evans et al. (2013)	*Hanssuesia sternbergi*; Brown and Schlaikjer (1943)	Short
CMN 9148	OF or DPF (uncertain); Evans et al. (2013)	*Hanssuesia sternbergi*; Sullivan (2003)	Tall
ROM 53555	OF or DPF (uncertain); Evans et al. (2013)	*Stegoceras validum*; Schott et al. (2011)	Tall
TMP 1972.027.0001*	Oldman Formation; Sullivan (2003)	*Gravitholus albertae*; Wall and Galton (1979)	Tall
TMP 1979.014.0853	OF or DPF (uncertain); Evans et al. (2013)	*Hanssuesia sternbergi*; Sullivan (2003)	Tall
TMP 1987.036.0363	OF or DPF (uncertain); Evans et al. (2013)	*Hanssuesia sternbergi*; Sullivan (2003)	Short
TMP 2017.012.0019	Lower 5 m of Dinosaur Park Formation; TMP collection records	*Hanssuesia sternbergi*; This study	Short
UALVP 2	22 m above Oldman/Dinosaur Park Formation Contact, Schott et al. (2011)	*Stegoceras validum*; Gilmore 1924; Schott et al. (2011)	Tall

Table 3. RMA regression results for linear frontoparietal measurements vs frontoparietal width in *Stegoceras validum* (= "*Hanssuesia sternbergi*" and "*Gravitholus albertae*").

Measurement	n	r^2	slope	ci	intercept	ci	p	allometry
H:N/N	42	0.74	1.76	1.37 – 2.11	-1.92	-2.55 – -1.22	2.72 E-13	+
H:N/Prf	42	0.66	1.62	1.29 – 1.93	-1.76	-2.33 – -1.19	5.47 E-11	+
H:Prf/Pl	51	0.70	1.76	1.47 – 2.06	-2.00	-2.56 – -1.49	1.51 E-14	+
H:Pl/Pso	52	0.72	1.81	1.54 – 2.09	-2.19	-2.71 – -1.72	2.14 E-15	+
H:Pso/Po	53	0.77	1.51	1.33 – 1.68	-1.49	-1.81 – -1.18	4.00 E-18	+
T:F/P	71	0.74	2.16	1.85 – 2.43	-2.31	-2.81 – -1.79	8.71 E-22	+
L:Prf	18	0.61	0.80	0.54 – 0.98	-0.26	-0.59 – 0.18	1.03 E-4	–
L:Pl	54	0.70	1.10	0.85 – 1.30	-0.85	-1.19 – -0.39	3.88 E-15	ISO
L:Pso	54	0.83	0.77	0.66 – 0.87	-0.08	-0.26 – 0.11	2.22 E-21	–
L:Po	37	0.89	0.85	0.75 – 0.95	0.03	-0.16 – 0.22	2.94 E-18	–
L:Sq	9	0.83	0.69	0.43 – 0.89	0.08	-0.25 – 0.55	5.84 E-4	–
L:F	42	0.59	0.57	0.45 – 0.66	0.63	0.46 – 0.84	2.64 E-9	–
L:P	25	0.86	0.72	0.59 – 0.83	0.43	0.25 – 0.66	3.27 E-11	–
W:N/Prf	45	0.77	0.93	0.81 – 1.05	-0.26	-0.48 – -0.04	3.62 E-15	ISO
W:Prf/Pl	52	0.82	0.75	0.66 – 0.82	0.30	0.17 – 0.44	1.46 E-20	–
W:Pl/Pso	55	0.92	0.75	0.70 – 0.80	0.44	0.35 – 0.53	1.95 E-31	–
W:Pso/Po	58	0.96	0.82	0.79 – 0.87	0.35	0.27 – 0.42	1.90 E-40	–
W:Po/stf/Sq	37	0.91	0.81	0.71 – 0.89	0.22	0.06 – 0.40	4.27 E-20	–

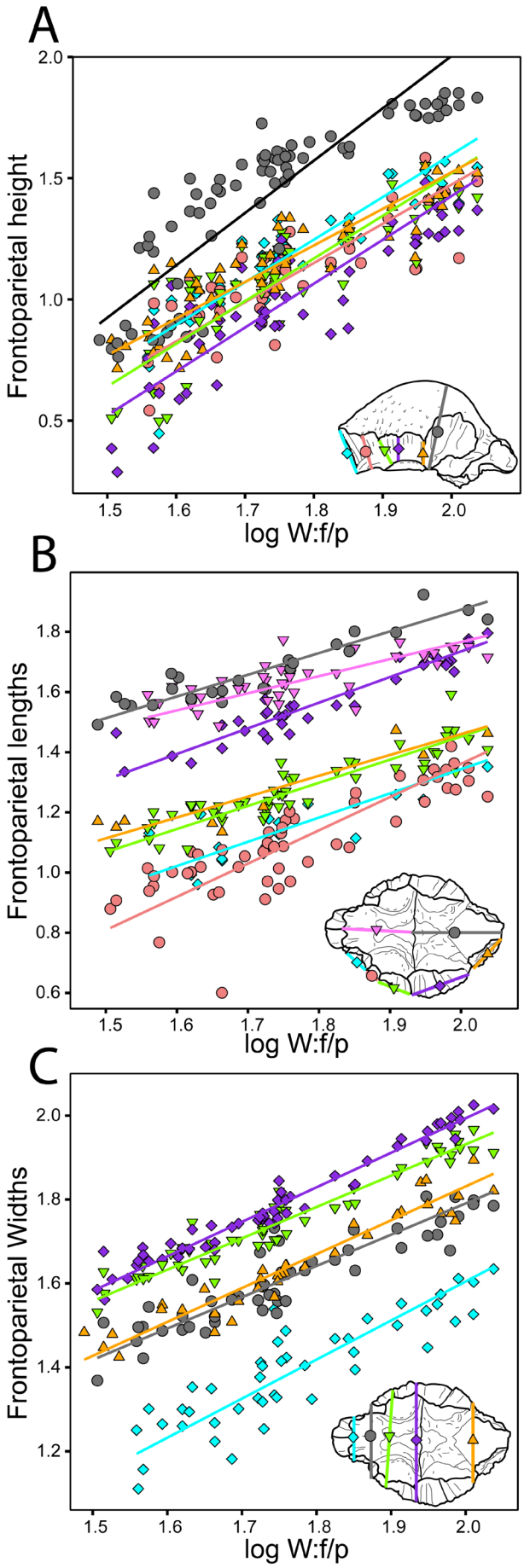

Figure 19. Frontoparietal allometry relative to frontoparietal width (W:F/P) in *Stegoceras validum*. A) RMA regressions of frontoparietal heights vs. W:F/P. Symbols: blue diamonds, H:N/N; coral circles, H:N/Prf; inverted green triangles, H:Prf/Pl; purple diamonds, H:Pl/Pso; orange triangles, H:Pso/Po; grey circles, T:F/P. B) RMA regressions of frontoparietal heights vs W:F/P. Symbols: blue diamonds, L:Prf; coral circles, L:Pl; inverted green triangles, L:Pso; purple diamonds, L:Po, inverted blue triangles, L:F, grey circles, L:P. C) RMA of frontal and parietal widths vs. W:F/P. Symbols: blue diamonds, W:N/Prf; grey circles, W:Prf/Pl; inverted green triangle, W:Pl/Pso; purple diamonds, W:Pso/Po; orange triangles, W:Po/stf/Sq. Allometric scaling within *Stegoceras validum* frontoparietals is largely consistent with the results of Schott et al. (2011).

(L:F) to 0.96 (W:Pso/Po). Frontoparietal widths regressed to W:F/P generally had the highest r^2 values, followed by frontoparietal lengths, then frontoparietal heights (including frontoparietal thickness).

All frontoparietal heights (including frontoparietal thickness) scale with positive allometry relative to W:F/P. The 95% confidence interval (CI) around the slopes of T:F/P and H:Pso/Po are exclusive, with T:F/P scaling with stronger positive allometry compared to H:Pso/Po. Otherwise, CI around slopes of frontoparietal heights relative to W:F/P all overlap each other. All frontoparietal lengths scale with negative allometry with respect to W:F/P, except for L:Prf, which scales isometrically relative to W:F/P. The 95% CI around the slope of L:Pso is higher than, and excludes the 95% CI of L:F. Similarly, the CI around the slope of L:Pl is higher, and excludes the 95% CI around the slope of both L:F and L:P. Otherwise, 95% CI around the slopes of linear measurements of the same allometric relationship overlap each other. The W:N/Prf is the only width that scales isometrically with respect to W:F/P. All other widths are negatively allometric with respect to W:F/P.

Phylogenetic Analyses

Parsimony analysis: The revised matrix used here resulted in 4529 MPTs. The strict consensus did not resolve any clades within Pachycephalosauria. A 50% majority rules consensus tree failed to recover a resolved Pachycephalosauridae (sensu Madzia et al. 2021), recovering a polytomy of *Colepiocephale lambei*, *Stegoceras validum*, *Wannanosaurus yansiensis* and a clade containing all pachycephalosaurines (100% of MPTs; Fig. 20A). Pachycephalosaurinae (all pachycephalosaurids more closely related to *Pachycephalosaurus wyomingensis* than to *Stegoceras validum*; Madzia et al. 2021) was recovered in a polytomy comprised of terminal taxa and one clade that

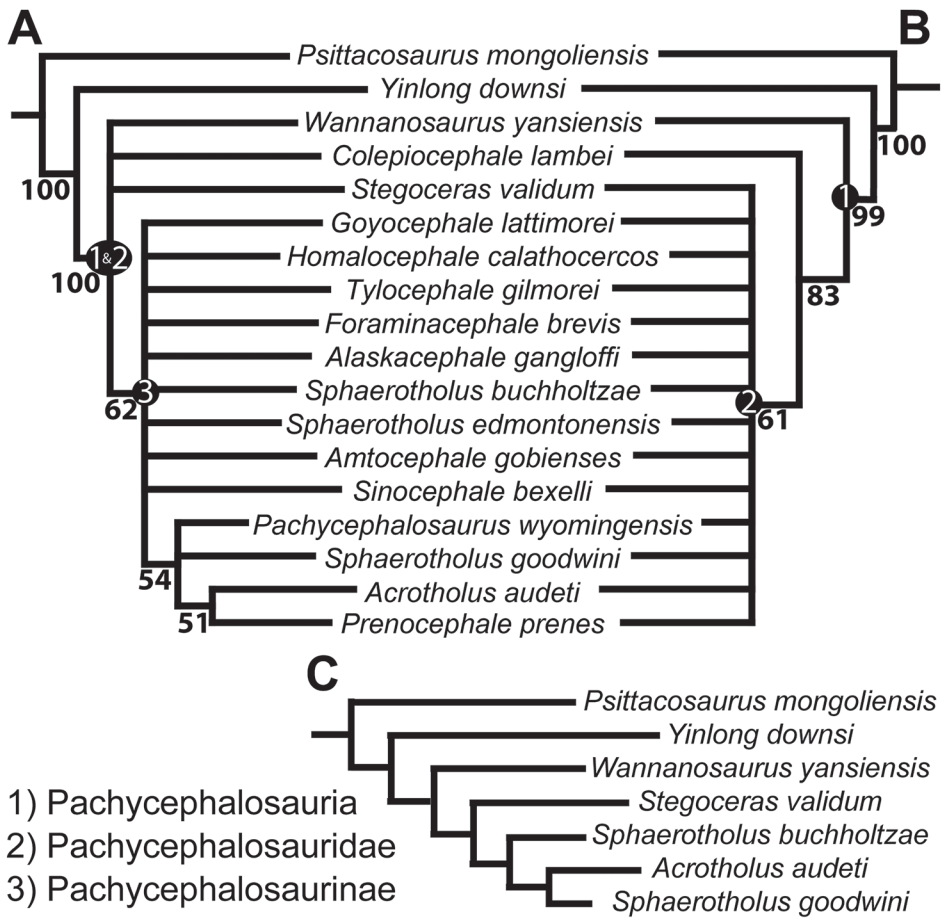

Figure 20. Majority rules (50%) consensus trees from parsimony and Bayesian analyses. A) Consensus tree of 4529 MPTs recovered from an exhaustive search parsimony analysis. Numbers by nodes indicate the percentage of MPTs in which they were recovered. B) Consensus tree of a Bayesian analysis. Posterior probabilities are presented as percentages at the base of the nodes. C) Agreement subtree of all MPTs. Previously named clades are labeled by their respective nodes where applicable.

contains *Pachycephalosaurus wyomingensis* and *Sphaerotholus goodwini*, and *Acrotholus audeti* + *Prenocephale prenes* (62% of MPTs). The sole clade within the pachycephalosaurine polytomy was recovered in 54% of the most parsimonious trees, and the clade *Acrotholus audeti* + *Prenocephale prenes* was recovered in 51% of the MPTs.

The agreement subtree pruned 11 pachycephalosaurians, which all had inconsistent relationships amongst the MTPs. These included: *Alaskacephale gangloffi*, *Amtocephale gobiensis*, *Colepiocephale lambei*, *Foraminacephale brevis*, *Goyocephale lattimorei*, *Homalocephale calathocercos*, *Pachycephalosaurus wyomingensis*, *Prenocephale prenes*, *Sinocephale bexelli*, *Sphaerotholus edmontonensis*, and *Tylocephale gilmorei*. The remaining five pachycephalosaurians formed successive sister taxa to a derived clade. *Wannanosaurus yansiensis*, *Stegoceras validum*, and *Sphaerotholus buchholtzae* were all successive sister taxa to a clade comprising *Acrotholus audeti* + *Sphaerotholus goodwini*.

Bayesian analyses: The majority rules Bayesian analysis (collapsing clades with less than 50% posterior probability) recovers *Colepiocephale lambei* as more derived than *Wannanosaurus yansiensis* (posterior probability; PP = 83%), but not as a pachycephalosaurid (equally related to *Pachycephalosaurus wyomingensis* and *Stegoceras validum*; Madzia et al., 2021) (Fig. 20B). Pachycephalosauridae was recovered as the sister taxon to *Colepiocephale lambei* in an unresolved polytomy (PP=61%).

The fully resolved Bayesian analysis recovers several clades corroborated by the parsimony analysis, as well as unique sister group relationships, although many of these have low support (PP<10; Fig. 21). *Wannanosaurus yansiensis* and *Colepiocephale lambei* are recovered as successive sister taxa to Pachycephalosauridae (sensu Madzia et al. 2021), which shows a high support value (PP=62%) and reflects the topology of the parsimony consensus in that both *Colepiocephale lambei* and *Stegoceras validum* are basal to pachycephalosaurines (Fig. 20A). Pachycephalosaurinae (all pachycephalosaurids more closely related to *Pachycephalosaurus wyomingensis* than to *Stegoceras validum*; Madiza et al. 2021) is moderately supported (PP=31%; Fig. 21).

Within Pachycephalosaurinae, two monophyletic clades are recovered, both with weak support (PP=8%; Fig. 21). One contains *Homalocephale calathocercos* sister to the clade *Alaskacephale gangloffi* + *Goyocephale lattimorei*, the latter showing modest support values (PP=23%). The other clade contains two clades; *Amtocephale gobiensis* + *Foraminacephale brevis* with relatively low support (PP=17%), and a clade

containing all taxa between *Pachycephalosaurus wyomingensis* and *Sinocephale bexelli*, which shows weak support (PP=9%). Within this weakly supported clade, *Sinocephale bexelli* is sister to all other representatives including a *Sphaerotholus* clade (*Sphaerotholus buchholtzae* + *Sphaerotholus edmontonensis*, PP=26%), and a clade containing *Acrotholus audeti, Pachycephalosaurus wyomingensis, Prenocephale prenes, Sphaerotholus goodwini,* and *Tylocephale gilmorei* (PP=21%). This clade is similar in its composition to a clade recovered in the parsimony analysis (Figs. 20A, 21). However, this clade also includes *Tylocephale gilmorei*, which forms a clade with *Acrotholus audeti* + *Prenocephale prenes* (PP=16%). The clade *Acrotholus audeti* + *Prenocephale prenes* was also recovered in the majority rules parsimony analysis, being recovered in

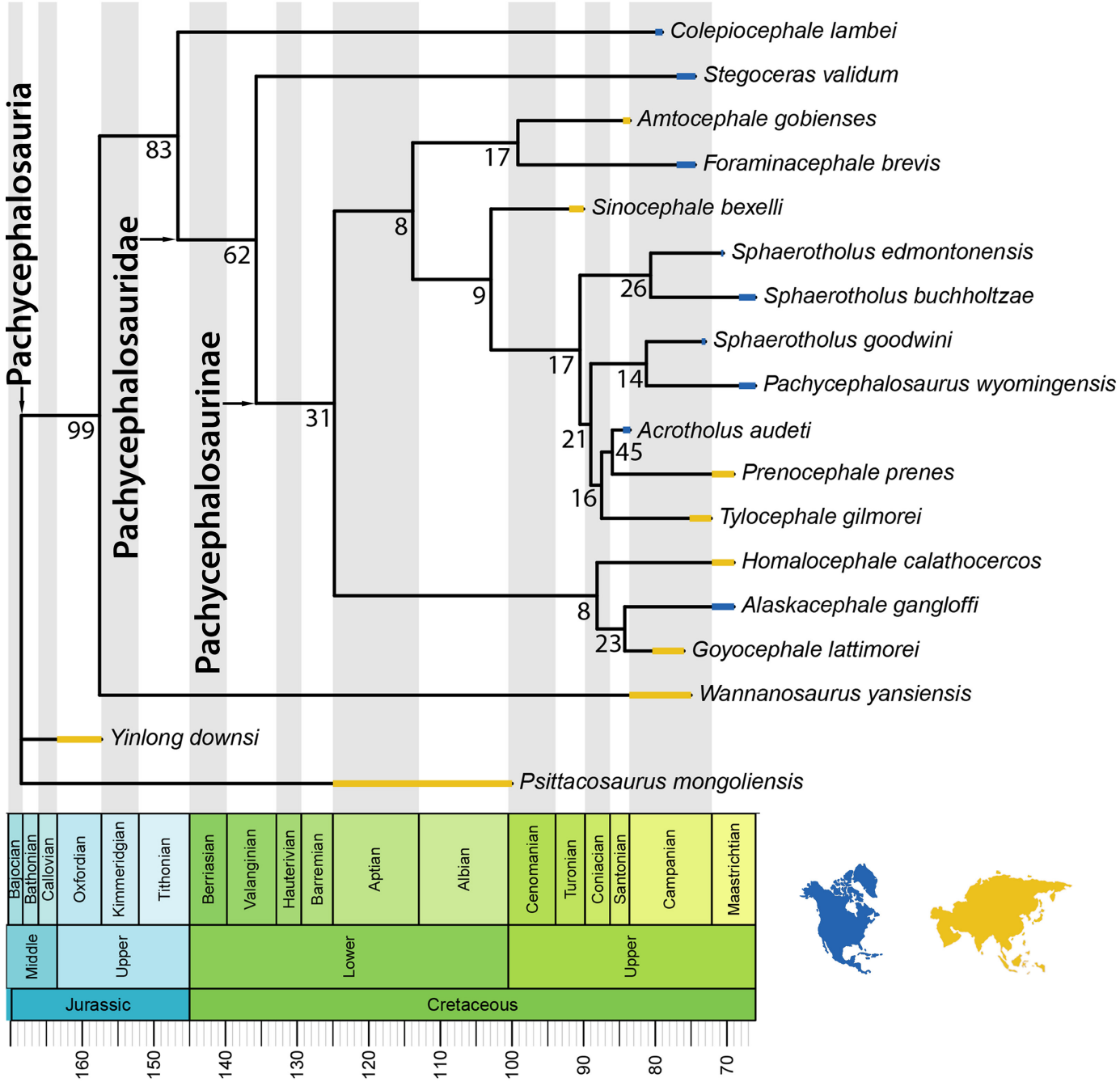

Figure 21. Time calibrated Bayesian tree with forced resolution. Time intervals are colour-coded to the region from which they were recovered (blue = North America; orange = Asia). Node support is given as posterior probabilities in percentages, at their respective nodes. The base of the tree is the default output of Mr. Bayes v 3.2.7 and not a real polytomy. *Yinlong downsi* is not unresolved with outgroup taxon, *Psittacosaurus mongoliensis*, and Pachycephalosauria. Previously named clades that were recovered are labeled with arrows directed to their respective nodes.

51% of the MPTs (Fig. 20A), although *Prenocephale prenes* was pruned when constructing the agreement subtree. Bayesian analysis recovers this clade with 45% posterior probability, one of the highest supports under the 50% threshold for majority (Fig. 21). A further difference between the parsimony and Bayesian analysis is the recovery of a sister relationship between *Pachycephalosaurus wyomingensis* and *Sphaerotholus goodwini* (PP=14%) rather than an unresolved relationship (Fig. 20A), although the support is relatively low (Fig. 21). This topology renders *Sphaerotholus* a polyphyletic genus with *Sphaerotholus goodwini* not just being sister to *Pachycephalosaurus wyomingensis*, but also nested within a more inclusive clade (exclusive of *Sphaerotholus buchholtzae* and *Sphaerotholus edmontonensis*) that has greater support (PP=21%) than its sister relationship.

Character support for recovered clades is fairly ambiguous, reflected in the generally low posterior probabilities due to large amounts of missing data (Supplemental Data 3). However, Pachycephalosauridae is supported by three unambiguous synapomorphies (28[1] closure of supratemporal fenestrae through ontogeny although this is polymorphic in *Stegoceras validum*, 32[2] frontoparietal doming includes supraorbitals, and 37[1] broad exposure of intersquamosal bar except in the most exclusive clade including P*achycephalosaurus wyomingensis* and *Prenocephale prenes* where it is restricted or absent (37[2]), and is polymorphic in *Stegoceras validum* - see Character List - Supplemental Data 2). Pachycephalosaurinae is supported by six unambiguous synapomorphies (12[1] a transversely flattened ischial-pubic peduncle, 15[1] an arched premaxilla-maxilla diastema, 34[0] inflated parietal that reaches the posterior margin of the skull, forming a downturned parietal (*Stegoceras validum* is polymorphic, TMP 1972.027.0001 shows this feature), 36[1] parietal squamosal bar below the primary node row is present and maintains the same depth, or slightly narrows laterally, 41[1] presence of a large squamosal corner node below the primary node row on the parietal squamosal bar, and 48[1] presence of nasal ornamentation). The clade (*Homalocephale calathocercos* + (*Alaskacephale gangloffi* + *Goyocephale lattimorei*)) is supported by two unambiguous synapomorphies (42[1] possession of at least two enlarged ventrolateral corner nodes on the squamosal (shared with *Pachycephalosaurus*), and 47[1] a convex dorsolateral skull margin along the postorbital and squamosal viewed dorsally (also observed in *Prenocephale prenes*). The clade containing *Alaskacephale gangloffi* and *Goyocephale lattimorei* is supported by enlarged dorsal ornamentation on the squamosal (49[1]), a feature also observed in *Pachycephalosaurus wyomingensis*. The most exclusive monophyletic clade containing *Foraminacephale brevis* and *Pachycephalosaurus wyomingensis* is supported by four unambiguous synapomorphies (35[1] the ventral margin of the squamosal viewed laterally, slopes steeply ventral laterally, 39[1] a row of small tubercles ventrally adjacent to the primary node row (this is lost in the most exclusive clade containing *Pachycephalosaurus wyomingensis* and *Prenocephale prenes* (39[0])), 40[0] nodes of the primary node row are all sub equally sized, and 42[0] possession of a single enlarged ventrolateral corner node (a second enlarged ventrolateral corner node is observed in *Pachycephalosaurus wyomingensis* 42[1])). The most exclusive monophyletic clade containing *Pachycephalosaurus wyomingensis* and *Sphaerotholus* spp. is supported by two synapomorphies (29[2] a posterodorsally inclined temporal chamber, except for *Sphaerotholus goodwini*, and 30[0] absence of grooves separating frontonasal boss from supraorbital lobes). *Pachycephalosaurus wyomingensis* and *Sphaerotholus goodwini* are united by a continuous, convex dorsal margin between the postorbital and posterior supraorbital and parietal (33[1]). This character state also unites *Sphaerotholus buchholtzae* and *Sphaerotholus edmontonensis*, although it is homoplastic with regards to *Pachycephalosaurus wyomingensis* and *Sphaerotholus goodwini*. The most exclusive clade containing *Pachycephalosaurus wyomingensis* and *Prenocephale prenes* is supported by four synapomorphies (27[1] the position of the bilateral depressed insertion area for the atlanto-occipital capsular membrane/ligament is dorsal to the foramen magnum, 37[2] a restricted or absent intersquamosal process of the parietal, 39[0] absence of minute tubercle ornamentation on the posterior wall of the squamosals (ornamentation is extensive over the posterior wall in *Tylocephale gilmorei* (39[2])), and 46[1] possession of enlarged circular nodes along the dorsolateral edge of the postorbital).

DISCUSSION

Validity of "*Gravitholus albertae*"

Some of the previous anatomical interpretations of TMP 1972.027.0001 were clearly influenced by the fusion of the peripheral elements to the frontoparietal (e.g., incipient incorporation of the posterior supraorbitals and postorbitals into the dome; misidentification of the nasal, prefrontals, left posterior supraorbital; Wall and Galton 1979; Sullivan 2003). However, other misinterpretations are apparent without a segmented model such the entire specimen representing a frontoparietal, the absence of squamosal nodes (Wall and Galton 1979; Longrich et al. 2010), and the presence of a parietosquamosal shelf (Williamson and Carr 2002).

Sullivan (2003) correctly noted that the dome width and thickness, as well as the pathological depression of TMP 1972.027.0001 should not be considered as diagnostic features. The dome is as thick as in some specimens of *Colepiocephale lambei* (e.g., TMP 2000.057.0001), "*Hanssuesia sternbergi*" (CMN 9148), and *Stegoceras val-*

idum (ROM 53555). The extreme dome width of TMP 1972.027.0001 while unique, is consistent with ontogenetic trends in *Stegoceras validum*, where the postorbital lateral shelf is reduced as the postorbitals are incorporated into the dome (Schott et al. 2011).

Giffin (1989a) presented endocranial measurements for numerous pachycephalosaurid specimens. In her text, she compared TMP 1972.027.0001 (W:F/P = 108.99 mm) to CMN 138 and UALVP 8501 (W:F/P = 53.1 mm and 38.81 mm respectively; the latter is currently regarded as *Foraminacephale brevis*; Sullivan 2003; Schott and Evans 2017). Giffin concluded that TMP 1972.027.0001 preserved a remarkably small endocranium (L:olf/soc = 34 mm, compared to 39 mm in CMN 138 and an estimated 29 mm in UALVP 8501 (which does not preserve the olfactory bulbs)), and supported the validity of "*Gravitholus albertae*". This assessment is here refuted as TMP 1972.027.0001 preserves an endocranial width that is not unique amongst Belly River Group pachycephalosaurians.

Giffin (1989a) additionally noted that the endocranial impression on TMP 1972.027.0001 was unique because the width across the olfactory bulbs is slightly wider than the width across the cerebrum. Interestingly, the same condition is apparent in the lectotype of *Stegoceras validum* (CMN 515). The width of the cerebral impression on the frontoparietal is extremely variable amongst Belly River Group pachycephalosaurians, and is not strongly correlated with frontoparietal size. TMP 1972.027.0001 does not possess a distinctly small endocranial impression, and should not be considered as a diagnostic feature of "*Gravitholus albertae*". Overall, specimens of *Colepiocephale lambei* and *Foraminacephale brevis* tend to have wider cerebral impressions on the frontoparietals, compared to "*Hanssuesia sternbergi*", *Stegoceras validum*, and TMP 1972.027.0001. This is not to say that the cerebrum is larger in the former taxa, only that the dorsal impression formed by the frontoparietal is wider as preserved. The laterosphenoid also contributes to the dorsolateral roof of the cerebrum (e.g., TMP 2000.026.0001; Fig. S1) and its preservation across specimens and taxa is variable. Measuring the width of the impression of the cerebrum along the frontoparietal suture may not accurately relate to the absolute width of the cerebrum. Instead, it may more accurately describe the relationship between the frontoparietal and laterosphenoid, and how they individually contribute to the endocranial roof, with the laterosphenoids restricting the exposure of the frontoparietal on the roof of the endocranium to varying degrees. Similar neurocranial variation is apparent in cf. *Prenocephale* (MPC-D 100/1207; Fig. 7B in Evans et al. 2018), where the cerebral fossa on the frontoparietal is separated from the impression of the olfactory bulbs by sutural surfaces for the neurocranial bones.

TMP 1972.027.0001 is morphologically consistent with a mature "end-stage" *Stegoceras validum*, and so is referred to this taxon. Unique features of TMP 1972.027.0001, such as a down-turned parietal and a dome that laterally extends beyond the lateral ridge are the logical end stages (or continuations) of previously recognised ontogenetic trends in *Stegoceras validum* – which include the reduction of the lateral and posterior shelves (Schott et al. 2011; Sternberg [1945] phrased the down-turned parietal as the opposite state of having a horizontal parietal shelf). Additionally, the smooth dorsal surface of the nasals is consistent with maturity, where the immature texture on the nasal (e.g., UALVP 2) has become smooth.

In addition to morphology, TMP 1972.027.0001 is histologically (based on SμCT images) consistent as a mature *Stegoceras validum*. Schott et al. (2011) observed a decrease in relative void space through ontogeny based on an ontogenetic series of HRCT images of *Stegoceras validum*. Void space (along a single HRCT coronal slice at the contact for the posterior supraorbital and postorbital) of juvenile *Stegoceras validum* (AMNH 5450) was calculated at 20.1%, whereas void space in the adult individual (ROM 53555) was calculated at 7.27% (Schott et al. 2011). Binary SμCT images of TMP 1972.027.0001 initially suggested it was more vascularized than juvenile *Stegoceras validum* (36.09% void space). However, SμCT images of TMP 1972.027.0001 are thinner and have a higher resolution than the HRCT images in Schott et al. (2011). When slice thickness and pixel sizes of SμCT images of TMP 1972.027.0001 are adjusted to be comparable to the HRCT images of ROM 53555, the relative void space is nearly identical (7.23% vs. 7.27%). Relative void space in mature specimens of *Acrotholus audeti* (TMP 2008.045.0001, 1.72%, slice thickness = 250 μm, pixel size = 118 μm by 118 μm; Evans et al. 2013), *Foraminacephale brevis* (TMP1987.050.0029, 0.37%, slice thickness = 250 μm pixel size = 244 μm by 244 μm; Schott and Evans 2017), and *Sphaerotholus buchholtzae* (DMNH EPV.97077, 2.5%; Woodruff et al. 2021; slice thickness = 240 μm, pixel size = 110 μm; Bourke et al. 2014) are less than in mature *Stegoceras validum*. TMP 1972.027.0001 is therefore histologically consistent with adult *Stegoceras validum* (ROM 53555). Differences in slice thickness and particularly pixel size should be considered in future studies that compare the amount of void space between binarized CT images of different specimens.

Nirody et al. (2022) calculated frontoparietal void density along all coronal HRCT slices imaged from frontoparietal domes of *Stegoceras validum*, at slice thicknesses and resolutions nearly identical to the SμCT images of TMP 1972.027.0001. Nirody et al. (2022) identified an increase in void density from flat-headed to partially domed specimens, opposite to the results of Schott et al. (2011). Nirody et al.

(2022) suggested the pattern observed by Schott et al. (2011) was due to a "single slice" analysis, whereas the Nirody et al. (2022) calculated void density and variation throughout the anteroposterior length of frontoparietals. However, the region analysed by Schott et al. (2011) (at the posterior supraorbital-postorbital contact; W:Pso/Po) shows relatively little interslice variation (~19-22% AMNH 5450, and ~31-37% in TMP 1984.005.0001), particularly compared to other regions of the frontoparietal that show much higher inter-slice variation in vascular density (anterior and posterior regions of the frontals and parietals respectively). AMNH 5450 and TMP 1984.005.0001 were rescanned by Nirody et al. (2022) at a resolution roughly twice that of the scanning parameters used by Schott et al. (2011) with slice thicknesses and resolutions within 4 μm of the SμCT images of TMP 1972.027.0001. We suggest that the difference in vascular percentage results between Nirody et al. (2022) and Schott et al. (2011) is the result of differing scanning parameters, particularly scanning resolution (slice thickness and pixel size). The higher resolution scans of Nirody et al. (2022) are more suitable to identify and binarize smaller void regions, particularly in the dense dorsal region (Zone III, Goodwin and Horner 2004), which is apparent when the CT images provided by both studies are compared. Zone III is proportionally much smaller in AMNH 5450 than in TMP 1984.005.0001 (Schott et al. 2011), which may explain why the vascular density percentages from the higher resolution images do not significantly differ from the lower resolution images studied by Schott et al. (2011).

Interestingly, the vascular density based on comparable CT image resolutions of TMP 1984.005.0001 (Nirody et al. 2022) and TMP 1972.027.0001 are nearly identical, whereas the vascular density of the adult UCMP 130051 was dramatically lower (~2-3% vascularity in the region surrounding W:Pso/Po). This is much denser than the adult vascularity percentage calculated by Schott et al. (2011) for ROM 53555, despite a much higher image resolution for UCMP 130051 (100 μm), compared to ROM 53555 (250 μm). The slice thickness and image resolutions of UCMP 130051 are more comparable to our SμCT images of TMP1972.027.0001 (50 μm), yet the difference in void densities between these specimens is greater than between ROM 53555 and TMP1972.027.0001. This may indicate that the frontoparietal dome of UCMP 130051 is uniquely dense, at least when compared to *Stegoceras validum*, and may support the referral of UCMP 130051 to a new taxon (see Goodwin 1990, Williamson and Carr 2002, Sullivan 2003, and Schott et al. 2009 for discussion on the taxonomic identity of UCMP 130051).

Validity of "*Hanssuesia sternbergi*"

Much of the revised diagnosis for "*Hanssuesia sternbergi*" proposed by Sullivan (2003) can be tested by morphometric analyses. The relative width of the frontoparietal dome must have been unique, as it is referenced three times in its revised diagnosis (anterior portion wide, posterior portion wide, and frontonasal boss broad; Sullivan 2003). Sullivan (2003) described the disproportionate width of "*Hanssuesia sternbergi*" as being unique amongst all known pachycephalosaurians. However, specimens of "*Hanssuesia sternbergi*" display a range of frontonasal boss width and anterior dome widths that are indistinguishable from other Belly River Group pachycephalosaurians. Frontoparietals of "*Hanssuesia sternbergi*" do appear to be posteriorly wider than specimens previously assigned to *Stegoceras validum*, although TMP 1972.027.0001 (herein referred to *Stegoceras validum*) fits well within the range of "*Hanssuesia sternbergi*" (Fig. 11C). Additionally, the relative posterior dome width amongst *Colepiocephale lambei* (which is hypothesised to have grown similar to *Stegoceras validum*; Schott et al. 2011) has a similar variance to the range observed between "*Hanssuesia sternbergi*" and *Stegoceras validum*, and demonstrates expected intraspecific variation in the temporal width of the parietal.

The relative frontoparietal width of "*Hanssuesia sternbergi*" is not distinctly wide amongst Belly River Group pachycephalosaurians, so it cannot be used as a diagnostic feature for the species. However, the posterior (parietal) dome is uniquely wide in *Foraminacephale brevis*, and distinguishes it from other Belly River Group pachycephalosaurians. This is observable in regressions comparing posterior dome width (W:Po/stf/Sq) to frontal length (L:F), as well as in the non-transformed and L:F proportionate PCA, where W:Po/stf/Sq loaded in the same direction that separated *Foraminacephale brevis* from other pachycephalosaurians. *Foraminacephale brevis* is unique amongst Belly River Group pachycephalosaurians in that dome inflation begins in the parietal (Schott and Evans, 2017), whereas dome inflation begins in the frontals in *Stegoceras validum* (the dome of *Colepiocephale lambei* likely grew similar to *Stegoceras validum*; Schott et al. 2011). The unique width across the temporal region of the parietal in *Foraminacephale brevis* may reflect the initial center of dome inflation on the parietal.

Similarly, the "more inflated" supraorbital lobes supposedly diagnostic of "*Hanssuesia sternbergi*" (Sullivan 2003) are not corroborated by RMA regressions. Supraorbital heights of "*Hanssuesia sternbergi*" are consistent with *Stegoceras validum* (including TMP 1972.027.0001). Sullivan (2003) did not qualify the shape of a "reduced" supraorbital lobe, although they described the supraorbital lobes (lateral or lateral prefrontal lobes in their text) as "not well developed" and positioned posterior to the frontonasal boss. This description may refer in part to the variation in the anteroposterior prominence of the frontonasal boss, as well as allometric

variation of frontoparietal widths. The supraorbital widths are negatively allometric with respect to the dorsal width at the frontal-parietal contact (W:F/P) in *Stegoceras validum*, whereas growth of the frontonasal boss is isometric (Schott et al. 2011). Thus, frontonasal bosses are proportionately wider compared to supraorbital widths in larger specimens, which results in smaller, indistinct supraorbital lobes that do not extend as medially as they do in smaller individuals. Furthermore, growth in the most posterior supraorbital width (W:Pso/Po) is likely less negatively allometric (closer to isometry) than the other two supraorbital widths. Thus, the posterior portion of the supraorbital lobes widens quicker, and blends the posterior extent of the supraorbital lobes with the posterior portion of the frontoparietal dome. In *Colepiocephale lambei*, the frontoparietal possesses a medial indentation along the most anterior portion of the sutural surface for the postorbital. This indentation may additionally restrict the height of the posterior supraorbital - postorbital contact, which lowers the posterior region of the supraorbital lobe, and perhaps results in "distinguished" supraorbital lobes (Schott et al. 2009).

The final purported diagnostic features of "*Hanssuesia sternbergi*" include the depressed parietal and reduced parieto-squamosal shelf. Only two referred specimens of "*Hanssuesia sternbergi*" preserve complete parietals, which makes assessing these states in most specimens difficult. The apices of the domes are positioned on the frontals in CMN 8817 (Fig. S9), TMP 1987.036.0363, and TMP 2017.012.0019 (Fig. S2), which results in the parietals being more shallowly anteriorly inclined than in *Stegoceras validum* (e.g., UALVP 2; Fig. 22). The parietal of CMN 9148 ("*Hanssuesia sternbergi*"), however, is steeply inclined, and the supraorbital lobes are almost indistinct (Fig. S10). Conversely, the parietal of CMN 38079 ("*Hanssuesia sternbergi*") appears shallowly inclined, although the supraorbital lobes are more distinct than they are in UALVP 2 (Fig. 5G-I in Sullivan, 2003).

The cranial dome of *Stegoceras validum* initially inflated from the frontals (Schott et al. 2011; Nirody et al. 2022). It progressively incorporated more of the parietal (and posterior shelf) and postorbitals through ontogeny (Schott et al. 2011), expanding posteriorly and laterally respectively. TMP 1972.027.0001 exemplifies the end-stage of these trends, whereby the posterior and lateral shelves are completely incorporated into the dome (Figs. 1, 2). Thus, a reduced parieto-squamosal shelf is an expected feature of mature *Stegoceras validum* (as hypothesised by Williamson and Carr 2002), and is not diagnostic to "*Hanssuesia sternbergi*". Variation in the timing or degree to which the parietal is incorporated into the dome may explain the "depressed" parietal, where delayed incorporation results in a disproportionately inflated frontal, compared to the

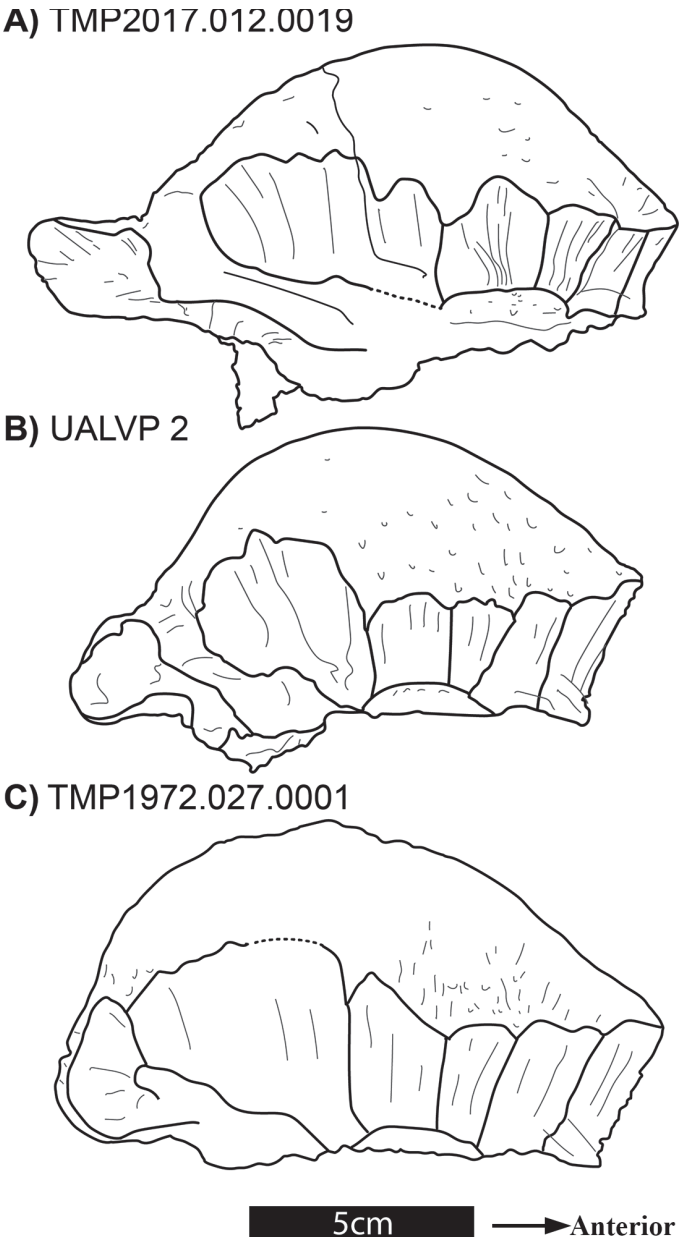

Figure 22. Frontoparietal variation in adult *Stegoceras validum*. Lateral line drawings of A) TMP 2017.012.0019. B) UALVP 2 (mirrored). C) TMP 1972.027.0001. Note that TMP 2017.012.0019 preserves an unambiguous depressed parietal portion of the dome and has a proportionately thinner frontonasal boss, whereas thicker frontonasal bosses (TMP 1972.027.0001 and UALVP 2) are concurrent with parietals that are more incorporated into the dome.

parietal. The ontogenetic timing of dome inflation may also be variable in *Stegoceras validum*. TMP 1978.019.0004, an isolated frontal of *Stegoceras validum*, exemplifies the variation between size (and presumably maturity) and dome development. It is the absolute longest frontal referred to *Stegoceras validum* (59 mm), yet shows no signs of doming. Instead, the dorsal surface is covered in distinctive tuberculate ornamentation (Sues and Galton 1983; Sullivan 2003).

Alternatively, a depressed parietal may represent a healed pathology. TMP 1992.002.0003, preserves a large resorptive pathology that covers nearly the entire dorsal surface of the parietal. If that individual had survived and continued growing, the resulting morphology would result in a "depressed" parietal relative to the mostly unaffected frontals.

Frontoparietal widths and supraorbital lobe inflation are not unique to "*Hanssuesia sternbergi*" among pachycephalosaurians, but are largely consistent with large specimens of *Stegoceras validum*. The depressed parietal of "*Hanssuesia sternbergi*" may also represent intraspecific, ontogenetic, or pathological variation. Additionally, "*Hanssuesia sternbergi*" is indistinct from other Belly River Group pachycephalosaurians in PCA of both $\log_{10}$-transformed and frontal length proportional linear measurements, respectively. For these reasons, we agree with previous studies (Galton 1971; Chapman et al. 1981; Maryańska et al. 2004) that refer "*Hanssuesia sternbergi*" to *Stegoceras validum* (see Schott et al. 2009 and Schott and Evans 2017 for discussion on the distinction of "*Hanssuesia sternbergi*" from *Colepiocephale lambei* and *Foraminacephale brevis* respectively). "*Hanssuesia sternbergi*" is largely separated from *Stegoceras validum* by the temporal width of the parietal in PC 2 the Belly River Group PCA based on non-transformed linear measurements. However, when compared to frontoparietal size, PC 2 scores of most "*Hanssuesia sternbergi*" fit comfortably along the tread line of *Stegoceras validum* (Fig. 16B). Only the holotype, CMN 8817, appears to have a distinct PC 2 score compared to *Stegoceras validum*. However, large specimens of *Colepiocephale lambei* have a greater variation in their PC 2 scores than "*Hanssuesia sternbergi*" and *Stegoceras validum* combined, demonstrating potential ranges that may be expected for intraspecific variation. Interestingly, when *Colepiocephale lambei* and *Foraminacephale* were excluded from PCA, "*Hanssuesia sternbergi*" and *Stegoceras validum* were not separated from one another. Inclusion of *Foraminacephale brevis* (which is largely separated by the temporal width of the parietal) exaggerates the distinction between "*Hanssuesia sternbergi*" and *Stegoceras validum* in PCA by pulling wider parietals closer together. When *Foraminacephale brevis* is removed, specimens referred to "*Hanssuesia sternbergi*" become indistinct from *Stegoceras validum*.

Schott and Evans (2017) recovered weak correlations between linear frontoparietal measurements of "*Hanssuesia sternbergi*" (replicated in this study; Tables S7, S10), and largely attributed this to the limited size range of available specimens. The small available sample of the taxon used in Schott and Evans (2017) and in this study may also contribute to weak or insignificant correlations between frontoparietal measurements. Schott and Evans (2017) also suggested the weak correlations indicated that "*Hanssuesia sternbergi*" comprise multiple species, with some specimens referable to *Stegoceras validum* or unidentified species. Indeed, CMN 9148 and TMP 1979.014.0853 consistently plot amongst *Stegoceras validum* in the PCA and RMA regressions of this study, whereas CMN 8817, TMP 1987.036.0363, and TMP 2017.012.0019 are distinguished from larger *Stegoceras validum* by shorter frontonasal bosses. If "*Hanssuesia sternbergi*" were to be considered valid, it is likely that many smaller specimens are currently misidentified as *Stegoceras validum*. However, frontonasal boss thickness variation is continuous amongst smaller specimens of *Stegoceras validum*, and some shorter bossed specimens (relative to their size) preserve squamosal ornamentation diagnostic to *Stegoceras validum* (CMN 138, ROM 64183, and TMP 1984.005.0001).

Frontoparietal Allometry in *Stegoceras validum* (= "*Hanssuesia sternbergi*" and "*Gravitholus albertae*")

Inclusion of TMP 1972.027.0001 and "*Hanssuesia sternbergi*" with other *Stegoceras validum* (including new specimens) in this analysis increased the strength of the regressions (r2 values) for most variables compared to the more restricted sample in Schott et al. (2011). Therefore, these specimens share a consistent frontoparietal growth pattern. The exception was frontoparietal thickness. Schott et al. (2011) noted that excluding flat-headed *Stegoceras validum* from regressions resulted in lower slopes of frontoparietal thickness, and conversely, excluding large frontoparietals increased the slope of frontoparietal thickness. They speculated that the positive allometry of frontoparietal heights relative to frontoparietal size may not be as extreme in larger frontoparietals, compared to smaller ones. Our inclusion of newly referred large *Stegoceras validum* further anchors the linear regression. This lowers the overall slope by 0.56 from the slope of the total sample RMA in Schott et al. (2011), similar to the exclusion of flatheaded specimens (Schott et al. 2011). It also reduces the 95% confidence interval around the slope compared to Schott et al.'s (2011) results (although they do overlap by 0.11). We agree with Schott et al. (2011) that the positive allometric scaling of frontoparietal thickness relative to frontoparietal width likely decreases through ontogeny, although future studies should explicitly test for this.

The inclusion of newly referred *Stegoceras validum* also resulted in lower slopes for all frontoparietal heights and widths (except for the width of the frontonasal boss) from the slopes calculated by Schott et al. (2011). Slopes for the lengths for the palpebral, posterior supraorbital, and parietal all decreased, whereas slopes for the contact length of the postorbital and the length of the frontal both increased.

Despite these differences, the 95% confidence interval around these slopes did overlap with those in Schott et al. (2011). Patterns of allometry were identical, except for the temporal width across the parietal and the lengths of the posterior supraorbital and postorbital, which scale with negative allometry with respect to the dorsal width across the frontal-parietal contact (W:F/P) (isometric in Schott et al. 2011).

Intraspecific Variation in Frontonasal Boss Thickness in Large *Stegoceras validum*

The PC 2 scores of both the $\log_{10}$-transformed and non-transformed PCA appeared to separate large *Stegoceras validum* into two clusters. These clusters differ in the height of the frontonasal boss, and are supported by Jenks Natural Break Optimization. While the PC 2 scores of large *Stegoceras validum* in the $\log_{10}$-transformed PCA failed the series of dimorphism tests outlined by Mallon (2017), they were significantly non-normally distributed (but not significantly multimodal) in the non-transformed PCA. The sample size of large *Stegoceras validum* frontoparietals is small (n = 9), and a larger sample size could easily corroborate or refute these results. Future analyses could also use other methods of assessing bimodality, such as Ameijeras-Alonso, Crujeiras, Rodrígez-Casal tests (Ameijeiras-Alonso et al. 2019; Moranti 2021). Regardless, frontonasal boss thickness is the feature with the highest degree of intraspecific variation not directly explained by frontoparietal size.

Stratigraphic separation of "thick-bossed" and "thin-bossed" specimens may suggest that these purported morphs represent distinct taxa, rather than a single taxon. Three large *Stegoceras validum* have known stratigraphic positions within the Belly River Group (Table 2). TMP 1972.027.0001, likely from the Oldman Formation, and UALVP 2 approximately 22 m above the Oldman-Dinosaur Park Formation contact (Schott et al. 2011) bracket TMP 2017.012.0019, which was collected from the lower 5 m of the Dinosaur Park Formation. Stratigraphic overlap of only three specimens may be dubious. Therefore, the taxonomic revisions concluded in this study should be revisited after a biostratigraphic analysis of taxonomically informative pachycephalosaurian remains from the Oldman and Dinosaur Park Formations, as well as with future discoveries of specimens with known stratigraphic positions.

Previous studies have explained intraspecific variation in frontoparietal thickness of similarly sized frontoparietals as sexual dimorphism (Galton and Sues 1983; Giffin 1989b) with the thicker-domed sex engaging in intraspecific dome-to-dome combat (Galton 1970; Chapman et al. 1981) or sexual display (Maryańska et al. 2004). The dome-dome combat hypothesis has been criticized based on the purported narrow contact areas (Carpenter 1997) and absence of internal sinuses in domes (Goodwin et al. 1998; Goodwin and Horner 2004). However, photoelastic analyses (Sues 1978) and Finite Element Analyses (Snively and Cox 2008; Snively and Theodor 2011) have demonstrated the pachycephalosaurid dome was structurally capable of withstanding forces induced from collision. The vertebral column and pelvic girdle of pachycephalosaurids are also suited to stabilising the body from dome-dome combat (see Moore et al. 2021 for review).

Pathologies consistent with dome-dome combat trauma are frequently observed on pachycephalosaurian domes (Peterson et al. 2013), and a histologically examined pathological specimen preserved bone remodeling features that form in response to high strain magnitude gradients (Dyer et al. 2021). In the *Stegoceras validum* sample of this study, these pathologies are restricted to specimens with taller frontonasal bosses throughout ontogeny, ranging from W:F/P of 46.07 mm (TMP 1992.002.0003) to 108.99 mm (TMP 1972.027.0001). The restriction of pathologies to relatively taller bossed *Stegoceras validum* is consistent with continuous (rather than discrete) intersexual variation, with the sex engaging in dome-dome combat tending to have thicker frontonasal bosses (although there is no statistically significant bimodality in frontonasal boss thickness). However, the sample of pathological specimens is low (n = 5). An increased sample of pathological specimens could strengthen or refute these results. If pathologies are discovered on "thinner-bossed" *Stegoceras validum*, than the variation in frontonasal boss thickness may represent interspecific, rather than intersexual variation.

Dome inflation begins in the frontals in *Stegoceras validum* (Schott et al. 2011; Nirody et al. 2022), and expands to the parietals and nasals (forming the frontonasal boss) to varying degrees. Frontonasal boss thickness is highly variable in *Stegoceras validum*. This may represent intersexual variation in the extent that the dome progresses from the frontal to include the posterior portion of the nasals (like the variation in the ontogenetic posterior progression of the dome onto the parietal). Large *Stegoceras validum* with proportionately thinner frontonasal bosses also possess unambiguous depressed parietals (considered a diagnostic feature of "*Hanssuesia sternbergi*"; Brown and Schlaikjer 1943; Sullivan 2003), although this feature is not explained by the linear measurements used in this analysis. Thus, the extent that the dome expands anterior and posterior from the frontals to the nasals and parietals, respectively, may represent intersexual variation in *Stegoceras validum*.

Pachycephalosaurian Diversity in the Belly River Group

Colepiocephale lambei, *Foraminacephale brevis*, and *Stegoceras validum* (including "*Gravitholus albertae*" and "*Hanssuesia sternbergi*"), are distinct from one another in

the PCA of non-transformed and frontal length proportionate PCA, whereas the PCA based on $\log_{10}$-transformed or frontoparietal width proportionate measurements mostly did not distinctly separate each taxon (see Supplemental Data 2 for discussion on measurement transformation methods for PCA). Although frontoparietal widths and supraorbital heights do not distinguish "*Hanssuesia sternbergi*", they can partially distinguish *Colepiocephale lambei* and *Foraminacephale brevis*. In these PCAs, as well as in bivariate analyses, *Foraminacephale brevis* is largely separated from other Belly River Group pachycephalosaurians by a wider temporal region of the parietal. Schott and Evans (2017) demonstrated this width scales with positive allometry with respect to the width at the frontoparietal contact, whereas that relationship is negatively allometric in *Stegoceras validum*. The cranial dome of *Foraminacephale brevis* begins inflating on the parietal and extends anteriorly onto the parietal through ontogeny, whereas the opposite occurs in *Stegoceras validum* (Schott et al. 2011, Nirody et al. 2022). The width of the temporal region of the parietal, in an ontogenetic series, may reflect the region of initial dome inflation. Although juvenile specimens of *Colepiocephale lambei* are unknown, the temporal width across the parietal is consistent with *Stegoceras validum*. We agree with Schott et al. (2011), who proposed that the frontoparietal dome of *Colepiocephale lambei* grew similar to *Stegoceras validum*, and further suggest that the dome of *Colepiocephale lambei* initially inflated from the frontals.

The relationship between supraorbital heights and frontoparietal thickness distinguishes *Colepiocephale lambei* from other Belly River Group pachycephalosaurians. In the PCAs based on non-transformed and L:F proportionate measurements, frontoparietal thickness is strongly negatively loaded in PC 3, the same direction that distinguished *Colepiocephale lambei*. All peripheral frontoparietal heights loaded positively, opposite to frontoparietal thickness. Amongst these height measurements the height at the contact for the posterior supraorbital and postorbital was the most positively loaded. This height is immediately adjacent to a lateral indentation in the side of the frontoparietal, which is diagnostic for *Colepiocephale lambei*.

Sullivan (2003) reported both TMP 1972.027.0001 and TMP 2000.026.0001 were derived from the Oldman Formation, and Evans et al. (2013) reported the same providence for TMP 2000.026.0001. This extends the temporal and stratigraphic range of *Stegoceras validum* from the Dinosaur Park Formation into the underlying Oldman Formation. Taxonomically informative pachycephalosaurian remains confidently derived from the lower portions of the Oldman Formation are uncommon, which has left a gap in pachycephalosaurian diversity within the Belly River Group. Schott and Evans (2017) reported *Foraminacephale brevis* from Unit 3 of the Oldman Formation in southern Alberta, which is time equivalent to the lower Dinosaur Park Formation in and around Dinosaur Provincial Park.

Implications for Pachycephalosaurian Diversity

Three species have been synonymised with *Stegoceras validum*: *Gravitholus albertae*, *Hanssuesia sternbergi*, and *Ornatotholus browni*. Many of the proposed diagnostic characters for these proposed species are now considered as individual or ontogenetically variable within *Stegoceras validum*. More species have been proposed to be synonymous with *Pachycephalosaurus wyomingensis*: *Dracorex hogwartsia*, *Pachycephalosaurus grangeri*, *Pachycephalosaurus reinheimeri*, *Stenotholus kohleri*, *Stygimoloch spinifer*, and *Tylosteus ornatum* (Galton 1971; Baird 1979; Sullivan 2003; Horner and Goodwin 2009). The skull roof of pachycephalosaurians underwent tremendous ontogenetic changes through an individual's life (Williamson and Carr 2002; Goodwin and Horner 2004; Horner and Goodwin 2009; Schott et al. 2009; Schott et al. 2011; Schott and Evans 2012; Goodwin and Evans 2016; Schott and Evans 2017; Woodruff et al. 2021). The frontoparietal dome morphology in particular forms the basis for many species diagnoses (*Acrotholus audeti*, Evans et al. 2013; *Amtocephale gobiensis*, Watabe et al. 2011; *Colepiocephale lambei*, Sternberg 1945, Schott et al. 2009; *Sinocephale bexelli*, Evans et al. 2021; "*Stegoceras novomexicanum*", Jasinski and Sullivan 2011, 2016; "*Stenotholus kohleri*", Giffin et al. 1988; *Sphaerotholus edmontonensis*, Brown and Schlaikjer 1943, Woodruff et al. 2021, "*Texacephale langstoni*", Longrich et al. 2010), although this is largely because less-taphonomically robust skeletal elements are rarely preserved (non-skull roof; Evans et al. 2013, Brown et al. 2013b). This makes identification of diagnostic frontoparietal features exceedingly difficult without knowledge of the ontogenetic sequence. Ignoring ontogeny, particularly in well sampled systems, results in erroneously overestimated pachycephalosaurian diversity. Despite the potential for overestimating their diversity, pachycephalosaurians still offer a unique glimpse into small-bodied dinosaur diversity that is less obscured by size-dependent preservational biases.

Further studies need to substantially address pachycephalosaurian diversity, and morphological changes during ontogeny. One of the interesting ontogenetic findings in this study is the potential for complete incorporation of a posterior parietal shelf into the frontoparietal dome, resulting in a "down-turned" parietal. This distinction in posterior parietal morphology has long been held as a strong taxonomic divider (Evans et al. 2021). One such example is the proposed distinction of "*Stegoceras novomexicanum*" (from the Fruitland Formation), and the slightly younger *Sphaerotholus goodwini* (Kirkland Formation) (Jasinski and

Sullivan 2016).Williamson and Brusatte (2016) postulated that NMMNH P33898 (the holotype of "*Stegoceras novomexicanum*") could represent an immature *Sphaerotholus goodwini* (amongst other taxonomic hypotheses). Jasinski and Sullivan (2016) argued "*Stegoceras novomexicanum*" was distinguished from the *Sphaerotholus goodwini* by the presence of a prominent posterior parietal shelf, whereas the cranial dome of *Sphaerotholus goodwini* extends to the posterior margin of the parietal, forming a "down-turned" parietal. Given that posterior parietal shelves may be entirely lost throughout ontogeny, as in *Stegoceras validum* (TMP 1972.027.0001), and that all specimens of "*Stegoceras novomexicanum*" are substantially smaller than specimens of *Sphaerotholus goodwini*, it may be possible that "*Stegoceras novomexicanum*" represents a juvenile ontogenetic stage of *Sphaerotholus goodwini*. A robust analysis of morphological variation amongst pachycephalosaurids from the Fruitland and Kirtland formations will be required to further test this hypothesis.

Pachycephalosaurian Interrelationships

Phylogenetic analyses based on our revised character matrix could not resolve many pachycephalosaurian interrelationships. This was likely because we excluded invalid/unsupported taxa and reassessed taxa known solely from juvenile material (*Goyocephale lattimorei*, *Homalocephale calathocercos*, and *Wannanosaurus yansiensis*) as uncertain for ontogenetically dependant characters. Although this adds greater uncertainty to phylogenetic hypotheses, it is appropriate to take caution in a priori assumptions of maturity given the available data. Sereno (2000) created the first comprehensive pachycephalosaurian morphological character matrix prior to much of the discussion around the maturity of flat-headed specimens (Goodwin et al. 1998 speculated that *Ornatotholus browni* represented immature *Stegoceras validum*, although Galton 1971 first described what would become the holotype (AMNH 5450) as a female morph of *Stegoceras validum*). Nearly every subsequent character matrix largely added onto Sereno's original matrix (Williamson and Carr 2002; Sullivan 2003), which along with the matrix of Maryańska et al. (2004) (they did not explicitly state if their matrix was based on Sereno 2000, although Maryańska et al. used fewer characters than Sereno) have been modified and amalgamated into the Evans et al. (2013) matrix. This has served as the predominant pachycephalosaurian character matrix for the past decade, with minor character additions and reassessments (Williamson and Brusatte 2016; Schott and Evans 2017; Woodruff et al. 2021; Evans et al 2021). Longrich et al. (2010) constructed a novel pachycephalosaurian character matrix, although it had little influence on the matrix created by Evans et al. (2013), and has not been subsequently used. Thus, until now, the pachycephalosaurian character assessments have not considered the uncertainty of ontogenetic dependent characters in taxa known solely from what are now recognised as juvenile animals.

The fragmentary anatomical record of most pachycephalosaurians is also a major contributor to uncertain phylogenetic relationships. There were relatively few characters for the number of included taxa in our dataset (as well as others; Sereno 2000; Williamson and Carr 2002; Sullivan 2003; Maryańska et al. 2004; Watabe et al. 2011; Evans et al. 2013, Schott and Evans 2017; Woodruff et al. 2021), which tends to recover fewer resolved relationships (e.g. Wiens 2004, although see Wiens 2003 for a discussion on the difference between missing data and undersampling characters) with poor node support (O'Reilly et al. 2018). More importantly, the character construction within the matrix is heavily focused on polarizing the ingroup, Pachycephalosauria, from the outgroup taxa, *Psittacosaurus mongoliensis* and *Yinlong downsi*. Sixteen of the 52 characters (31% of characters) distinguish pachycephalosaurians from the outgroup. However, many of these are unknown in most pachycephalosaurians, and more material could make them phylogenetically informative for ingroup relationships. Six characters define an apomorphic feature of terminal taxa (this is more impactful on the parsimony analyses than Bayesian). This results in 30 potentially phylogenetically informative characters for 16 ingroup terminal taxa (< 2 characters per ingroup terminal taxon). Additionally, pachycephalosaurians are only assessed for ~47% of the character matrix (~57% of the "informative" characters) due to their overall fragmentary nature of their remains. This missing data likely has a major impact in recovered hypotheses of phylogenetic relationships (Wright and Hillis 2014). Bayesian methods have been demonstrated to better deal with the effects of missing data and homoplasy in simulated datasets. Therefore, Bayesian methods were employed here to examine hypothetical relationships, regardless of node support, which is still majorly impacted by the percentage of unscored characters for most taxa within our analysis (Supplemental Data 3). Future discoveries, particularly of non-dome related skeletal elements, will provide more anatomical data to resolve these uncertain assessments. Many of the apparent synapomorphic character states of Pachycephalosauria (in this data matrix) are unknown for most pachycephalosaurians due to limited material (e.g., elongate posterior sacral ribs; character 2[1]). It is possible that some of these are synapomorphic for certain groups of pachycephalosaurians, rather than the whole group.

Despite the relatively unresolved topologies in this study, there are intriguing results. The Bayesian analyses recovered some degree of support for a Pachycephalosauridae that does not include *Colepiocephale lambei*, although this relationship was unresolved in maximum parsimony analysis,

and *Colepiocephale lambei* was not included in the agreement subtree of MPTs. Our Bayesian analyses are the first results to suggest a dome-headed non-pachycephalosaurian may not be descended from the most recent common ancestor of *Stegoceras validum* and *Pachycephalosaurus wyomingensis*. This division is based largely on the retention of open supratemporal fenestrae, and lack of incorporation of peripheral elements in the frontoparietal dome during ontogeny in *Colepiocephale lambei*. This character distribution demonstrates vulnerabilities for a taxon-based definition for Pachycephalosauridae. As our understanding of taxonomic diversity and character evolution within Pachycephalosauria increases, taxon-based definitions for clades may make composition of these clades more ephemeral. Adoption of character based clade definitions may resolve these issues if convention demands all dome-headed pachycephalosaurians be distinguished from flat-headed members. Overall, the assignment of *Colepiocephale lambei* as a pachycephalosaurid or non-pachycephalosaurid pachycephalosaurian is ambiguous between parsimony and Bayesian methods.

None of the MPTs nor the fully resolved Bayesian tree recovered a monophyletic *Sphaerotholus*, inconsistent with recent phylogenetic analyses (Woodruff et al. 2021; a monophyletic *Sphaerotholus* was recovered in the 50% consensus tree of Evans et al. 2021). The agreement subtree of all MPTs recovered a paraphyletic *Sphaerotholus*, with *Sphaerotholus goodwini* more closely related to *Acrotholus audeti* than to *Sphaerotholus buchholtzae* (*Sphaerotholus edmontonensis* was not included in the agreement subtree). Woodruff et al. (2021) reported four characters uniting *Sphaerotholus*: characters 33(1), 35(1), 36(2), and 42(1) of their analysis (character 42 appears erroneously reported as character 52 in their figure 14). All these characters were modified to various extents in our analysis (see Supplemental Data 2 for detailed explanations).

Given that *Sphaerotholus goodwini* is the type species of *Sphaerotholus* (Williamson and Carr 2002), *Sphaerotholus buchholtzae* and *Sphaerotholus edmontonensis* may be erroneously assigned to *Sphaerotholus* based on the 50% majority and fully resolved Bayesian tree. Alternatively, the agreement subtree of all MPTs suggests that *Acrotholus audeti* may instead belong to *Sphaerotholus*. However, given overall uncertainty in pachycephalosaurian interrelationships in both analyses, we refrain from reassigning species to different genera.

Despite poor node support in the resolved Bayesian tree, compelling anatomical similarities support the position of *Sphaerotholus goodwini* within the most exclusive monophyletic clade containing *Pachycephalosaurus wyomingensis* and *Prenocephale prenes*. *Sphaerotholus goodwini* shares four characters with these other taxa (27[1], 37[2], 39[0], and 46[1]) that distinguishes it from *Sphaerotholus buchholtzae* (27[0], 37[1], 39[1], and 46[0]). *Sphaerotholus edmontonensis* is only scored for one of these characters: 37[1] possession of a broad intersquamosal process of the parietal. Interestingly, *Sphaerotholus* spp. and *Pachycephalosaurus wyomingensis* share the feature of a confluent dorsal border across the contact between the frontoparietal dome, posterior supraorbital, and postorbital (Ch. 33[1]). Although none of the supports in the most exclusive monophyletic clade that contains *Sphaerotholus* spp. and *Prenocephale prenes* are above 50% PP, they generally show higher support than most other derived nodes within the tree. A similar clade was recovered in the 50% majority rule consensus parsimony tree (Fig. 20A). Of all the pachycephalosaurines, only *Pachycephalosaurus wyomingensis*, *Sphaerotholus goodwini*, and *Acrotholus audeti* + *Prenocephale prenes* were recovered in a distinct clade. Additionally, the relationship between *Acrotholus audeti* and *Sphaerotholus* spp. (excluding *Sphaerotholus edmontonensis*) is recovered in both the resolved Bayesian tree (Fig. 21) as well as the agreement subtree (Fig. 20C), suggesting strong corroborative support for these relationships. Without question, more specimens will provide better resolution in hypotheses of pachycephalosaurian phylogeny. However, the study here shows hypothetical relationships worth investigating further, which could benefit from targeted sampling.

Characterizing Pachycephalosaurians

The history of pachycephalosaurian taxonomy has been rife with controversy and post hoc diagnostic corrections (including this study), largely because pachycephalosaurians underwent incredible ontogenetic transformations in life. Generating robust species diagnoses requires multiple specimens of various ontogenetic stages (*Colepiocephale lambei*, Schott et al. 2009; *Foraminacephale brevis*, Schott and Evans 2017; *Sphaerotholus buchholtzae*, Woodruff et al. 2021; *Stegoceras validum*, Schott et al. 2011; Schott and Evans 2012). Species propositions based on morphological criteria are hypotheses that can be tested through comparison with other specimens and taxa. With the known phenomenon of drastic ontogenetic transformations in pachycephalosaurian taxa, caution should be used in diagnosing specimens as species without sufficient overlap with semaphoronts of other taxa. Doing so may inflate the ongoing problems in pachycephalosaurian taxonomy.

The other problem that comes with major morphological transformations through ontogeny is one of generating morphological character statements for postulating phylogenetic relationships. The characters we use are the primary hypotheses of relationship (Patterson 1982; de Pinna 1991) and they must be tested with increasing observations through additional samples. Characters were tested here

for their logical and biological independence (Wilkinson 1995; Hawkins et al. 1997), as well as general character construction (Simões et al. 2017) in order to produce primary hypotheses (morphological character statements) of relationships that better reflect the current data of pachycephalosaurian specimens. Topological relationships recovered in this study varied from previous studies, primarily in the exclusion of *Colepiocephale lambei* from Pachycephalosauridae, and the polyphyletic/paraphyletic relationship of *Sphaerotholus* spp. This is not to say that these hypotheses are superior to previous hypotheses, but simply that adjusting character statements prior to analysis has a large impact on the pattern of relationships produced via phylogenetic analysis (Simões et al. 2017).

Morphological characters are not fixed data points, but rather conceptualized similarities between specimens representing species. They require re-evaluation as our knowledge of intraspecific variation (ontogeny, sexual dimorphism, allometry) improves and new taxa are proposed. We hope that more studies will incorporate this practice of re-evaluation more regularly, particularly when inserting new taxa into an existing framework. Many of the characters in this matrix would greatly benefit from quantitative analysis to provide statistical support for differentiating character states (e.g., Powers et al. 2020; Powers et al. 2022). Constructive discourse between researchers on hypotheses of homology should be the desired goal.

CONCLUSIONS

This study utilized SμCT images of TMP 1972.027.0001 ("*Gravitholus albertae*") to address the taxonomic problems proposed by this specimen. SμCT imaging is suitable for identifying the fused contacts in TMP 1972.027.0001 and may be an appropriate method for future studies of large, fused pachycephalosaurid skulls. "*Gravitholus albertae*" cannot be distinguished from *Stegoceras validum* based on its original diagnosis. Morphological differences between TMP 1972.027.0001, "*Hanssuesia sternbergi*" and historically identified *Stegoceras validum* are explained by ontogenetic patterns and allometry. Thus, "*Gravitholus albertae*" and "*Hanssuesia sternbergi*" are synonymous with *Stegoceras validum*, which reduces the diversity of North American pachycephalosaurids during the Campanian. The thickness of the frontonasal boss has a high degree of intraspecific variation. Posttraumatic pathologies, consistent with intraspecific cranial combat are restricted to specimens with relatively thicker frontonasal bosses for their size, and suggests that variation in frontonasal boss thickness may represent continuous, non-discreet intersexual variation.

A revised pachycephalosaurian phylogenetic character matrix incorporating ontogenetic uncertainties, novel interpretations, and excluding invalid/unsupported taxa resulted in a relatively unresolved Pachycephalosauria. Despite this lack of resolution, *Colepiocephale lambei* may be a non-pachycephalosaurid pachycephalosaurian (unresolved), and there is some support for a polyphyletic/paraphyletic *Sphaerotholus*. To improve our understanding of pachycephalosaurian systematics, future works should aim to quantitatively dichotomize character states based on clusters within continuous data.

ACKNOWLEDGEMENTS

B. Strilisky, B. Sanchez, T. Courtenay provided access to TMP 1972.027.0001 and assistance during TMP collections visits. C. Coy and H. Gibbins provided access to the UALVP collections. D. Evans and K. Seymour provided access to the ROM collections. T. Bond, S. Gasilov, D. Miller, and A. Panahifar of the CLS are thanked for their technical support and expertise. J. Richard provided the photograph used in Fig 1C. D. Evans and C. Woodruff provided HRCT data for ROM 53555. WitmerLab at Ohio University provided access to the segmented frontoparietal model of UALVP 2 originally appearing in The Visible Interactive Pachycephalosaur, the collection of which was funded by NSF grants to LM Witmer. The files were downloaded from www.MorphoSource.org, Duke University. C. Dyer assisted with a collection visit to the TMP. F. Sperling, C. Sullivan, R. Wilkinson, D. Maranga, D. Evans, M. Rhodes, G. Funston, and C. Dyer all provided valuable discussions and/or reviewed earlier drafts of this manuscript. C. Brown and E. Snively provided valuable comments and criticisms that have greatly improved this manuscript. This research was supported by funding from the Ontario Graduate Scholarship awarded to A.D. Dyer, and further funding was provided by a DRI Student Project grant to M.J. Powers, and an NSERC Discovery grant (#2017-04715) to P.J. Currie.

LITERATURE CITED

Ameijeiras-Alonso, J., R.M. Crujeiras, and A. Rodríguez-Casal. 2019. Mode testing, critical bandwidth and excess mass. TEST 28:900–919.

Baird, D. 1979. The dome-headed dinosaur *Tylosteus ornatus* Leidy 1872 (Reptilia: Ornithischia: Pachycephalosauridae). Notulae Naturae 456:1–11.

Bourke, J.M., W.R. Porter, R.C. Ridgely, T.R. Lyson, E.R. Schachner, P.R. Bell, and L.M. Witmer. 2014. Breathing life into dinosaurs: tackling challenges of soft-tissue restoration and nasal airflow in extinct species. The Anatomical Record 297:2148–2186.

Brown, B., and E.M. Schlaikjer. 1943. A study of the troödont dinosaurs with the description of a new genus and four new

species. Bulletin of the American Museum of Natural History 82:115–150.

Brown, C.M., D.C. Evans, N.E. Campione, L.J. O'Brien, and D.A. Eberth. 2013. Evidence for taphonomic size bias in the Dinosaur Park Formation (Campanian, Alberta), a model Mesozoic terrestrial alluvial-paralic system. Palaeogeography, Palaeoclimatology, Palaeoecology 372:108–122.

Brown, C.M., D.C. Evans, M.J. Ryan, and A.P. Russell. 2013. New data on the diversity and abundance of small-bodied ornithopods (Dinosauria, Ornithischia) from the Belly River Group (Campanian) of Alberta. Journal of Vertebrate Paleontology. 33:495–520.

Carpenter K. 1997. Agonistic behaviour in pachycephalosaurs (Ornithischia: Dinosauria): a new look at head-butting behaviour. Contributions to Geology, University of Wyoming 32:19–25.

Chapman, R.E., P.M. Galton, J.J. Sepkoski, and W.P. Wall. 1981. A morphometric study of the cranium of the pachycephalosaurid dinosaur *Stegoceras*. Journal of Paleontology 55:608–618.

de Pinna, M.C. 1991. Concepts and tests of homology in the cladistic paradigm. Cladistics 7:367–394.

Dyer, A.D., A.R.H LeBlanc, M.R. Doschak, and P.J. Currie. 2021. Taking a crack at the dome: histopathology of a pachycephalosaurid (Dinosauria: Ornithischia) frontoparietal dome. Biosis: Biological Systems 2:248–270.

Eberth, D.A., and A.P. Hamblin. 1993. Tectonic, stratigraphic, and sedimentologic significance of a regional discontinuity in the upper Judith River Group (Belly River wedge) of southern Alberta, Saskatchewan, and northern Montana. Canadian Journal of Earth Sciences 30:174–200.

Evans, D.C., C.M. Brown, H. You, and N.E. Campione. 2021. Description and revised diagnosis of Asia's first recorded pachycephalosaurid, *Sinocephale bexelli* gen. nov., from the Upper Cretaceous of Inner Mongolia, China. Canadian Journal of Earth Sciences 58:981–992.

Evans, D.C., S. Hayashi, K. Chiba, M. Watabe, M.J. Ryan, Y.-N Lee, P.J. Currie, K. Tsogtbaatar, and R. Barsbold. 2018. Morphology and histology of new cranial specimens of Pachycephalosauridae (Dinosauria: Ornithischia) from the Negmet Formation, Mongolia. Palaeogeography, Palaeoclimatology, Palaeoecology 494:121–134.

Evans, D.C., R.K. Schott, D.W. Larson, C.M. Brown, and M.J. Ryan. 2013. The oldest North American pachycephalosaurid and the hidden diversity of small-bodied ornithischian dinosaurs. Nature Communications 4:1–10.

Galton, P.M. 1971. A primitive dome-headed dinosaur (Ornithischia: Pachycephalosauridae) from the Lower Cretaceous of England and the function of the dome of pachycephalosaurids. Journal of Paleontology 45:40–47.

Galton, P.M. and H.-D. Sues. 1983. New data on pachycephalosaurid dinosaurs (Reptilia: Ornithischia) from North America. Canadian Journal of Earth Sciences 20:462–472.

Geist, V. 1966. The evolution of horn-like organs. Behaviour 27:175–214.

Giffin, E.B. 1989a. Pachycephalosaur paleoneurology (Archosauria: Ornithischia). Journal of Vertebrate Paleontology 9:67–77.

Giffin, E.B. 1989b. Notes on pachycephalosaurs (Ornithischia). Journal of Paleontology 63:525–529.

Giffin, E.B., D.L. Gabriel, and R.E. Johnson. 1987. A new pachycephalosaurid skull (Ornithischia) from the Cretaceous Hell Creek Formation of Montana. Journal of Vertebrate Paleontology 7:398–407.

Gilmore, C.W. 1924. On *Troodon validus*: an orthopodous dinosaur from the Belly River Cretaceous of Alberta. University of Alberta Department of Geology Bulletin 1:1–43.

Goloboff, P.A., and S.A Catalano. 2016. TNT version 1.5, including a full implementation of phylogenetic morphometrics. Cladistics 32:221–238.

Goodwin, M.B. 1990. Morphometric landmarks of pachycephalosaurid cranial material from the Judith River Formation of northcentral Montana; pp. 189–201 in K. Carpenter and P.J. Currie (eds.). Dinosaur Systematics: Approaches and Perspectives. Cambridge: Cambridge University Press.

Goodwin, M.B., E.A. Buchholtz, and R.E. Johnson. 1998. Cranial anatomy and diagnosis of *Stygimoloch spinifer* (Ornithischia: Pachycephalosauria) with comments on cranial display structures in agonistic behavior. Journal of Vertebrate Paleontology 18:363–375.

Goodwin, M.B., and D.C. Evans. 2016. The early expression of squamosal horns and parietal ornamentation confirmed by new end-stage juvenile *Pachycephalosaurus* fossils from the Upper Cretaceous Hell Creek Formation, Montana. Journal of Vertebrate Paleontology 36:e21078343.

Goodwin, M.B., and J.R. Horner. 2004. Cranial histology of pachycephalosaurs (Ornithischia: Marginocephalia) reveals transitory structures inconsistent with head-butting behaviour. Paleobiology 30:253–267.

Hammer, Ø., D.A.T. Harper, and P.D. Ryan. 2001. PAST: Paleontological statistics software package for education and data analysis. Palaeontologia Electronica 4:1–9.

Hawkins, J.A., C.E. Hughes, and R.W. Scotland. 1997. Primary homology assessment, characters and character states. Cladistics 13:275–283.

Jasinski, S.E., and R.M. Sullivan. 2011. Re-evaluation of pachycephalosaurids from the Fruitland-Kirtland transition (Kirtlandian, Late Campanian), San Juan Basin, New Mexico, with a description of a new species of *Stegoceras* and a reassessment of *Texacephale langstoni*. New Mexico Museum of Natural History and Science Bulletin 53:202–215.

Jasinski, S.E., and R.M. Sullivan. 2016. The validity of the Late Cretaceous pachycephalosaurid *Stegoceras novomexicanum* (Dinosauria: Pachycephalosauridae). New Mexico Museum of Natural History and Science Bulletin 74:107–115.

Kilmer, J.T., and R.L. Rodríguez. 2017. Ordinary least squares regression is indicated for studies of allometry. Journal of Evolutionary Biology 30:4–12.

Lambe, L.M. 1902. New genera and species from the Belly River series (mid-Cretaceous). Geological survey of Canada Contributions to Canadian Palaeontology 3:25–81.

Lehman, T.M. 2010. Pachycephalosauridae from the San Carlos and Aguja formations (upper Cretaceous) of West Texas, and observations of the frontoparietal dome. Journal of Vertebrate Paleontology 30:786–798.

Longrich, N.R., J. Sankey and D. Tanke. 2010. *Texacephale langstoni*, a new genus of pachycephalosaurid (Dinosauria: Ornithischia) from the upper Campanian Aguja Formation, southern Texas, USA. Cretaceous Research 31:274–284.

Mallon, J.C. 2017. Recognizing sexual dimorphism in the fossil record: lessons from nonavian dinosaurs. Paleobiology 43:495–507.

Maryańska, T. 1990. Pachycephalosauria; pp. 564–577 in D.B. Weishampel, P. Dodson, and H. Osmólska (eds.). The Dinosauria. Berkeley: University of California Press.

Maryańska, T., R.E. Chapman, and D.B. Weishampel. 2004. Pachycephalosauria; pp. 464–477 in D.B. Weishampel, P. Dodson and H. Osmólska (eds.). The Dinosauria, second edition. Berkeley: University of California Press.

Maryańska, T., and H. Osmólska. 1974. Pachycephalosauria, a new suborder of ornithischian dinosaurs. Palaeontologica Polonica 30:45–120.

Motani, R. 2021. Sex estimation from morphology in living animals and dinosaurs. Zoological Journal of the Linnean Society 192:1029–1044.

Moore, B.R.S., M.J. Roloson, P.J. Currie, M.J. Ryan, R.T. Patterson, and J.C. Mallon. 2022. The appendicular myology of *Stegoceras validum* (Ornithischia: Pachycephalosauridae) and implications for the head-butting hypothesis. PLoS ONE 17(9):e0268144.

Nirody, J.A., M.B. Goodwin, J.R. Horner, T.L. Huynh, M.W. Colbert, D.K. Smith, and D.C. Evans. 2022. Quantifying vascularity in the frontoparietal dome of *Stegoceras validum* (Dinosauria: Pachycephalosauridae) from high resolution CT scans. Journal of Vertebrate Paleontology e2036991.

Owen, R. 1842. Report of British fossil reptiles, Pt II. Report of the British Association for the Advancement of Science 11:60–204.

O'Reilly, J.E., M.N. Puttick, D. Pisani, and P.C. Donoghue. 2018. Probabilistic methods surpass parsimony when assessing clade support in phylogenetic analyses of discrete morphological data. Palaeontology 61:105–118.

Patterson, C. 1982. Morphological characters and homology; pp. 21–74 in K.A. Joysey and A.E. Friday (eds.). Problems of Phylogenetic Reconstruction, volume 21. London and New York: Academic Press.

Peterson, J.E., C. Dischler, N.R. Longrich. 2013. Distributions of cranial pathologies provide evidence for head-butting in dome-headed dinosaurs (Pachycephalosauridae). PLoS ONE 8:e68620.

Peterson, J.E., and C.P. Vittore. 2012. Cranial pathologies in a specimen of *Pachycephalosaurus*. PLoS ONE 7:e36227.

Powers, M.J., C. Sullivan, and P.J. Currie. 2020. Re-examining ratio based premaxillary and maxillary characters in Eudromaeosauria (Dinosauria: Theropoda): divergent trends in snout morphology between Asian and North American taxa. Palaeogeography, Palaeoclimatology, Palaeoecology 547:109704.

Powers, M.J., M. Fabbri, M.R. Doschak, B.A.S. Bhullar, D.C. Evans, M.A. Norell, and P.J. Currie. 2022. A new hypothesis of eudromaeosaurian evolution: CT scans assist in testing and constructing morphological characters. Journal of Vertebrate Paleontology 41:e2010087.

Ryan, M.J., and D.C. Evans. 2005. Ornithischian dinosaurs; pp. 313–348 in P.J. Currie and E. Koppelhus (eds.). Dinosaur Provincial Park: A Spectacular Ancient Ecosystem Revealed. Bloomington: Indiana University Press.

Schott, R.K., and D.C. Evans. 2012. Squamosal ontogeny and variation in the pachycephalosaurian dinosaur *Stegoceras validum* Lambe, 1902, from the Dinosaur Park Formation, Alberta. Journal of Vertebrate Palaeontology 32:903–913.

Schott, R.K., and D.C. Evans. 2017. Cranial variation and systematics of *Foraminacephale brevis* gen. nov. and the diversity of pachycephalosaurid dinosaurs (Ornithischia: Cerapoda) in the Belly River Group of Alberta, Canada. Zoological Journal of the Linnean Society 179:865–906.

Schott, R.K., D.C. Evans, M.B. Goodwin, J.R. Horner, C.M. Brown, and N.R. Longrich. 2011. Cranial ontogeny in *Stegoceras validum* (Dinosauria: Pachycephalosauria): A quantitative model of pachycephalosaur dome growth and variation. PLoS ONE 6:e21092.

Schott, R.K., D.C. Evans, T.E. Williamson, T.D. Carr, and M.B. Goodwin. 2009. The anatomy and systematics of *Colepiocephale lambei* (Dinosauria: Pachycephalosauridae). Journal of Vertebrate Paleontology 29:771–786.

Seeley, H.G. 1887. On the classification of the fossil animals commonly named Dinosauria. Proceedings of the Royal Society of London 43:165–171.

Simões, T.R., M.W. Caldwell, A. Palci, and R.L. Nydam. 2017. Giant taxon-character matrices: quality of character constructions remains critical regardless of size. Cladistics 33:198–219.

Smith, R.J. 2009. Use and misuse of the Reduced Major Axis for line-fitting. American Journal of Physical Anthropology 140:476–486.

Snively, E., and A. Cox. 2008. Structural mechanics of pachycephalosaur crania permitted head-butting behavior. Palaeontologica Electronica 11:3A.

Snively, E., and J.M. Theodor. 2011. Common functional correlates of head-strike behavior in the pachycephalosaur dinosaur *Stegoceras validum* (Ornithischia, Dinosauria) and combative artiodactyls. PLoS ONE 6(6):e21422.

Starck, J.M., and A. Chinsamy. 2002. Bone microstructure and developmental plasticity in bird and other dinosaurs. Journal of Morphology 254:232–246.

Sternberg, C.M. 1945. Pachycephalosauridae proposed for dome-headed dinosaurs, *Stegoceras lambei* n. sp., described. Journal of Paleontology 19:534–538.

Sues, H.-D. 1978. Functional morpholoogy of the dome in pachycephalosaurid dinosaurs. Neues Jahrbuch für Geologie und Paläontologie Monatshefte 8:459–472.

Sues, H.-D., and P.M. Galton. 1987. Anatomy and classification of the North American Pachycephalosauria (Dinosauria: Ornithischia). Paleontographica Abteilung A 198:1–40.

Sullivan, R.M. 2000. *Prenocephale edmontonensis* (Brown and Schlaikjer) new comb. and *P. brevis* (Lambe) new comb. (Dinosauria: Ornithischia: Pachycephalosauria) from the upper Cretaceous of North America. New Mexico Museum of Natural History and Science Bulletin 17:117–190.

Sullivan, R.M. 2003. Revision of the dinosaur *Stegoceras* Lambe (Ornithischia, Pachycephalosauridae). Journal of Vertebrate Paleontology 23:181–207.

Sullivan, R.M. 2006. A taxonomic review of the Pachycephalosauridae (Dinosauria: Ornithischia). New Mexico Museum of Natural History and Science Bulletin 35:347–365.

Wall, W.P. and P.M. Galton. 1979. Notes on pachycephalosaurid dinosaurs (Reptilia: Ornithischia) from North America, with comments on their status as ornithopods. Canadian Journal of Earth Sciences 16:1176–1186.

Watabe, M., K. Tsogtbaatar, and R.M. Sullivan. 2011. A new pachycephalosaurid from the Baynshire Formation (Cenomanian-Late Santonian), Gobi Desert, Mongolia. New Mexico Museum of Natural History and Science Bulletin 53:489–497.

Wiens, J.J. 2003. Missing data, incomplete taxa, and phylogenetic accuracy. Systematic Biology 52:528–538.

Wiens, J.J. 2004. The role of morphological data in phylogeny reconstruction. Systematic Biology 53:653–661.

Wilkinson, M. 1995. A comparison of two methods of character construction. Cladistics 11:297–308.

Williamson, T.E., and S.L. Brusatte. 2016. Pachycephalosaurs (Dinosauria: Ornithischia) from the Upper Cretaceous (upper Campanian) of New Mexico: A reassessment of *Stegoceras novomexicanum*. Cretaceous Research 62:29–43.

Williamson, T.E. and T.D. Carr. 2002. A new genus of derived pachycephalosaurian from western North America. Journal of Vertebrate Paleontology 22:779–801.

Woodruff, D.C., M.B. Goodwin, T.R. Lyson and D.C. Evans. 2021. Ontogeny and variation of the pachycephalosaurine dinosaur *Sphaerotholus buchholtzae*, and its systematics within the genus. Zoological Journal of the Linnean Society 193:563–601.

Wright, A.P. and D.M. Hillis. 2014. Bayesian analysis using a simple likelihood model outperformed parsimony for estimation of phylogeny from discrete morphological data. PLoS ONE 9:e0109210.